POLITECNICO DI TORINO

Master's Degree in Ingegneria Aerospaziale

Master's Degree Thesis

Analysis of the behaviour of flax fibre's biocomposites under static and dynamic loads.

Supervisors

Prof. Erasmo CARRERA

Prof. Marco PETROLO

Prof. Frédéric LACHAUD

Candidate

DAVID PLANAS

APRIL 2020

Summary

Composite materials are not new, they have been leading the way in the construction of technologically cutting- edge structures for several decades, specially in the field of aeronautics. In the last few years their use has, however, jumped to some other sectors. The main reason for this popularisation for "earthlier" applications, has been the deepening in their knowledge, specially regarding their manufacturing and maintenance processes, what has caused without any doubt a cheapening in their use. On the other hand, in the last two decades it has arisen across all industries, fields, sectors and social layers of population a raising awareness of care taking of the planet, what has caused an important ecological wave, as resources are limited and the human being is consuming them at an accelerated rate. As a consequence of this deeper knowledge in composites and following this ecological upward tendency, bio composite materials appeared in the 90's. Among these bio composites the flax fibre is gaining an important role due to its characteristics, which keep a good balance between weight/density and mechanical properties. VESO- Concept is a company settled in Toulouse whose aim is to develop complete organic elements made up with bio composite materials. This thesis fits within the BOPA project, a project between VESO- Concept and ISAE- SUPAERO, the Institut superieur de l'aeronatique et de l'espace. Final objective of this project is the characterization of the behaviour of plies made of flax fibre, specially regarding damage. Models of damage will be developed following others authors theories and they will be put to test taking advantage of the powerful tools that represent the currently finite elements programs. To compare results, real experiments will be carried out. At the same time these experiments will be replicated with FEM program. Experiments will put the bio composite elements under static loads (three point bending test and fracture test) and dynamic loads, through an impact test. Results comparison will help to analyse the validity of the models and improve them.

Acknowledgements

A mi familia, por su apoyo incondicional

Table of Contents

List of Tables

List of Figures

Chapter 1

Introduction

BOPA is a project which is being held between ISAE-SUPAERO and a company called VESO-CONCEPT, specialized in composite materials. The objective of the project is to develop complete organic elements made from bio-composite materials able to compete with the classic inorganic composite panels.

Composite materials are defined as those materials which are made of the union, chemical or not, of two or more different materials, in order to achieve a combination of properties that is not possible to get in the original material. A composite material can be defined as the macroscopic combination of a reinforcement material and a different material that acts as a binder or matrix, and that has a differentiated and recognizable interphase (Guemes et. al, 2012) [1]. Materials can be considerate as composites when they fulfil the following conditions:

1. They are made of two or more components which can be physically distinguished and mechanically divisible.

2. They present several phases chemically different, completely insoluble between them and separated by an internphase. Each one of the components must maintain its identity and they cannot react between them.

3. Their mechanical properties are superior to the simple addition of the properties of their components, what is called synergy.

The reinforcement material, in the form of discontinuous phase, provides the interesting mechanical properties. Meanwhile the matrix, that surrounds the reinforcement material and causes the whole element to be a monolithic structure, is responsible of holding the fibres together, of transferring the loads on it, and of the thermal and environmental resistance.

As aeronautic materials, they present a series of clear advantages when faced with traditional materials. This has favoured a considerable increase in the use of these materials in the last decades. This can be seen when comparing the weight of composite material faced with the operational empty weight. In veteran airplanes such as the Airbus A320-100 (1987) composites are a 15% of the OEW, while in newer ones such as the Airbus A-350 XWB (2013) this percentage is above 50%.

Figure 1.1: Airbus A350-XWB [2]

In the typical conception of a composite material, with a series of fibres orientated under a direction, and a matrix acting as a binder between them, it is seen the clear objective pursued with the use of these materials. They are intended to offer good mechanical properties in the direction of the fibre, which will be placed in the direction of the main stresses, and poorer properties in the unloaded directions, achieving through this anisotropy a weight reduction when compared with an isotropic material that would have same properties in all directions. As construction with composites is "modular", more plies can be applied in the most loaded directions, while a few ones are put in the unloaded ones, ensuring through this way that they are not totally abandoned and achieving the weight reduction.

A bio-composite is a composite material whose matrix and reinforcement have an animal or vegetable origin. Matrix are usually compounded of polymers which come from renewable and nonrenewable resources, while bio-fibres typically come from biological origins, e.g. recycled wood, fibres from crops (cotton, hemp or flax) etc.

The main difference for this kind of composites is that they are biodegradable, renewable, in some cases completely recyclable, and cheaper, and therefore pollute the environment less. This is the reason why there has been heightened interest in its use in recent years, due to the increasing concern with the environmental change and pollution and the sustainability of using resources such as petroleum, which is a usual base for many polymers, for example. In addition, natural fibres usually have lower manufacturing costs than conventional composites and are easily processed, and are suited for a wider range of applications, such as packaging, building, automobiles, aerospace, military applications, electronics, consumer products and medical industry (prosthetic, bone plate, orthodontic archwire, and composite screws), and research, as is the case of this thesis.

One of the most important advantages of natural fibres is their low density, which results in a higher specific tensile strength and stiffness than glass fibres, besides of its lower manufacturing costs. Natural fibres have a hollow structure, which gives insulation against noise and heat. Bio-composites may be employed alone, or complementing other materials, like carbon or glass fibre. Some side- effect advantages are that they improve health and safety in their production, are lighter in weight when compared with traditional materials, have a pleasant visual appeal, similar to the one of wood, and are environmentally superior.

In this sense, a project called BOPA is being held between ISAE-SUPAERO (Institut Superior de l'Aéronautique et de l'Espace) and a company called VESO-CONCEPT, settled in Toulouse and which is specialized in composite and bio-composite materials. The aim of the project in a long term scale is to develop complete organic elements made of bio-composite materials able to compete with the classic inorganic composite panels.

The project is guided in the university by Prof. Frédéric Lachaud, from the Research and Development department DMSM (Département Mécanique des Structures et Matérieux). Since BOPA has an environmental and eco-friendly background, this project is considered of high interest and this is the reason why the project is partially financed by ADEME (Agence de l'Environnement et de la Maîtrise de l'Énergie).

ADEME is a public institution under the supervision of the French ministry of Ecological Transition and the ministry of Superior Education, Research and Innovation. Regarding the aim of the project, the main fibre that is being used and tested is the flax fibre. Glass fibre is also being studied within BOPA project but not in this thesis. Flax fibre has a unique series of properties that make it interesting for the manufacturing of composite panels, presenting high values of Young modulus and ultimate stress, which does not allow construction of primary but secondary structures at a fewer weight than other non biodegradable composites.

As the goal is to develop pre-preg plies with correct mechanical properties when compare with classic composite solutions, specific engineering applications are being studied, that is the case for example of corrugated panels, in order to substitute the classical honeycomb core sandwich solutions.

To reach the final goal, the whole project is divided in several steps:

1. Characterization of the mechanical properties of plies made of flax fibre, including the damage modelization.
2. Study the use of organic matrix in place of epoxy or phenolic resin.
3. Development of a completely organic ply.

The project is still in its first phase, and that is why the characterization of the flax fibre is being studied in plies made of epoxy resin, instead of using an organic matrix.

Chapter 2

Problem approach

As previously explained, the main goal of this thesis is to collaborate in the BOPA project, through the characterization of the mechanical properties of the bio flax composite materials.

The characterization is not easy, as the main problem is that these fibres do not present a linear behaviour, in other words, their stiffness matrix is not constant throughout the loading phase. As its obvious, there is a point at which the material fails and the stiffness is sharply decreased, but through the loading phase until that point the stiffness is neither constant, but suffers from a degradation that is not given for example in isotropic metals (or at least not in such a strong way, as all the materials suffer from small internal imperfections with growing mechanisms such as dislocations in metals).

Therefore, the main objective for this characterization is the creation of damage models able to replicate the behaviour of these materials when submitted to two types of loads, static and dynamic. The static load will be typically a three point bending test whereas the dynamic load will be the low velocity impact of a mass.

In order to do so, plies made up of flax fibre and epoxy matrix are being manufactured in the laboratory. These plies are later being used for creating several elements with different shapes and ply configurations that are tested in different analysis, later explained. According to the results of these tests, several damage models are studied, created and applied. These models are then put to test with models created in a FEM program, equal to the real tested ones. The program used is ABAQUS, as it allows a simple implementation of the characterization of different kinds of materials through means of routines written in several programming languages such as C or FORTRAN. After, results are out taken from ABAQUS and compared with the real test results in order to validate the degree of approximation with reality of the chosen damage model.

It is important, in order to understand later the damage model, that the flax fibre when used for the creation of the plies is used with a fabric configuration, this is, fibre has been weaved in a warp and a weft direction , as shown in figure 2.1. The plies used are not pre-preg plies, but the liquid epoxy is distributed with the help of a brush, filling the gaps in the weaved configuration and also between a ply and the next one. After that, the configuration of stacked plies is cured in an autoclave or in a normal oven creating the negative pressure with the help of a vacuum bag.

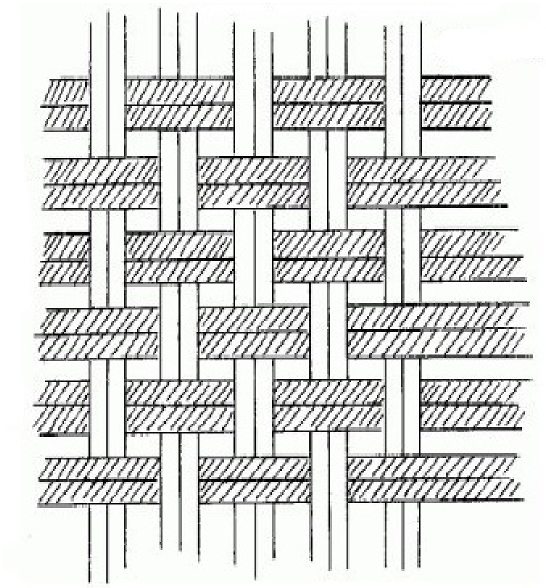

Figure 2.1: Warp and weft scheme [3]

Taking this into account, a mathematical model based on mechanics of materials has been adopted. The model is used for 3D analysis and its adapted for a 2D analysis on ABAQUS too.

2.1 Mathematical model

This chapter means to explain the mathematical model inside the theory of strength of materials used, and which are the different properties which are meant to be characterized. This mathematical model is important as it is necessary in order to understand later the damage models that will be implemented.

For most of the analysis, models are created with volumetric (3D elements). This is done to achieve the best possible approach to reality. However, sometimes is interesting to prepare first a 2D model of the part, in order to carry out a faster simulation and see if results are as expected, and if it is therefore logic and worthy to prepare later a more complex and time – consuming 3D model. 2D models are mesh with plane elements (shell elements) and the mathematical model implemented in the routine differs slightly from the one used for three dimensions ones.

For all the analysis carried out in this work, a theory of linear elasticity will be considered. This law, also known as Hooke law, establishes a linear evolution of stress when face with strain. When considering the most generic case, this means that the stiffness tensor (here called C) will be constant with the time, and will be therefore made of constants terms.

This Hooke law can be expressed as:

$$\vec{\sigma} = \overline{\overline{C}} : \vec{\epsilon} \tag{2.1}$$

Being $\overline{\overline{C}}$ a 6x6 matrix for the 3D case of stresses. Different notations can be used for $\vec{\sigma}$ as:

$$\vec{\sigma} = \{\sigma_1 \ \ \sigma_2 \ \ \sigma_3 \ \ \sigma_4 \ \ \sigma_5 \ \ \sigma_6\}^T = \{\sigma_{11} \ \ \sigma_{22} \ \ \sigma_{33} \ \ \tau_{12} \ \ \tau_{13} \ \ \tau_{23}\}^T \tag{2.2}$$

And the same happens with $\vec{\epsilon}$:

$$\vec{\epsilon} = \{\epsilon_1 \ \ \epsilon_2 \ \ \epsilon_3 \ \ \epsilon_4 \ \ \epsilon_5 \ \ \epsilon_6\}^T = \{\epsilon_{11} \ \ \epsilon_{22} \ \ \epsilon_{33} \ \ \gamma_{12} \ \ \gamma_{13} \ \ \gamma_{23}\}^T \tag{2.3}$$

It is useful to remember that :

$$\epsilon_4 = \gamma_{12} = 2\epsilon_{12} \qquad \epsilon_5 = \gamma_{13} = 2\epsilon_{23} \qquad \epsilon_6 = \gamma_{23} = 2\epsilon_{23} \tag{2.4}$$

Since it is intended to model damage and non linearities, its obvious that our final matrix will not be constant, so changes in the Hooke's law will be introduced, multiplying the terms of the constant matrix C with factors that will not be constant, obtaining therefore $\overline{\overline{C_D}}$, the stiffness damaged matrix. This will be explained later.

Composite materials belong to a group of materials called orthotropic materials. An orthotropic material properties vary along three mutually-orthogonal twofold axes of rotational symmetry at a given point. They are considered a subgroup inside anisotropic materials, as their material properties differ when measured from different directions.

Attending to the on-ply configuration explained before, the material considered will be an orthotropic material with three axes mutually perpendicular (although later some simplifications will be introduced): the one in the warp direction, the weft direction one, and the perpendicular to this plane, called stacking direction, where there is epoxy.

Attending to this the undamaged stiffness matrix will look like this:

$$\overline{\overline{C}} = \begin{bmatrix} C_{11} & C_{12} & C_{13} & 0 & 0 & 0 \\ C_{21} & C_{22} & C_{23} & 0 & 0 & 0 \\ C_{31} & C_{32} & C_{33} & 0 & 0 & 0 \\ 0 & 0 & 0 & C_{44} & 0 & 0 \\ 0 & 0 & 0 & 0 & C_{55} & 0 \\ 0 & 0 & 0 & 0 & 0 & C_{66} \end{bmatrix} \tag{2.5}$$

And will depend exclusively of these nine independent constants.

$$E_1 \quad E_2 \quad E_3 \quad \nu_{12} \quad \nu_{13} \quad \nu_{23} \quad G_{12} \quad G_{13} \quad G_{23} \tag{2.6}$$

It must be kept in mind that the following expression is always true:

$$\frac{E_i}{\nu_{ij}} = \frac{E_j}{\nu_{ji}} \tag{2.7}$$

The form of the terms will be the following:

$$\begin{gathered}
C_{11} = \frac{1 - \nu_{23}\nu_{32}}{E_2 E_3 \Delta} \\
C_{12} = \frac{\nu_{21} + \nu_{31}\nu_{23}}{E_2 E_3 \Delta} = \frac{\nu_{12} + \nu_{32}\nu_{13}}{E_1 E_3 \Delta} \\
C_{13} = \frac{\nu_{31} + \nu_{21}\nu_{32}}{E_2 E_3 \Delta} = \frac{\nu_{13} + \nu_{12}\nu_{13}}{E_1 E_2 \Delta} \\
C_{22} = \frac{1 - \nu_{13}\nu_{31}}{E_1 E_3 \Delta} \\
C_{23} = \frac{\nu_{32} + \nu_{12}\nu_{31}}{E_1 E_3 \Delta} = \frac{\nu_{23} + \nu_{21}\nu_{13}}{E_1 E_2 \Delta} \\
C_{33} = \frac{1 - \nu_{12}\nu_{21}}{E_1 E_2 \Delta} \\
C_{44} = G_{12} \\
C_{55} = G_{13} \\
C_{66} = G_{23}
\end{gathered} \tag{2.8}$$

Being Δ :

$$\Delta = \frac{1 - \nu_{12}\nu_{21} - \nu_{23}\nu_{32} - \nu_{31}\nu_{13} - 2\nu_{21}\nu_{32}\nu_{13}}{E_1 E_2 E_3} \tag{2.9}$$

1. The stiffness in the warp and weft directions are very similar and can be approximated by the same one.

   $$E_1 = E_2$$

   Due to equation 2.7, the Poisson modulus will obey to:

   $$\nu_{12} = \nu_{21}$$

2. The shear modulus in the planes 23 and 13 will be considered to be the same as they slightly differ from one to another.

   $$G_{13} = G_{23}$$

2.1.1 2D Case

In a in plane stress case, for a shell, the stresses and strains vectors will be:

$$\vec{\sigma} = \{\sigma_{11} \;\; \sigma_{22} \quad \tau_{12}\}^T \tag{2.10}$$

$$\vec{\epsilon} = \{\epsilon_{11} \;\; \epsilon_{22} \;\; \gamma_{12}\}^T \tag{2.11}$$

So the system remains like in 2.1 :

$$\vec{\sigma} = \overline{\overline{C}} : \vec{\epsilon}$$

In order to have the stiffness matrix that relates the stresses vector with the strains one, it will be necessary to carry out a static condensation of the stiffness matrix previously calculated for the 3D case.

$$\begin{bmatrix} \sigma_{11} \\ \sigma_{22} \\ \tau_{12} \end{bmatrix} = \begin{bmatrix} H_{11} & H_{12} & 0 \\ H_{21} & H_{22} & 0 \\ 0 & 0 & H_{33} \end{bmatrix} \begin{bmatrix} \epsilon_{11} \\ \epsilon_{22} \\ \gamma_{12} \end{bmatrix} \tag{2.12}$$

Operating, the elements will be the following:

$$\begin{gathered} H_{11} = C_{11} - \frac{C_{13}^2}{C_{33}} \\ H_{22} = C_{22} - \frac{C_{23}^2}{C_{33}} \\ H_{12} = C_{12} - \frac{C_{13}C_{23}}{C_{33}} \\ H_{33} = C_{44} \end{gathered} \tag{2.13}$$

Being $C_{11} \quad C_{12} \quad C_{22} \quad C_{13} \quad C_{23} \quad C_{44}$ the ones of the 3D case.

Finally, in table 2.1, values of the different parameters are presented.

Property	**Value**
E_1	17500 MPa
E_2	17500 MPa
E_3	8000 MPa
G_{12}	1900 MPa
G_{13}	1500 MPa
G_{23}	1500 MPa
ν_{12}	0.06
ν_{13}	0.06
ν_{23}	0.06

Table 2.1: Properties of the manufactured flax fibre ply

These values have been obtained through several tensile tests in each direction. However, as told, flax fibre presents non linearities during the loading phase that affect these values. Next chapter will intent to give an explanation to the reason and origin of these non linearities. Objective is not the characterisation of these values, but to create reliable damage models able to represent efficiently this behaviour presented by the flax fibre.

Chapter 3

Flax fibre non linearities

This chapter's aim is to give and explanation to the non linearities found when working with flax fibre, and that make necessary the implementation of damage models that reproduce these non linearities and changes in the stiffness matrix. To do so, is necessary to have a closer view into the morphological features of the flax as a plant.

Figure 3.1: Flax plant [4]

Flax, is a bast fibre plant, and, since it is one of the oldest agricultural crops and most widely spread, it has been largely used mainly in textile. Its applications for construction regarding the bio-composites have begun to be exploited in the last two decades.

On figure 3.2 pictures taken with the SEM (Scanning electrone microscope) are shown. In them it is possible to see the cross section of the fibres, with diameters within the 10 and 20 µm. It can be easily seen how the cross sections have not well defined borders, sometimes sharply and sometimes rounded. Outside the fibre, fibrenodes can be seen as perpendicular dislocations. These dislocations, distinctive of the flax fibre, have an origin which is not fully understood. In these regions enzymes and moisture penetrate, modifying the mechanical properties of the fibre. They have been recognized as a source of weak points in tensile tests and can be also in implicate compression failure (Mussig & Stevens, 2010) [5] .

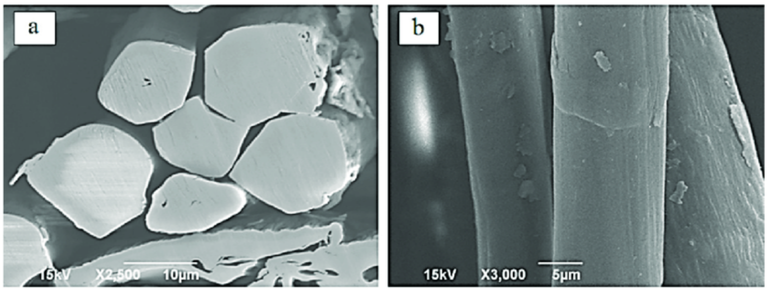

Figure 3.2: SEM pictures of a sectioned flax fibre [6]

As other natural fibres, the flax cells have a cellular wall which is the responsible for the mechanical stability. Its constitutive molecules are stiff cellulose fibril, embedded in matrix of complex macromolecules such as hemicelluloses, pectins and lignin. The cellular wall is composed of one or more layers with different thicknesses depending on the stage of development. (Mussig & Stevens, 2010)

When the flax plant reaches maximum height and shape, cells start to synthesise a new secondary wall that begins to grow in the stem. This new secondary wall, known as S2 zone, is very important and will determine final properties.

This secondary wall is thick, in comparison with the others, and in it cellulose fibrils are helix winding parallel to each other around the cell, figure 3.3.

The angle of the parallel cellulose microfibrils to the longitudinal cell axis is labeled as MFA, cellulose microfibril angle, and it greatly determines the mechanical properties. For bast fibre this angle goes from 0º to 10°, in flax fibre it is around 10°. For seed hairs fibre as cotton, MFA values round 5°-12°, while for wood fibres it can reach higher values, around 30°-45°. (Mussig & Stevens, 2010)

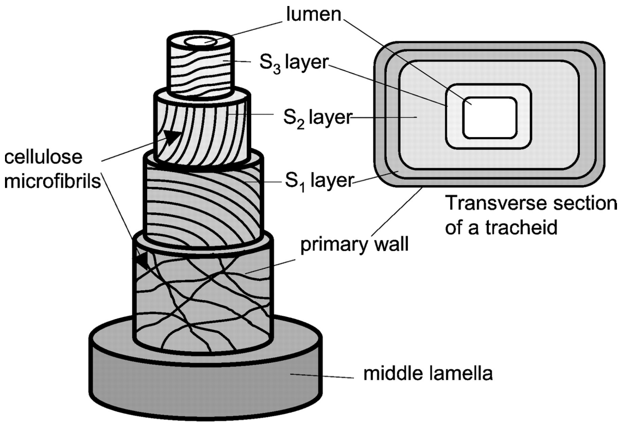

Figure 3.3: Fibre cell wall organization [5]

As a summary, it can be said that those fibres useful for the industrial application are long and cellulose-rich fibres, and are fully developed between the outer skin and the inner core of the plant stem.

In table 3.1 some of the main properties of the most common bio-fibres are shown. Values shown great variability as fibres properties are very influenced by the climate in which they have been cropped, the manufacturing process etc. As it can be seen, flax fibre properties are among the best in natural fibres and this is one of the reasons of their huge popularisation for their employment in bio composite materials.

Fibre	MFA [º]	Young's modulus [GPa]	Ultimate stress [MPa]	Density	Elongation at break %
Flax	10	27.6-160	345-1100	1.39-1.5	1.5-5
Hemp	6	30-60	199	1-1.40	-
Jute	7-9	2.7-12.6	345-1500	1.3-1.46	7-8
Soft wood	7-45	0.88	199	-	-
Sisal	1.061	9.4-24	468-640	1.35-1.45	3-7.4
Banana	1.061	3.4-32	54-789	1.3-1.35	2-7
PALF	1.061	6.26-24.6	170-635	1.44	3
Cotton	6	5.5-12.6	287-597	-	-

Table 3.1: Main bio-fibres properties (P. Asokan and others, 2012) [7]

In the following diagrams it is shown how the thickness of the cell wall layers and their cellulose fibril orientations play a dominant role in the mechanical properties, with the Young modulus increasing when density does so, and it can be seen too how the non-linear behaviour is increased with MFA.

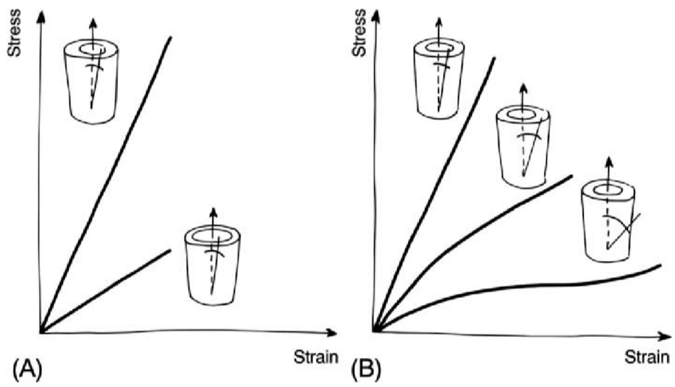

Figure 3.4: Stress–strain curves of (A) low- and high-density fibre with constant MFA and (B) fibres with different microfibril angles [5]

Fibre length is another aspect to take into account as it is responsible too for the appearance of non- linearities. When a fibre is submitted to a tensile tension, there appears a tensional flow between the fibrils and with it micro shear stresses in addition to the axial ones and consequently deformations which are responsible for the appearance of non linearities.

Finally, the last source of variability comes with the treatment given to the plies in the impregnation process with the resin, together with the curing process parameters.

This chapter is intended to be useful in order to understand why the natural fibres have in general more variability regarding their properties than the chemically-obtained fibres such as aramodic, carbon or fibreglass.

Chapter 4

Damage model

In order to characterize correctly the properties of the flax fibre composites, and regarding, as it has been explained, their nonlinear behaviour, it is necessary to introduce a correct damage modeling.

In this chapter they will be explained the different theories that have been adapted for modeling the damage, the different kinds of damages that have been considered and the elements which are needed for their correct application.

In order to conduct the tests with FEM models, ABAQUS has been chosen due to its functionality regarding the possibility of introducing subroutines in order to change the properties and behaviour of the materials. In this sense, UMAT routine has been chosen for conducting the static analysis while VUMAT is the chosen one for the dynamic tests.

4.1 Types of damages

Three different kinds of damage have been taken into account for a static analysis. These ones are the diffuse damage, the failure damage, and the viscous damage.

1. **Diffuse damage**

   The diffuse damage is a damage that degrades the stiffness matrix during the loading phase, and therefore creates the non linearities present in the curve stress-strain characteristic of the flax fibres. Although any material has a constant stiffness during loading phase, as all materials have internal imperfections that degrade the stiffness matrix, these ones are more significant in the flax fibre and lead to a much greater degradation than for example in metals. It will be seen later how the form of the curve in this loading phase can be approached by a logarithmic function.

2. **Failure damage**

   The failure damage is a failure whose mission is to define the ultimate load that leads to the fracture of the fibre or matrix. Failure is of course present in all materials, but what is not common among them is the form of the curve after the failure, which can vary. Metals are typical examples of the formation of neck sections after the tensile strength in which the section is drastically reduced but some stiffness is maintained. In flax fibre the failure form has been proven to depend on some factors related with measurable properties of the material, such as the fibre energy released rate. Failure damage evolution can be approached by an exponential form, as will be explained later.

3. **Viscous regularization**

   The third kind of damage is the viscous damage. Viscous damage is an artificial procedure, more than a damage, that has been used for stabilizing the numerical simulation in the static analysis, and that is used to ensure the convergence of the solution which is a typical issue when trying to solve problems which involved non linear effects. It has been used only in the static case and will be later explained.

4.2 Diffuse damage

Diffuse damage is the first one to act on the ply as it's a damage in charge of degrading the matrix, this is, creating the non-linear behaviour during the loading phase. As it has been said, this smoothing of the stiffness is due to the presence of fibrenodes in the flax fibre, which are perpendicular dislocations that deteriorate the mechanical properties. However, this damage does not appear straight from the beginning. In the model, a series of conditions have to be accomplished in order for this damage to be active. The damage model that has been used for programming the routine is based on the one of Ladeveze- Le Dantec model, 1992 [8].

First, in order to understand how this damage is acting, a real test conducted in the laboratory is going to be briefly explained. In this test a typical sample for a tensile test was put to test. A tensile traction test was conducted on several directions. These directions are: the direction taken as reference (0°), also called warp, the direction perpendicular to this one (90°), also called weft, and a 45° direction for the first one, in order to measure the in-plane/in-ply shear stress. As expected results are very similar for warp and weft because, as it has been said, in a fabric in-ply configuration the properties are the same in both directions due to the fact that fibre is weaved in both directions.

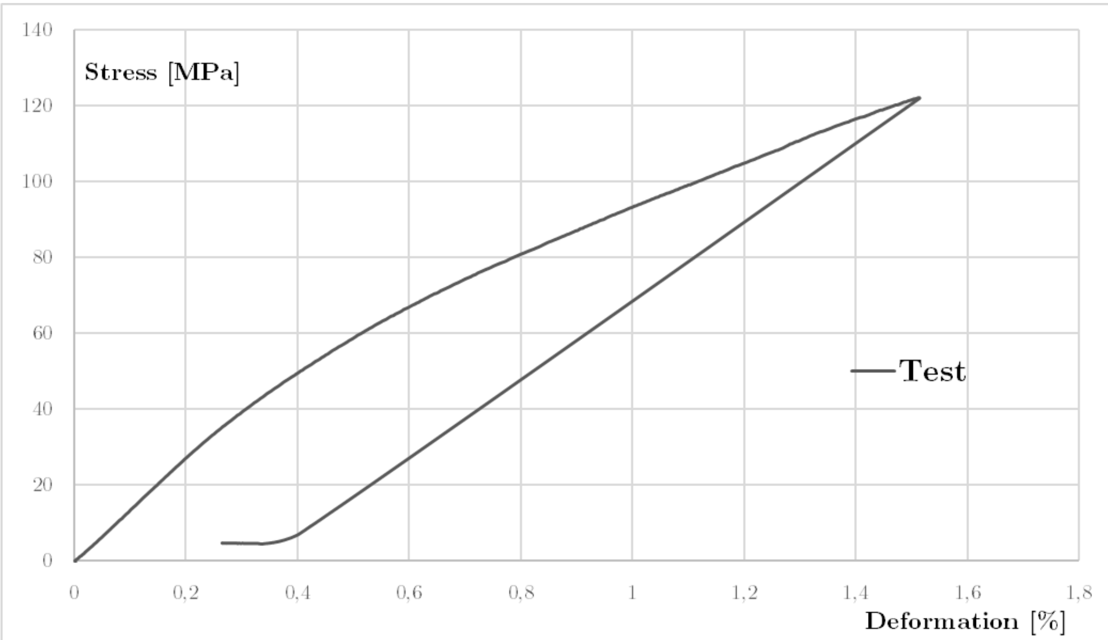

Figure 4.1: Stress- Strain plot in the warp direction

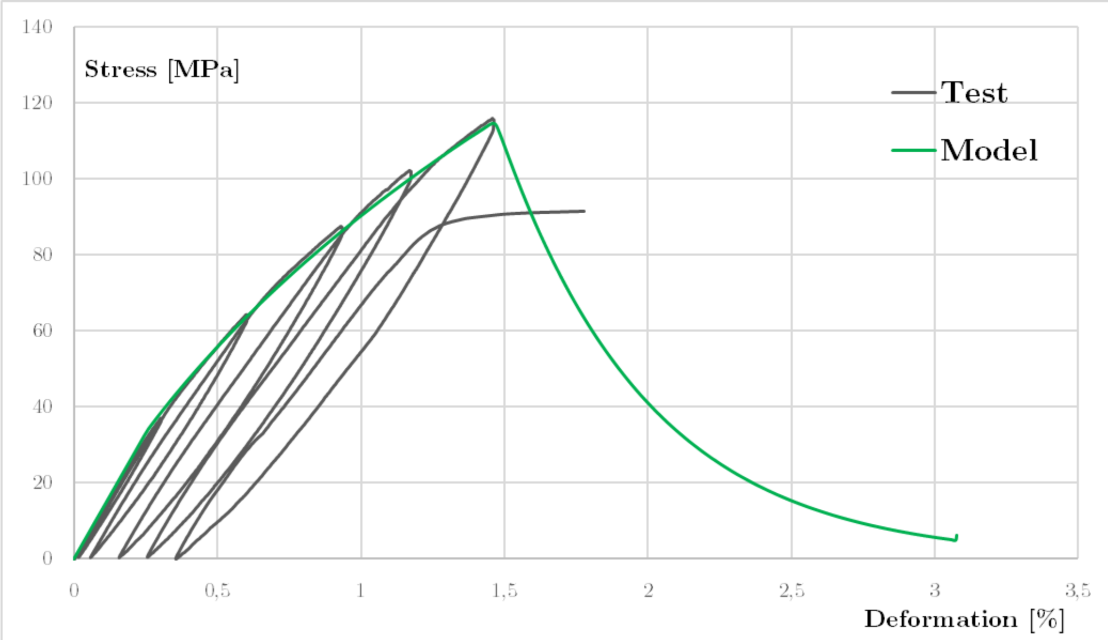

Figure 4.2: Stress- Strain plot in the weft direction

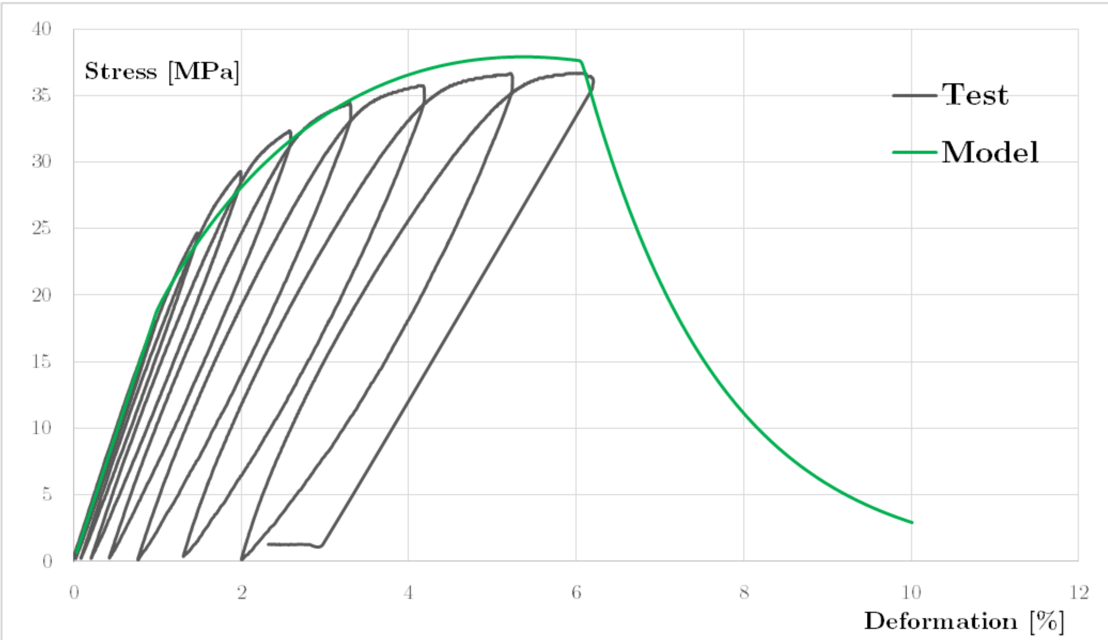

Figure 4.3: Shear tress- Strain plot in the in-plane lamina

Figure 4.1 shows the test in the warp direction, figure 4.2 the test in the weft direction, and figure 4.3 the shear stress test. In figure 4.1 there has only been one loading and unloading phase, while in figures 4.2 and 4.3 the failure was achieved through five loads and unloads cycles. The curves achieved with the final damage model are also shown in the last two in green colour.

It can be seen in the three tests, how after a small linear zone there begins a nonlinear zone which consists in a decrease in the slope that essentially reduces the stiffness. Basically this decrease in the slope can be modeled by a damage d that is going to be acting in the stiffness term in that direction in the form $\sigma = E(1-d)\epsilon$, and this damage "d" zone can be approached by a logarithmic function that is going to depend of the elastic energy together with some fitter constants in order to approach it to the curve in the tests, all this would be explained lately.

Two things can be remarked. First one is that tests have been pushed until failure of the samples, around deformations of 1.5 % for for warp and weft directions ($\epsilon_{11} = \epsilon_{22} = 0.015$) and 6 % for the shear strain in 12 plane ($\gamma_{12} = 0.06$).

Second one is that the undamaged stiffness can be calculated with the slope of the first linear zone before the initiation of the diffuse damage. This value has some variability mainly due to the negative pressure when the resine is cured in the oven or autoclave. In the tests above this value for warp and weft is around 13000 MPa, as they were cured in an oven applying a vacuum bag and therefore having a negative pressure of 1 atm, while some other samples tested register higher values due to the fact that they were cured in an autoclave where in addition to the vacuum bag an additional negative pressure is applied. In this second case the stiffness registered for the warp and weft is around 17500 MPa.

To explain how this damage has been modeled, the stress-strain plot in weft direction, is taken as example.

The load is applied with 5 charges, each one with increasing load. The stress-strain curve is the one of figure 4.2, registering therefore 5 maximums in stress, and 5 minimums in strain (the point from which each charge restarts).

The model here has been inspired by the one of P.Lavedeze & E. Le Dantec (1992). In general damage in one of the directions of the ply can be model through a term d that is going to influent in the stiffness matrix in the form:

$$E_d = E(1-d) \tag{4.1}$$

The elastic energy is:

$$Y = \frac{1}{2} E\, \epsilon^2 \tag{4.2}$$

And the stress is:

$$\sigma = E_0(1-d)\epsilon \tag{4.3}$$

Therefore Y can be expressed too as:

$$Y = \frac{1}{2} \frac{\sigma^2}{E_0(1-d)^2} \tag{4.4}$$

And the damage can be expressed as:

$$d = 1 - \frac{E_i}{E_0} \tag{4.5}$$

Being E the stiffness in that direction. What is done is registering the different stiffness modulus E in the tensile direction, calculating then as:

$$E_i = \frac{\sigma_{maximum_i}}{\epsilon_{reestart_i}}$$

And with this way five values of the damage are calculated. Then, this damage is represented in front of the square root of the elastic energy. The curve is interpolated and approached through a logarithmic function. The value of the fitting constants depends on the system of units used, which is usually different between explicit and implicit simulations. The values for creating the plot are shown in table 4.1. For this direction, the value of $E_0 = 13146 MPa$ (Although in table 2.1 another value is presented, because, as explained, this sample was cured with fewer negative pressures than the used later).

Stress [MPa]	ϵ	$E_i[GPa]$	d_i	$\sqrt{Y}$
36.98	0.3	12326	0.06236	0.24323
64.2	0.607	10576	0.19548	0.49213
87.4	0.927	9428	0.28283	0.75157
102.1	1.17	8726	0.33621	0.94858
115.7	1.4587	7931	0.39667	1.12265

Table 4.1: Values for creating the diffuse damage tendency curve in the weft direction

With the values of the table 4.1 the curve of the figure 4.4 can be plotted. With these values it is possible to get a logarithmic tendency curve, which is the one that approaches better to the curve, and get the law for the evolution of the damage that is going to be used, written in figure 4.4 too.

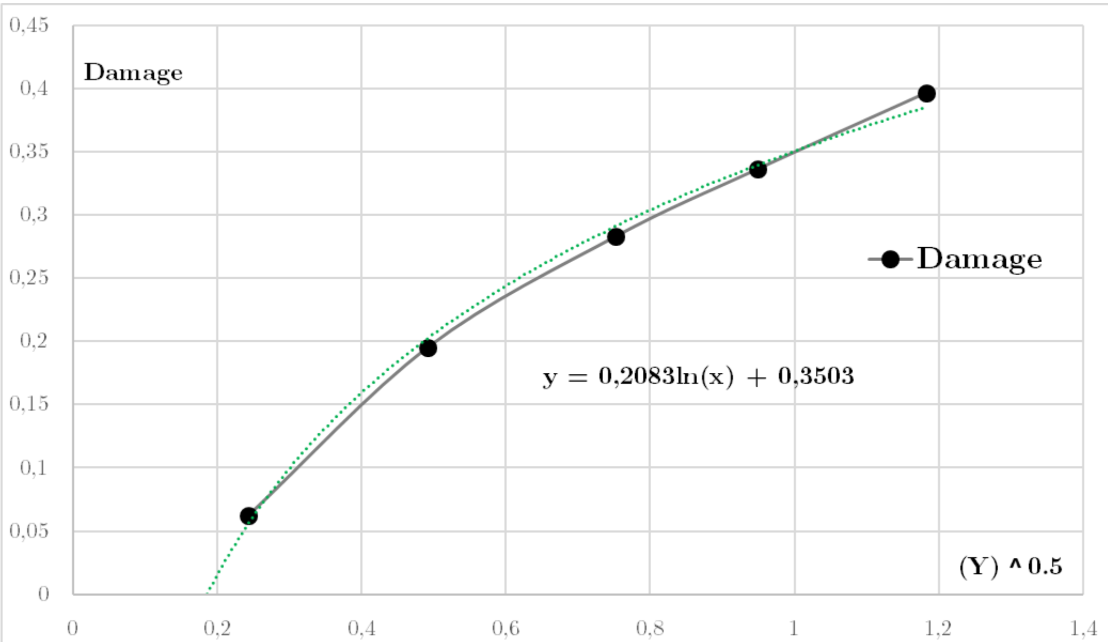

Figure 4.4: Evolution of damage and logarithmic tendency curve for the weft direction

This evolution of damage is valid whenever the strain is comprised between a minimum and a maximum. The minimum value of the strain can be obtained through the elastic energy when the value of the damage is zero, while the maximum value is taken at the point in the test where the failure damage is initiated. This exact process is repeated for the other two main directions of the stress, the warp and the in-ply shear.

As a summary, for the diffuse damage model, there are three damage evolution variables present that are going to degrade the stiffness matrix. They are three as each one of them will act in a direction of the space, one for the warp direction, one for the weft direction, and one for the in-ply shear direction.

The damage activation is based on a threshold for the damage value. If same of the following relations is accomplished, then there will start to be damage in that direction. These relations or thresholds are:

$$\begin{aligned} FD_1 &= \frac{1}{2}\epsilon_1^2 C_1 > FD_{01} \\ FD_2 &= \frac{1}{2}\epsilon_2^2 C_2 > FD_{02} \\ FD_3 &= \frac{1}{2}\gamma_{12}^2 C_{44} > FD_{03} \end{aligned} \tag{4.6}$$

FD_{01} , FD_{02} and FD_{03} can be seen as the minimum values of strain energy above which the diffuse damage starts to act. In fact, as it has been seen, the first thing to do is to interpolate the logarithmic function and after these minimum thresholds can be obtained.

After that, the damaged is computed (if the threshold value is exceeded in that direction) as:

$$\begin{aligned} D_{d1} &= c_0 + c_1\, ln(\sqrt{FD_1}) \\ D_{d2} &= c_2 + c_3\, ln(\sqrt{FD_2}) \\ D_{d3} &= c_4 + c_5\, ln(\sqrt{FD_3}) \end{aligned} \tag{4.7}$$

As has been said, c_0 , c_1 , c_2 , c_3 , c_4 , c_5 are fitting constants whose value depends on the units used, something that will differ between static and dynamic analysis.

And the damaged stiffness matrix $\overline{\overline{C_D}}$ when considering just diffuse damage is the one shown below:

$$\begin{bmatrix}(1-D_{d1})C_{11} & (1-D_{d2})C_{12} & (1-D_{d2})C_{13} & 0 & 0 & 0\\ C_{21} & (1-D_{d2})C_{22} & (1-D_{d2})C_{23} & 0 & 0 & 0\\ C_{31} & C_{32} & C_{33} & 0 & 0 & 0\\ 0 & 0 & 0 & (1-D_{d3})C_{44} & 0 & 0\\ 0 & 0 & 0 & 0 & C_{55} & 0\\ 0 & 0 & 0 & 0 & 0 & C_{66}\end{bmatrix}$$

Two things must be said regarding the behaviour of the diffuse damage. First, the diffuse damage has memory, this is, even if strain is reduced, the value of the damage does not do so, and therefore the stiffness lost in one direction cannot be recover. Second, when the strain reaches the point in which the failure begins, the diffuse damage does not increase more even if the strain do so.

4.3 Failure damage

The failure damage is the one in charge of defining the ultimate load which will lead to the break and failure of the ply. Model is based on the one implemented by Linde et al, 2004 [9]. Original author considered that material was damaged with two variables, which represented the damage in the fibre and in matrix. Here, model has been adapted, and there will be three different kinds of damages, for warp direction, weft direction and one for failure of the matrix in shear. Criteria for initiation of damage is given by the following equations. Once again, if some of the relations is true, then the damage will start in that direction.

$$
\begin{aligned}
FF_1 &= \sqrt{\frac{\epsilon_1^2}{\tilde{\epsilon}_{T1}\tilde{\epsilon}_{C1}} + \frac{\epsilon_1(\tilde{\epsilon}_{C1} - \tilde{\epsilon}_{T1})}{\tilde{\epsilon}_{T1}\tilde{\epsilon}_{C1}}} > 1 \\
FF_2 &= \sqrt{\frac{\epsilon_2^2}{\tilde{\epsilon}_{T2}\tilde{\epsilon}_{C2}} + \frac{\epsilon_2(\tilde{\epsilon}_{C2} - \tilde{\epsilon}_{T2})}{\tilde{\epsilon}_{T2}\tilde{\epsilon}_{C2}}} > 1 \\
FF_3 &= \frac{\gamma_{12}}{\tilde{\gamma_{12}}} > 1
\end{aligned}
\tag{4.8}
$$

Where $\tilde{\epsilon}_{T1}$, $\tilde{\epsilon}_{C1}$, $\tilde{\epsilon}_{T2}$, $\tilde{\epsilon}_{C2}$, $\tilde{\gamma}$ are the strains at which failure occurs, "1" & "2" stands for warp and weft directions, and "T" & "C" for traction and compression. Meanwhile, $\tilde{\gamma}$ is the in-plane shear strain in which failure occurs but for shear stress. While the criteria for warp and weft is a bit more complex, following the model of Linde et al, 2004, the one written for the failure in shear just implies that when the shear strain is above the one of failure, failure damage starts. The damage, when activated, will take the form :

$$
\begin{aligned}
D_{f1} &= 1 - \frac{e^{(1-FF_1)\frac{C_{11}\tilde{\epsilon}_{T1}^2 CELENT}{G_{fib}}}}{FF_1} \\
D_{f2} &= 1 - \frac{e^{(1-FF_2)\frac{C_{22}\tilde{\epsilon}_{T2}^2 CELENT}{G_{fib}}}}{FF_2} \\
D_{f3} &= 1 - \frac{e^{(1-FF_3)\frac{C_{44}\tilde{\gamma_{12}}^2 CELENT}{G_{mat}}}}{FF_3}
\end{aligned}
\tag{4.9}
$$

The curve has an exponential form to represent the drop of the curve after the failure. How this curve has been model can be seen in figures 4.2 and 4.3, in green, which represents the plot achieved with the numeric model. This is also valid for 4.1 but this curve has not been plotted here.

Two magnitudes that appear in the evolution of damage must be explained.

1. **"G" energy released rate**

   The energy released rate represents the released energy when a crack advances per unit of new area created. It will be explained later, as a whole experiment was designed in order to characterise it, but it is a very important magnitude and plays a key role in the fracture of mechanics, and it is important to have a correct value in order to create a reliable damage model. As a composite material is being considered, this magnitude is not the same in all the directions, but there is one for the direction of the fibre, this is, warp and weft direction, and another one for the matrix, in the shear failure, as can be found in Linde et al, 2004. The values used are shown in table 4.2.

Magnitude	**Value** $\frac{N}{mm}$
G_{fib}	10
G_{mat}	0.5

Table 4.2: Values used for the energy released rates

2. **Celent**

   Parameter "*CELENT*" means to represent the characteristic length of the element. In an ideal case the length used should be the one of the element which is perpendicular to the fibre direction and to the stacking direction. However, ABAQUS gives in a length by default that does not match with this one, but instead, is the cubic root of the volume in a 3D element or the square root of the surface in a 2D one.

Obviously, best strategy for getting the correct *CELENT* from ABAQUS is to mesh all the models with perfect cubic elements, where the cubic root is equal to any side. However, this is generally not possible, since as will be discussed later, there are parts of the model with very small thicknesses which need a denser mesh, but have very large lengths, or are connected with other parts that do have large lengths, and therefore they cannot be meshed with the same element size in the two directions, because if so there would be a lot of elements and computation time would increase drastically whereas the precision would barely change.

As a brief summary, a small code was programmed in order to get a more accurate *CELENT* that the one given by ABAQUS. To do so, *CELENT* was calculated through a small algorithm with the coordinates of the nodes of the element. The problem was that the only way found to give these lengths (one per element) after to ABAQUS, was to write them in a .txt file, so that the routine could after read them. However, for this to be possible, computations should be run with just one core, otherwise the correct order was not kept, as computation with several cores (parallel computation) divides the model and calculates magnitudes at the same time, including the reading from this .txt file. Therefore this algorithm was only used in the model prepared for the study of the energy released rate, which will be described later, as this model was faster to compute and computation with just one core was affordable in terms of time. Further about *CELENT* calculus can be seen in appendix A.

So in case there was damage in all directions, and considering just the failure damage, the damaged stiffness matrix $\overline{\overline{C_D}}$ would have the form:

$$\begin{bmatrix} (1-\mathrm{D}_{f1})C_{11} & (1-\mathrm{D}_{f1})(1\text{-}D_{f2})C_{12} & (1-\mathrm{D}_{f1})C_{13} & 0 & 0 & 0 \\ \mathrm{C}_{21} & (1-\mathrm{D}_{f2})C_{22} & (1-\mathrm{D}_{f3})C_{23} & 0 & 0 & 0 \\ \mathrm{C}_{31} & \mathrm{C}_{32} & \mathrm{C}_{33} & 0 & 0 & 0 \\ 0 & 0 & 0 & (1-\mathrm{D}_{f1})(1\text{-}D_{f2})(1\text{-}D_{f3})C_{44} & 0 & 0 \\ 0 & 0 & 0 & 0 & \mathrm{C}_{55} & 0 \\ 0 & 0 & 0 & 0 & 0 & \mathrm{C}_{66} \end{bmatrix}$$

4.4 Viscous regularization

Viscous regularization is a procedure used for stabilizing the numerical simulation based on an artificial damping (Bak M., n.d.) [10]. Finite element analysis, like any numerical procedure, can exhibit convergence difficulties when trying to solve problems involving nonlinear effects. Often, the convergence issues in a structural analysis come from a sudden change in stiffness, such as might occur when a constitutive law has a sudden change in the slope of the stress-strain curve. This is what is exactly happening in the case studied. There is a linear behavior, due to the constant elements presented in the stiffness matrix, until the damage initiation criteria is accomplished, and the damage starts, causing a change in the slope (a change in the Jacobian matrix). In fact this happens twice, at the beginning of the diffuse damage and of course at the beginning of the failure.

A particular example given by Bak of a sudden change in stiffness that causes convergence difficulties is modeling delamination using the bilinear cohesive zone material law. This kind of law is very similar to the one used in the routine for the failure damage (and in fact it is the one used in one of the two models that will be analyzed in the chapter were energy released rate is discussed) and can be used for illustrate how is viscous regularization achieved. In this law, if it is represented the interface traction with the interface separation, the initial slope represents the linear elastic material behavior of the interface. When the peak traction is achieved at a certain separation, damage is initiated, and the traction-separation response is represented by a downward slope. The stress-strain curve of this behaviour can be seen in figure 4.5.

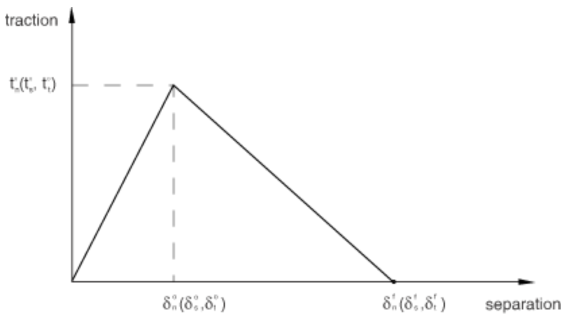

Figure 4.5: Stress-strain curve in a cohesive zone material law [11]

This softening can eventually lead to the maximum separation, at which point the interface is failed and can open freely. The bilinear cohesive zone law uses a damage parameter (d) to define the current state of the interface. At damage initiation , damage is zero, and as the separation increases, the damage will increase until it reaches a maximum value of one at failure . At any point on the softening slope, the reduced stiffness of the damaged interface is equal to $(1-d)K$, where K is the elastic undamaged stiffness of the interface. Although the bilinear cohesive zone model can be a useful tool in modeling delamination behavior, the sudden change of stiffness at the peak, and the subsequent negative softening slope of the bilinear law, causes convergence problems.

It is at this point when according to Bak, viscous regularization appears to provide stability to the numerical solution. In viscous regularization, the traction-separation law allows stresses to be outside the limits set by the law. This causes the tangent stiffness matrix of the softening material to be positive for sufficiently small time increments.

The value of the viscous damage (d_v) can be calculated from the current damage (d), the viscosity parameter, and the time step used in the analysis (d_t). The viscous damage value is then substituted for the regular damage value to calculate updated tractions, and is also used to update the tangent stiffness matrix. With a small value of the viscosity parameter η , the rate of convergence is improved without compromising the results. In addition, the viscous energy dissipation is usually available as a result quantity so that the analyst can compare to the strain energy to verify that this damping procedure is not adding artificial stiffness to the system.

The larger values of viscosity over-estimate the positive tangent stiffness effect, since it is expected that the bilinear interface law behavior will show a sharp peak at damage initiation. Guidelines for verifying a valid solution would include further reduction of the viscosity value until the change in response is insignificant, and reviewing the viscous energy dissipation to determine if it is a negligible percentage of the strain energy in the system. As with any numerical damping scheme, the lower the viscosity value, the more accurate the results, the lower the viscous energy, but the longer the analysis run time (Bak M., n.d.).

In our case the law implemented for the viscous regularization is the following:

$$d^v_{t+\Delta t} = \frac{\Delta t}{\eta + \Delta t} d_{t+\Delta t} + \frac{\eta}{\eta + \Delta t} d_t \tag{4.10}$$

This viscous is applied to both failure and diffuse damage.This viscous regularization was implemented as in a previous version of the routine the damages were not well defined and the Jacobian had not been calculated, but estimated, and therefore models run with the routine present convergence problems. Although later the Jacobian was analytically- calculated and implemented in the routine, and therefore the convergence of the solution suffered a great improvement, it was decided to keep the viscous regularization with very low values of η that maintain convergence stability and do not barely change the response.

4.5 Final damaged matrix and input properties

At this point it can be presented the final stiffness matrix $\overline{\overline{C_D}}$ if all the damages where acting at the same time, the three of the diffuse damage and the three of the failure one, after having been calculated with the viscous regularization.

$$\begin{bmatrix} (1-D_{f1})(1-D_{d1})C_{11} & (1-D_{f1})(1-D_{f2})(1-D_{d2})C_{12} & (1-D_{f1})(1-D_{d2})C_{13} & 0 & 0 & 0 \\ C_{21} & (1-D_{f2})(1-D_{d2})C_{22} & (1-D_{f3})(1-D_{d2})C_{23} & 0 & 0 & 0 \\ C_{31} & C_{32} & C_{33} & 0 & 0 & 0 \\ 0 & 0 & 0 & (1-D_{f1})(1-D_{f2})(1-D_{f3})(1-D_{d3})C_{44} & 0 & 0 \\ 0 & 0 & 0 & 0 & C_{55} & 0 \\ 0 & 0 & 0 & 0 & 0 & C_{66} \end{bmatrix}$$

It must also be explained how are the values involved in the calculus of the damaged stiffness matrix (and its differentiated matrix, the Jacobian) given to ABAQUS and which are the values that have been selected.

The values needed for the calculus of C_d and for its Jacobian, are all the three stiffness, E_1 , E_2 and E_3 , the three shear modulus G_{12} , G_{13} and G_{23} , and the three poisson modulus ν_{12} , ν_{13} and ν_{23}. Their values can be found on table 2.1. Values of the energy released rates for fibre and matrix are also necessary, they can be found in this chapter in table 4.2. To continue, the values for the strains at failure are also necessary $\tilde{\epsilon}_{T1}$, $\tilde{\epsilon}_{C1}$, $\tilde{\epsilon}_{T2}$, $\tilde{\epsilon}_{C2}$, $\tilde{\gamma}$, the values used are shown in table 4.3. These values have been selected as they are the ones in which failure is given, what can be seen in figures 4.1, 4.3 and 4.2. Values for compression have been estimated similar to the ones in traction, so the same value is used. The final parameter is η , used for the viscous regularization and which is used in implicit analysis. For this analysis the value used was $\eta = 0.001$.

All these parameters are directly introduced into ABAQUS through the ABAQUS model, in the definition of the material through the properties vector. Subroutines UMAT and VUMAT are then given this vector by ABAQUS and read all the values for the calculus of C_d and its Jacobian matrix. It must also be said that the system of units is not the same in implicit and explicit analysis and therefore the units of all these parameters must be adapted depending on the kind of simulation and the subroutine that is being used.

Magnitude	**Value**
$\tilde{\epsilon}_{T1}$	0.0145
$\tilde{\epsilon}_{C1}$	0.0145
$\tilde{\epsilon}_{T2}$	0.0145
$\tilde{\epsilon}_{C2}$	0.0145
$\tilde{\gamma}$	0.06

Table 4.3: Values used for the strains at failure

To end this chapter, it must be said that the procedure followed to calculated the jacobian matrix of this final damaged stiffness matrix C_d , has been exposed in appendix B.

Chapter 5

Static analysis

This chapter is intended to explain the static analysis carried out, necessary in order to model the behaviour and damage when the flax fibre panels are submitted to static loads.

To begin with, a summary of how does the UMAT routine works will be done. This routine, together with VUMAT, are the two given by ABAQUS in order to run simulations introducing the "User-defined mechanical material behaviour" concept. UMAT is used for implicit analysis, while VUMAT is used for explicit analysis, and it has been the one selected in order to simulate the damage in the bio composite material.

To continue, the three point bending test will be introduced. This test was the chosen one in order to compare the results between a real model and a model prepared in ABAQUS for the static load case. The real experiment together with the one carried out in ABAQUS will be explained. Finally, the results of the two will be compared in order to evaluate the degree of reliability of the model.

Finally, the fibre energy released test will be explained too. This test was simulated in ABAQUS, where several models where run. Real test was intended to be done too, but it was not possible in the end. The purpose is to measure and characterise the fibre energy released rate, a magnitude that plays an important role in the failure damage model.

5.1 UMAT routine

During the next section, it will be explained how does the subroutine UMAT works through a brief explanation and scheme. It is important to explain who does the routine works as a lot of time has been spent in its writing in order to obtain simulations with results in compliance to those of the real tests. Some of the following notes have been summarised from [12].

UMAT subroutine is one of the subroutines given by ABAQUS in order to enlarge the capacities and allow the user to perform more precise and control simulations. UMAT and VUMAT are the subroutines proportioned to use when none of the existing material models included in the ABAQUS material library accurately represents the behavior of the material to be modeled. As a summary, UMAT allows the user to define the mechanical behaviour of the material, by defining the stiffness matrix, together with its Jacobian matrix, in order to perform non linear analysis. In general, UMAT and VUMAT interfaces make it possible to define any (proprietary) constitutive model of arbitrary complexity.

The Abaqus routines can be written in Fortran, C and C++, although the most used language is Fortran and that is why it has been the chosen one.

For static analysis, a step is normally defined for every load case. The step has therefore associated a list of loads and boundary conditions. It has also associated a time, although this time is not important in static analysis, as it does not have any relationship with the real physical time. Each step is composed of a number of increments. In each increment there is therefore an increment in the loads, and inside each increment there will be an iteration in which the static equilibrium will be tried to be achieved within the increments given. If equilibrium is not achieved, then another iteration within the same increment will take place and a new increments for the loads will be defined, these ones smaller than in the previous iteration. Overwhelming the maximum number of iterations for each increment is, for example, one of the cases of abortion of the analysis, as convergence is considered not to be achieved.

In UMAT a series of variables are passed in to the routine by ABAQUS. In the routine new variables are calculated, using some of these, and then are passed back to ABAQUS in order to perform the calculus.

Between the variables passed in, the main one is the strain vector, which is passed through an array that contains the total strains at the beginning of the increment, and another array that contains the strain increments in the iteration.

After this, a series of variables must be defined inside the routine in order to be passed back. As it has been said the most important one is the array of stresses, which is passed in as the stress tensor at the beginning of the increment and must be updated in this routine to be the stress tensor at the end of the increment.

Both UMAT and VUMAT require a proper definition of the constitutive equation, which requires the explicit definition of stress (Cauchy stress for large-strain applications).

It is necessary to transform the constitutive rate equation into an incremental equation, using a suitable integration procedure, in general:

- Forward Euler (explicit integration)
- Backward Euler (implicit integration)

The other important variable, in addition to the stress, that is necessary to calculate in ABAQUS/Standard UMAT is the Jacobian. For small-deformation problems (e.g., linear elasticity) or large-deformation problems with small volume changes (e.g., metal plasticity), the consistent Jacobian is

$$J = \frac{\partial \triangle \sigma}{\partial \triangle \epsilon}$$

where $\triangle\sigma$ is the increment in (Cauchy) stress and is the increment in strain. (In finite-strain problems, is an approximation to the logarithmic strain.)

Furthermore, it is likely to require the solution-dependent state variables, which are variables of interest associated to each point and from which is interesting to have information at the end of the analysis; i.e. the value of each damage.

Solution-dependent state variables (SDVs) are values that can be defined to evolve with the solution of an analysis. It is the user's responsibility to calculate the evolution of the SDVs within the subroutine; ABAQUS just stores the variables for the user subroutine.

Space must be allocated to store each of the solution-dependent state variables defined in a user subroutine.

Finally it can also be returned to ABAQUS the SSE, SPD, SCD, the specific elastic strain energy, plastic dissipation, and creep dissipation, respectively. They have no effect on the solution, except that they are used for energy output.

As a summary:

The following quantities are available in UMAT:

- Stress, strain, and SDVs at the start of the increment
- Strain increment, rotation increment, and deformation gradient at the start and end of the increment
- Total and incremental values of time, temperature, and user-defined field variables
- Material constants, material point position, and a characteristic element length
- Element,integration point,and composite layer number(for shells and layered solids)
- Current step and increment numbers

The following quantities must be defined:

- Stress
- SDVs
- Material Jacobian

The following variables may be defined:

- Strain energy, plastic dissipation, and "creep" dissipation
- Suggested new (reduced) time increment

It is important to say that ABAQUS runs the routine in order, first once for each integration point (also called Gauss point) inside an element, and then for all the elements.

In the next page, figure 5.1, a simple scheme of the functioning of the routine is shown.

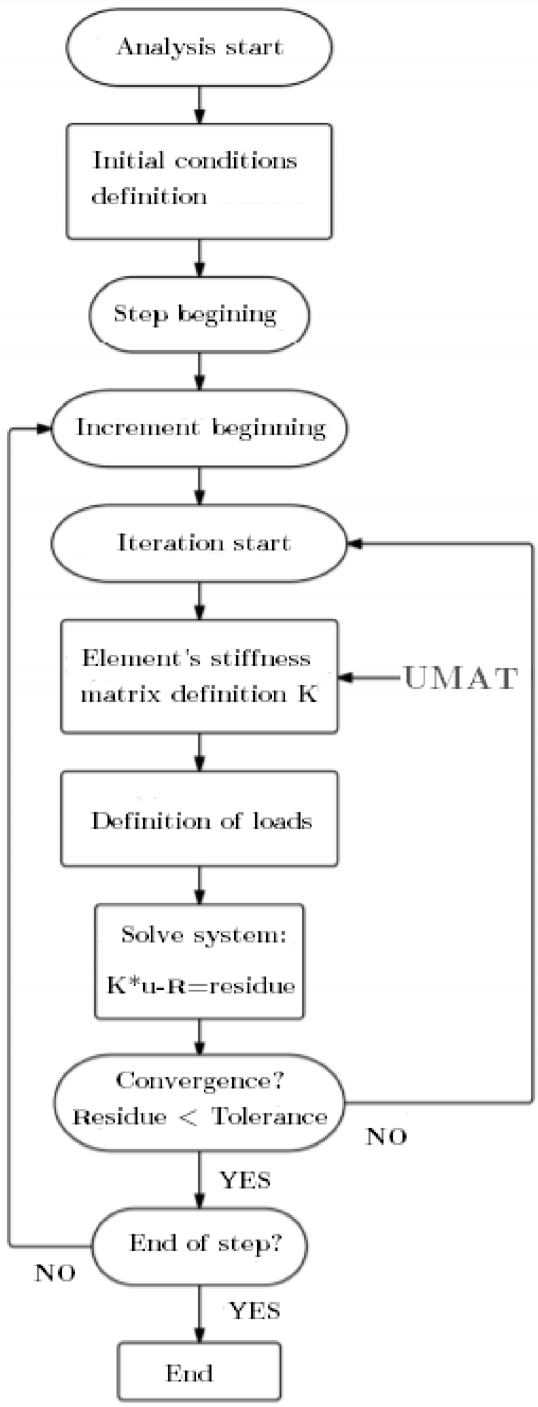

Figure 5.1: UMAT Scheme

Criteria for the stress and strain vector used in UMAT can be seen below. This is important when coding and as will be seen later, criteria for these two vectors differs from UMAT to VUMAT.

$$\vec{\epsilon} = [\epsilon_{11} \quad \epsilon_{22} \quad \epsilon_{33} \quad \gamma_{12} \quad \gamma_{13} \quad \gamma_{23}]$$

$$\vec{\sigma} = [\sigma_{11} \quad \sigma_{22} \quad \sigma_{33} \quad \tau_{12} \quad \tau_{13} \quad \tau_{23}]$$

Finally in table 6.1 the system of units used for the implicit analysis is given. It is important to remind that as almost all FEM programs, ABAQUS has not built-in dimensions, and it must be ensured that work is done with all magnitudes in consistent units. International system of units or multiples from this one are strongly recommended. Obviously the parameters that must be read from ABAQUS by UMAT, which were discussed at the end of chapter 4, must respect the chosen system of units.

Quantity	**Unit**
Length	mm
Force	N
Mass	ton
Time	s
Stress	MPa
Energy	N · mm (mJ)
Density	ton/mm^3

Table 5.1: System of units used for implicit analysis

5.2 Three Point Bending Test

5.2.1 Introduction

The three point bend test is a classical experiment in mechanics, for characterizing the modulus of elasticity in bending E_f flexural stress σ_f flexural strain ϵ_f and the flexural stress–strain response for a material in the shape of a beam. This test is performed on a universal testing machine (tensile testing machine or tensile tester) where the material is laid horizontally over two points of contact and with a force that is applied to the top through one or two points (this would be a four point bending test) of contact.Force is applied until the fail of the sample occurs (Zweben et. al, 1979) [13].

The main advantage of a three-point flexural test is the ease of the specimen preparation and testing, as it is more affordable than a tensile test. This is the main reason why this was the chosen test for the static case. However, this method has also some disadvantages: the results of the testing method are sensitive to specimen and loading geometry and strain rate (Zweben et. al).

The ultimate goal of the three point bending test is the plot of the applied load with the displacement. Assuming that the lower elements that support the sample (in this test they are two cylinders) are fixed, then the load is the one that is applied in the upper element (in this test this element has a rectangular shape), and the displacement is the one of a point of this element (assuming that it can be model as rigid, since its Young modulus is several times higher than the one of the material tested). This plot has some similarities to the one of the uni-axial stress-strain plot in any direction, slope will be linear until a point, where it will begin to decrease (this will mean that diffuse damage has been initiated), and after a maximum (which represents a global failure of the sample), slope will drop with the shape of a sort of exponential function.

The three point bending test has been performed according to ASTM C393 / C393M-16, Standard Test Method for Core Shear Properties of Sandwich Constructions by Beam Flexure, [14]. A scheme of the three point bending test is shown in figure 5.2 . The main parameters taken in the test are shown in table 5.2.

Load cell	10 kN
Displacement measurement	LVDT
Velocity	6 mm/min
Sample dimension	75 x 200 x 12 mm
Contact	10 mm rigid barr

Table 5.2: Three point bending test parameters

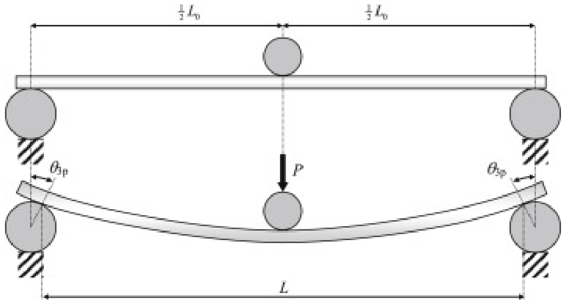

Figure 5.2: Three point bending test scheme [15]

According to ASTM Standard, it's possible to calculate the core shear ultimate stress $\tau_{ultimate}$, core shear yield stress τ_{yield}, and the facing stress σ_{facing}, through the equations:

$$\tau_{ultimate} = \frac{P_{max}}{(d+c)b}$$

$$\tau_{yield} = \frac{P_{yield}}{(d+c)b}$$

$$\sigma facing = \frac{P_{max}}{(d+c)b}$$

Where:

- t = facing thickness
- c = core thickness
- d = sandwich thickness
- b = sandwich width

The model which has been tested for this experiment, can be seen in figure 5.3. It consist on two skins with a corrugated section between them. It is of course made of flax fibre and epoxy plies. More detailed geometric aspects of the model will be shown in next chapter, where the FEM model will be introduced.

The results for this model test are shown below, in table 5.3.

P_{max} [N]	$\tau_{ultimate}$ [MPa]	σ_{facing} [MPa]	**Bending Stiffness [N/mm].**
2040	174	1.27	577

Table 5.3: Values for the test

5.2.2 FEM model

This subsection is intended to present the model which was prepared in ABAQUS in order to simulate the three point bending test carried out. Showing the FEM model will also be a way to introduce the geometry and characteristics of the real model and also some test parameters. The real model was built with some measure specifications, regarding the length, width and the geometry and measures of the cross section and those have been the pursued when creating the FEM model in ABAQUS. This model has been meshed with C3D8R brick elements.

The model tested consist on a corrugated panel, with a cross-section "W" shape, which can also be called omega panel, and which is between two flat skins. Some images of the model can be seen in figures 5.3, 5.4 and 5.4. Figure 5.3 shows a general view in order to have an idea of the configuration, while 5.4 shows again a general view but without the upper skin, and figure 5.5 shown a lateral view in order to see better the cross- section.

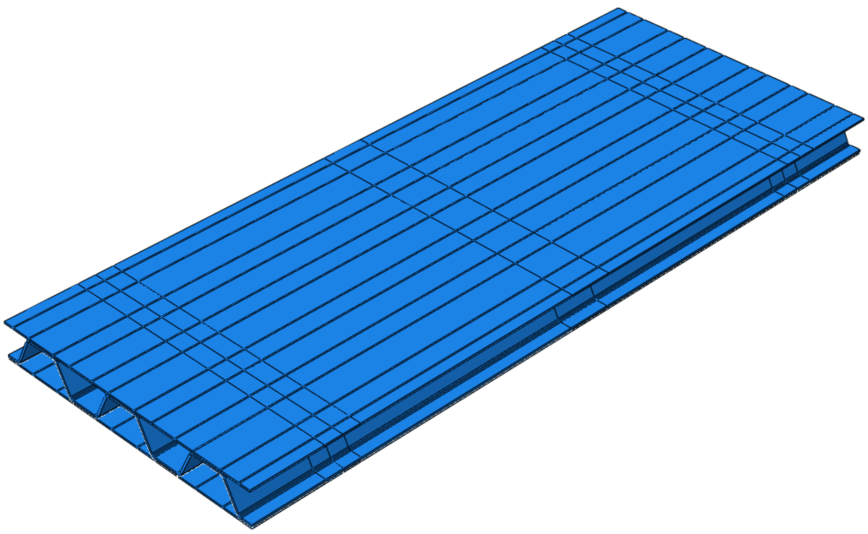

Figure 5.3: General view of the FEM model for the 3 point bending test

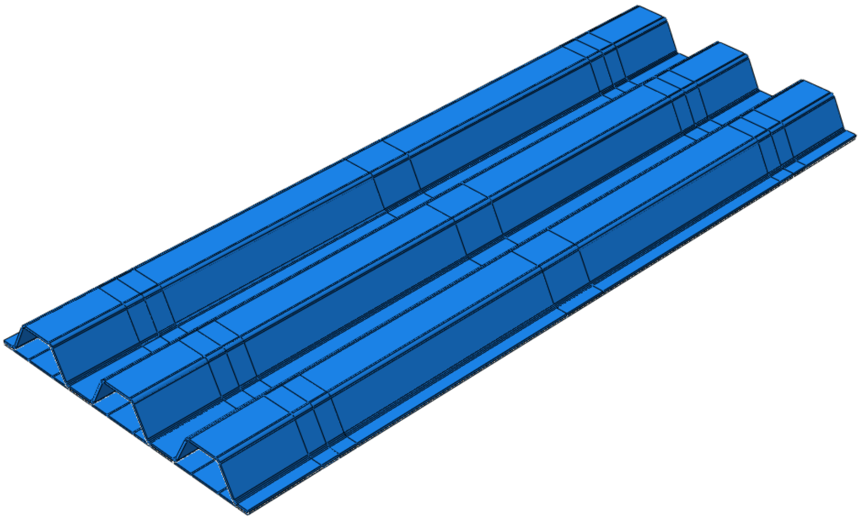

Figure 5.4: View of FEM model without upper skin

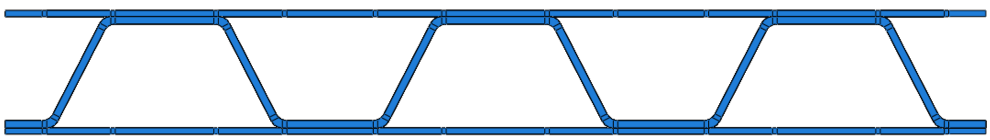

Figure 5.5: View of the cross- section of the FEM model

Main measures of the model are shown in table 6.4.

Measure]	**Value [mm]**
Length	200
Width	80
Height	10.1
Skin thickness	0.5
Corrugated panel thickness	0.6

Table 5.4: Main measures of the three point bending test model

Figure 5.6 shows the distance between the elements (two cylinders and a rectangle) that are used to create the bending during the test. Dimensions of these elements are also shown. In the upper element (the rectangle) there were introduced 1 mm fillet radius in order to smooth the stresses that can appear in the contact when there are not round corners. As told before, this rectangle and the cylinders were meshed as rigid since their stiffness is several times the one of the panel.

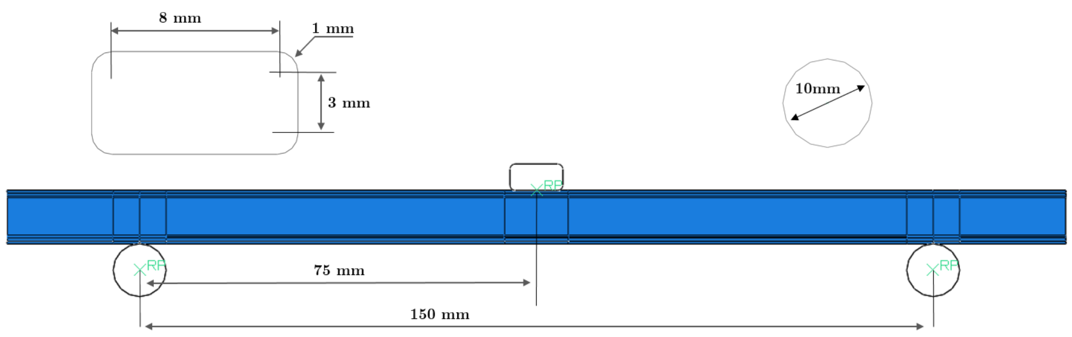

Figure 5.6: Main measures of the three point bending test

Meshing

Meshing is one of the most critical parts of the pre-processing of the design. The mesh is the degree of approximation that the model has with reality. The denser the mesh, the closer it is to reality. However, a very dense mesh will also need a more powerful computer to be able to run the analysis. In addition, putting a very large number of elements, this is, making a very dense mesh, does not necessarily mean that this mesh is good, and can become a useless way of consuming resources. It is possible to obtain very truthful results with a not very dense but well done mesh, and that is exactly what it is intended (Dueñas, 2014) [16].

In order for a mesh to be considered as good, basically three things should be tried to be achieved.

1. Have a structured mesh. Structured meshes are those formed by a set of nodes (or control volumes) that can be uniquely identified by a group of ordered indexes (i, j, k) in 3D or (i, j) in 2D.

2. Elements with good characteristics. In order to do so, two aptitudes will be remarked.

   - First, a good relationship between the proportions of the sides of the elements should be achieved. The less disproportionate they are the better. To measure this disproportion, there exists in all FEM programs what is called the "Aspect Ratio". The exact definition of the aspect ratio is defined for a four-sided element as the ratio between the maximum semi-sum of two opposite sides and the semi-sum of the other two opposite sides. This parameter should be tried be kept under 5, which in a rectangular element means that one side cannot be 5 times larger than the other. Elements must be therefore made as square as possible.
   - The other factor to watch out is related to the angles between the sides of the elements, and that is distortion. An undistorted element will be a square or a perfect rectangle with all 4 angles at 90 degrees, while a very distorted element will have irregular angles. To do this FEM programs normally present some sort of "Jacobian" tool, which analyzes the distortion of the elements by measuring their Jacobian, and colors them with a color scale according to that value. If the distortion of the elements in an area is large, poor quality results can be produced locally.

   Is important to be careful since if the excessively disproportionate or distorted elements are in a non-critical area, the false results can stop instead of spreading, but if these elements are located in a critical area, the results can affect the whole model and a good approximation to reality would not be achieved.

3. At the edge of a joint between two surfaces, the nodes of one and the other must coincide, that is, the side of an element that is on the edge must belong entirely to the element on the surface on the other side of the edge, and only to that element. For this to happen, it is essential to have broken the surfaces in a correct way.

As a summary, a mesh will be good if it is fine enough, is structured and its elements are not too distorted or disproportionate, but rather compact and square.

Model was meshed with brick elements, in particular C3D8R elements, while reduced integration was not activated. Mesh can be seen in figures 5.7 and 5.8.

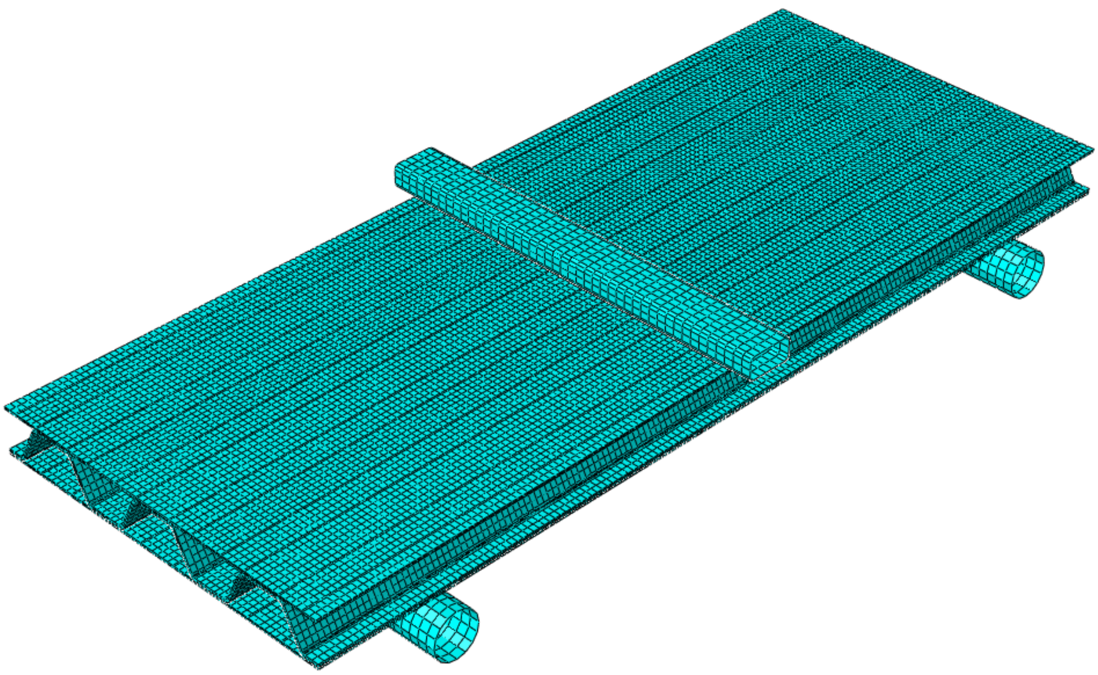

Figure 5.7: General view of the mesh in the three point bending test model

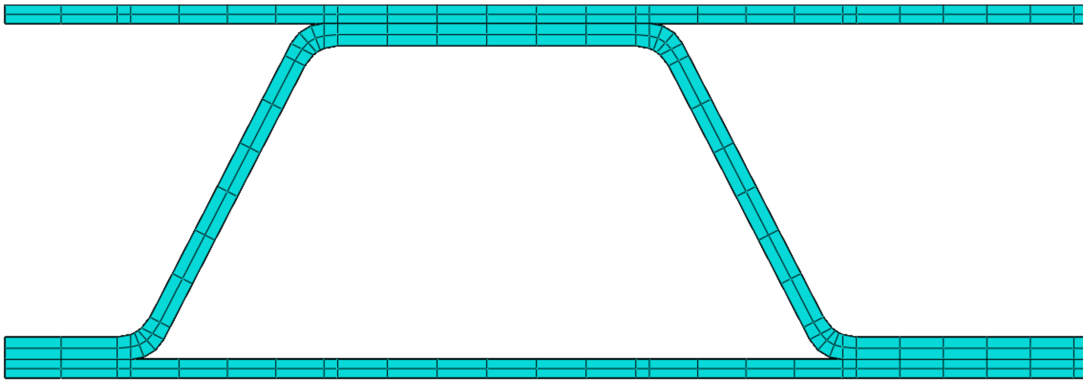

Figure 5.8: Detailed cross-section view of the mesh in the three point bending test model

Figure 5.8 is important as it shows something that was discussed when *celent* was introduced. In order to get good results at least two elements have to be put in the thickness of the corrugated panel and the skin. As the skin has the smallest thickness (0.5 mm) this means that elements are going to have a minimum dimension of 0.25 mm. If perfect cubic elements are wanted, this would mean, and taking into account that one skin measures 200 x 80 x 0.5 mm^3, that just one skin would have 512000 elements. To have so many elements would increase a lot computation time without reporting barely any improvement in the degree of compliance with reality of the results. For this reason, elements which need to have small thickness (all of the model, since the thickness dimension of the skins is 0.5 mm and the one of the corrugated panel is 0.6 mm) have lengths of five times their thickness. Five is chosen since as told before, a value above 5 would compromise the quality of the elements, while low values would imply more elements and higher computation times.

5.2.3 Results and results comparison

The following section will present the results for the introduced corrugated panel. Al it has been already told, main result from a three point bending test is the plot of the applied load (or the reaction load from the sample) with the displacement of the element that applies the load.

A total of 5 samples were tested under the three point bending test. Two of them failed after with a "lower skin tensile failure" mode, while three did under a compressive mode involving buckling of the upper skin. Results for the plot load-displacement of all the cases are shown in figure A.2, and are compared with the results extracted from ABAQUS.

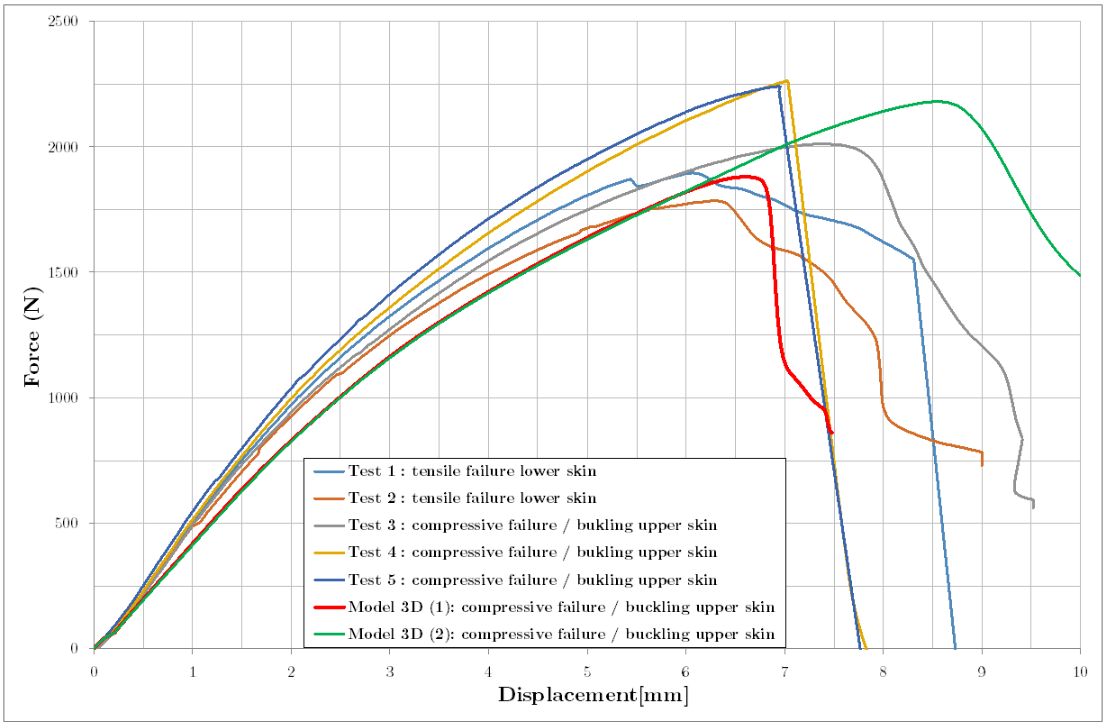

Figure 5.9: Load vs displacement, three point bending test

Curves from ABAQUS tests are red and green ones. Green curve has been produced with the values of the failure strains at table 4.3, while red curve was done with values $\tilde{\epsilon}_{T1} = \tilde{\epsilon}_{C1} = \tilde{\epsilon}_{T2} = \tilde{\epsilon}_{C2} = 0.0112$ and some value for $\tilde{\gamma}$. In both cases, curve develops through the same path, but the value of these terms affects the point in which failure presents, being this last one a better approximation to real curves.

Overall, results can be rated as good. Slope is near the one that have shown experimental tests. This slope smoothes due to the effect of the diffuse damage following a very similar shape and tendency. Failure is given at the around the same value of displacement, and the exponential function achieves a good modeling regarding the drop of the curve after the failure.

Slope is however slightly lower than in the real tests, and this seems to be related with the fact that there is a very small in time (but in a way remarkable in terms of load) drop of the slope at the beginning of the curve. When revising the model it is seen that it appears in some element (in contact with the element on which is applied the load) diffuse damage straight from the beginning. This indicates that there may be some contact problem that is producing some stress in these elements from the initial instant, what could explain this small drop in the curve at the beginning.

As in two of the real tests, the mechanism of failure in the simulation carried out in ABAQUS has been the buckling of the upper skin. Figure 5.10 shows the situation of the upper skin after failure. Buckling of this skin can be seen.

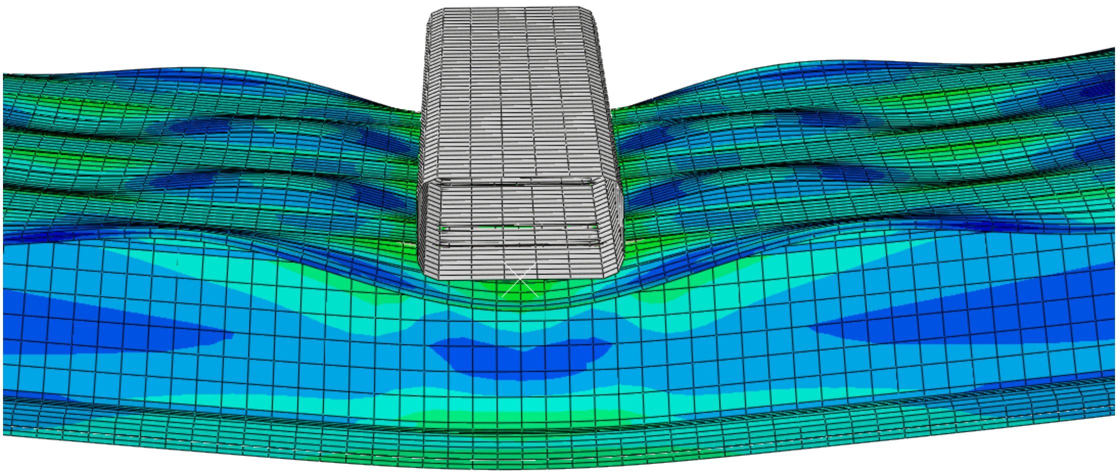

Figure 5.10: View of the buckling of the upper skin

Images from results have been left below. Figures 5.11 to 5.18 show the value of the different damages at the final time. In figures 5.14 and 5.18 the upper skin has been removed to show the internal cross section as it is greatly damaged by the shear stress. Table 5.5 shows the code for the different damages. For identifying a damage through an SDV, only image's caption should be payed attention, but not each image's legend.

SDV	Magnitude
SDV 1	Failure fibre damage, 11 direction
SDV 2	Failure fibre damage, 22 direction
SDV 3	Failure matrix damage, 12 direction
SDV 4	Diffuse fibre damage, 11 direction
SDV 5	Diffuse fibre damage, 22 direction
SDV 6	Diffuse matrix damage, 12 direction

Table 5.5: SDV association

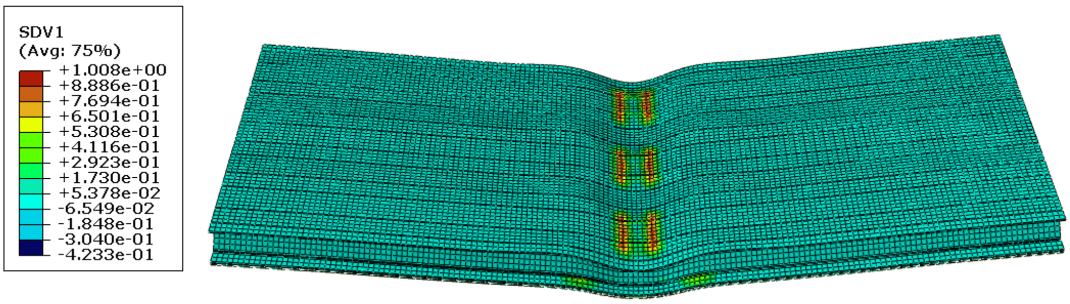

Figure 5.11: Three point bending test, SDV 1

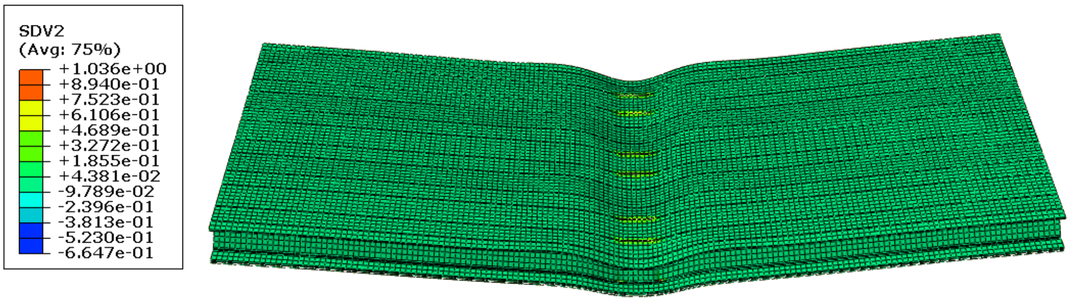

Figure 5.12: Three point bending test, SDV 2

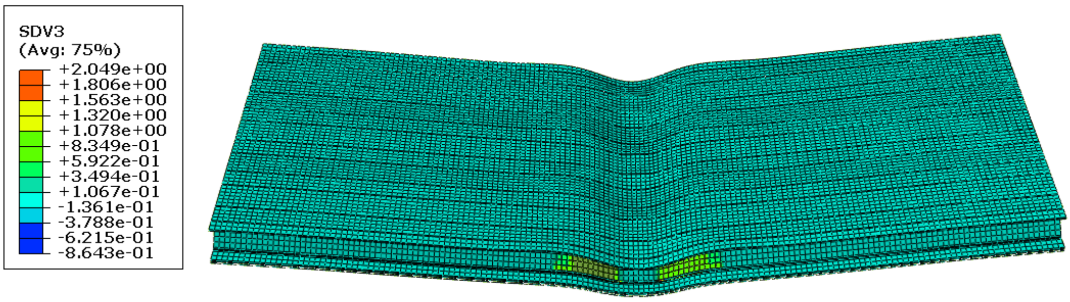

Figure 5.13: Three point bending test, SDV 3

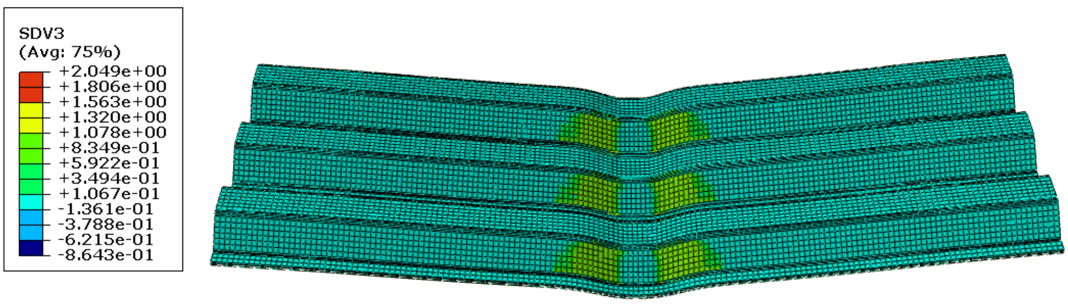

Figure 5.14: Three point bending test, SDV 3, upper skin removed

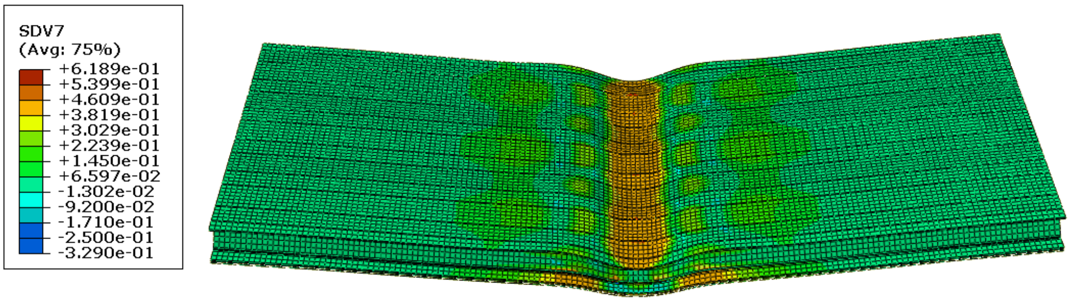

Figure 5.15: Three point bending test, SDV 4

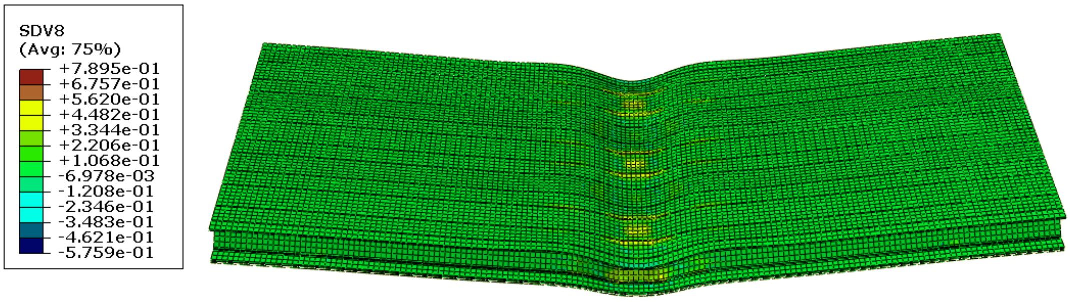

Figure 5.16: Three point bending test, SDV 5

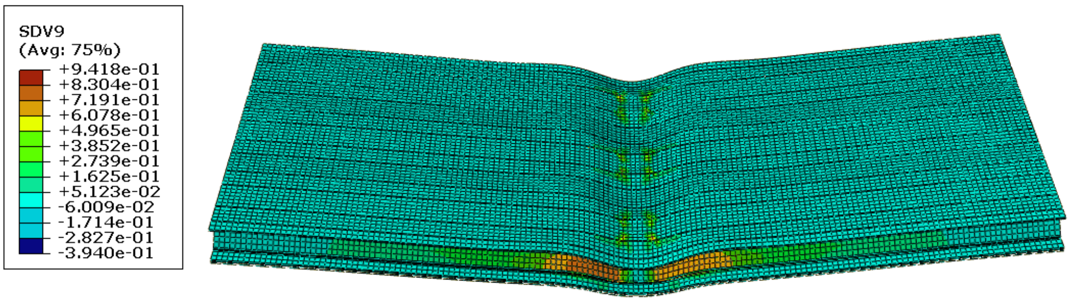

Figure 5.17: Three point bending test, SDV 6

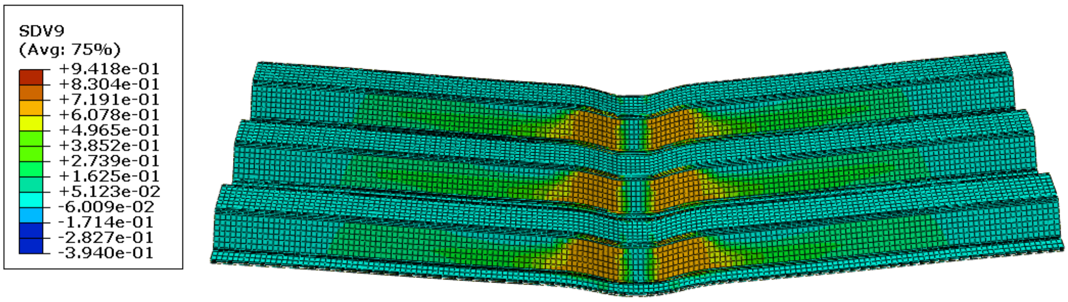

Figure 5.18: Three point bending test, SDV 6, upper skin removed

5.3 Fibre energy released rate

5.3.1 Introduction mathematical background

The fracture energy rate is the energy released per-unit-area as the material undergoes a fracture with the propagation of a crack. The fracture energy can be understood as the decrement in total potential energy necessary for the creation of new surface in the fracture, divided by this increment in the fracture surface area.

The fibre fracture energy rate is the energy released per-unit-area when the fracture is having place in a plane perpendicular to the fibre direction, as the tensile strengths have the direction of the fibre. Do not confuse the fracture energy rate with the critic energy rate (which has been called through all this thesis "energy released rate", as they are not exactly the same, difference will be explained later).

The reason why the characterization of the fibre and matrix energy released rates is important is due to the fact that they are important magnitudes for the creation of damage models in the case of bio composites as they develop an important role in the fracture models developed, and they appear in the calculus of the damage for the fracture damage. Their correct characterization and evaluation is therefore important for the overall robustness of the model.

For the all simulations carried out, and as the real value of this fibre energy released rate was still not characterised, a value of $Gc_{fib} = 10\frac{N}{mm} = 0.001\frac{J}{mm^2}$ was used.

For the matrix energy released rate the value used was $Gc_{mat} = 0.5\frac{N}{mm} = 0.0005\frac{J}{mm^2}$.

For fibre this value was estimated from a carbon fibre and epoxy ply. Previous tests (identically to the one that will be explained here) show that the this value for carbon is around $Gc_{fib} = 100000\frac{J}{mm^2} = 100\frac{N}{mm}$. Taking as hypothesis that this value is proportional to the stiffness or Young's modulus in the fibre direction, and taking into account that the stiffness of carbon is around 135000 $\frac{N}{mm^2}$ and the one of the flax fibre is around ten times less, around 15000 $\frac{N}{mm^2}$, Gc_{fib} can be estimated to be $Gc_{fib} = 10\frac{N}{mm} = 0.001\frac{J}{mm^2}$.

The value for the matrix Gc_{mat} is known as previous test had been conducted in shear with epoxies very similar to the one used for the ply here.

5.3.2 Mathematical Background

The study of fracture generally involves the characterization of the released or dissipated energy when there is propagation of a crack (Médeau V. 2019) [17]. This quantification of the energy is support by the Griffith analysis, thought the introduction of the rate of energy released G. This rate has been introduced by Griffith (Griffith, 1921) [18], and is used as support for mechanics of fracture.

This theory is valid for a big variety of materials. It is made the hypothesis that the the behaviour of the material remains linear elastic - fragile in all the structure, except in a infinitesimal zone in the point of fracture. This infinitesimal point in the crack is the only source of dissipation (Médeau V., 2019).

Theoretically, the mechanics of fracture affirms that the influence of this small zone in the global behaviour is negligible. The criteria for the propagation of a crack is supported by an energetic balance between the structural properties dependent of the loads and the material parameters (Chaboche, 2001) [19] :

- For each crack it is associated a rate of released energy G (fracture energy rate), that is the elastic energy released by the structure per infinitesimal transversal growth of the crack, proportional to the area.

- Crack advances if G is able to compensate the necessary surface energy for the advance of the crack (rate of restitution of the critic energy Gc, the magnitude intended to characterise and that has been called until this point as energy released rate).

On the contrary, if the released elastic energy is not sufficient for creating a new fracture surface the crack does not advance.

Considering an structure of thickness e_p, that has a fissure placed in a, of an infinitesimal lenght δa, figure 5.19 the energetic balance can be written in a quasi-static state as:

$$G\, e_p\, \delta a = \delta W - \delta U \tag{5.1}$$

δW is the work done by the exterior forces during the propagation of the crack and δU is the variation of elastic energy stored in the structure. For a given displacement u, the exterior work is written as $\delta W = P(u,a)\delta u$. Equation 5.1 is therefore transformed into:

$$G\, e_p\, \delta a = P(u,a)\delta u - (\left.\frac{\partial U(u,a)}{\partial u}\right|_a \delta u + \left.\frac{\partial U(u,a)}{\partial a}\right|_a \delta a) \tag{5.2}$$

If a system without propagation of fracture or quasi-static is considered, it is had $P(u,a) - \frac{\partial U(u,a)}{\partial u} a = 0$ and therefore the G can be expressed as

$$G = -\frac{1}{e_p}\frac{\partial U(u,a)}{\partial a} \tag{5.3}$$

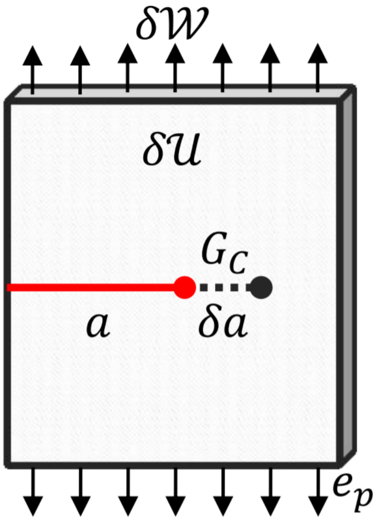

Figure 5.19: Scheme of the crack propagation in the theory of Griffith [17]

So as a summary:

- If $G < Gc$: crack does not advance.
- If $G = Gc$: crack advance in a quasi-static way, all the released energy is consumed in the propagation and creation of new surface.
- If $G > Gc$: the crack propagates in a dynamic way, the excess of released energy not used for creating surface is transformed into kinetic energy K, and this term will appear in the energetic balance of previous equation.

As it can be seen, the experimental objective is to determine the value Gc, one of the most important ones when trying to understand the fracture mechanics. This parameter, correctly named "Critic released energy rate" is considered to be a material parameter independent of the studied structure, the propagation history, the applied loads and the size and form of the present mechanic fields. Through this dissertation is has been named as "fibre energy relased rate" (since it is intended to characterise this value in that direction).

5.3.3 Method of the Areas for determination of Gc

To continue, the method used for the determination of Gc will be explained. The method of areas is the most directed method for the estimation of the critic released energy rate. It estimates the Gc taking differences in the equation 5.3, calculated between two instants of propagation 1 and 2 , 5.20. The variation of elastic energy is divided by the new surface created when the crack has advanced a distance $\triangle a$. (Médeau V., 2019) [17].

Gc can be interpreted as the difference of areas below the curve Force - Displacement between two points.This method is not supported by solid hypothesis and is valid in order to give a good estimation, in any context. It has not, however, an unconditional reliability and it can show some errors when the variation of the crack longitude is very small.

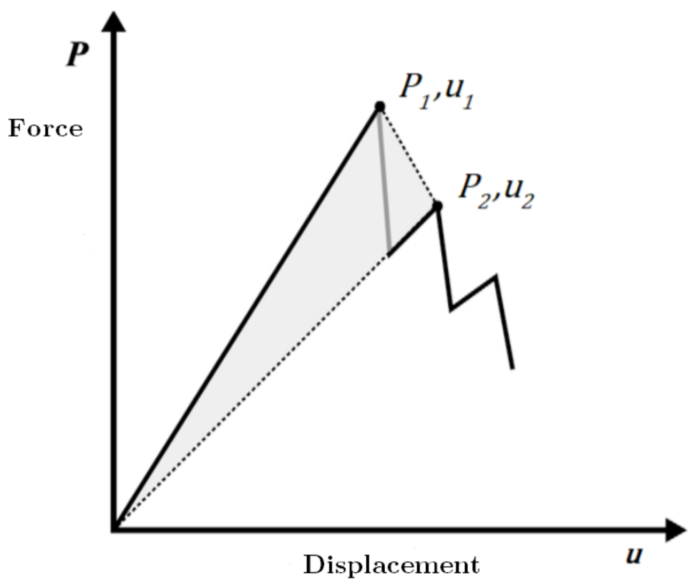

Figure 5.20: Graphic interpretation of the method of areas [20]

This method has been the used for calculating Gc with the results of the analysis given by ABAQUAS and it is the planned one for extracting the magnitude in the real tests.

5.3.4 Characterization and experimental test

The energy released rate test is conducted according to ASTM D5528-13 [21] "Standard Test Method for Mode I Interlaminar Fracture Toughness of Unidirectional Fiber-Reinforced Polymer Matrix Composites", and is performed with a traction machine.

The objective of the test will be to evaluate the fibre fracture energy of a sample made of the stacking of several plies of flax fibre which has been weaved and later impregnated in epoxy and which has been cured in the oven. A picture of the sample is shown in figure 5.21.

In the test the sample has a precrack made and the tensile stress is applied through a traction machine. The tension is practised through two cylinders that cross the sample by two drilled holes. Tension is applied pulling from these two cylinders from each side with the pull machine, and propagating therefore the precrack which starts to advance through a plane perpendicular to the fibre. An scheme can be seen in figure 5.22.

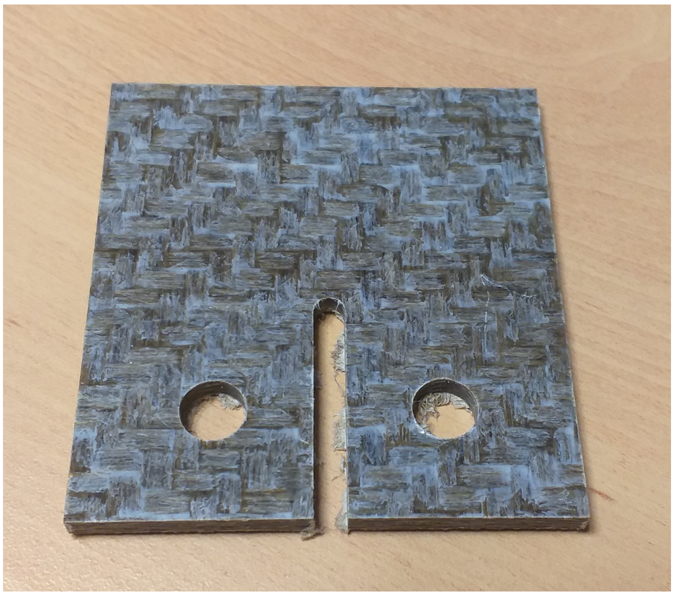

Figure 5.21: Sample for the characterization of the critic energy released rate

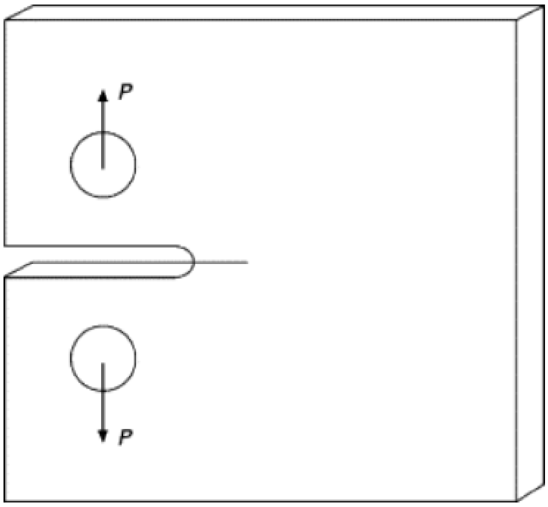

Figure 5.22: Scheme of the test

The initial sample was prepared by the group of operators of DMSM department. The execution of the drilled holes can be seen in figure 5.23.

Figure 5.23: Execution of through holes in the sample

In order to perform the precrack in the middle a diamond- edge cutter is used, in order to let the crack start by that point. Process can be seen in figure 5.24 and the sample with the precrack done in figure 5.25. As explained, the crack will develop through a fracture plane which will be perpendicular to the fibre direction.

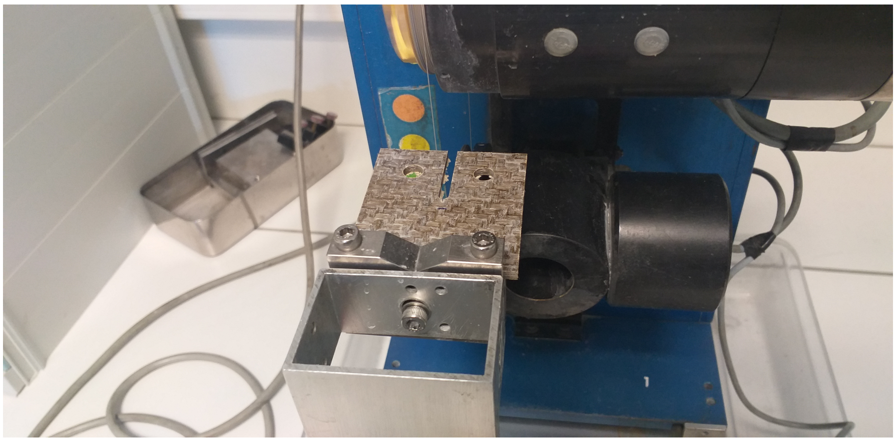

Figure 5.24: Execution of the precrack with the diamond- edge cutter

Figure 5.25: Sample with the precrack in the middle

The main characteristics of the sample can be seen in table 5.6. The rest of measures can be found in figure 5.22.

Characteristic	**Value [mm]**
Length	65
Width	60
Thickness	4
Drilled holes diameter	8
Hole separation at the beginning	28
Precrack thickness	0.3
Precrack length	6

Table 5.6: Main measures of the sample

After that, the strain gauge, commercialy branded as KRAK-GAGE is placed. The following has been directly reproduced from the FRACTOMAT manual of instructions, [22]. The KRAK-GAGE is essentially a thin film electrical cracklength transducer bonded on a component or specimen. It provides an infinite resolution DC voltage output proportional to the cracklenght. It consists of a thin metal foil and of a flexible backing which provides a convenient bonding and insulating to a test specimen. The photo-etched shape of the KRAK GAGE gives a strongly linear relationship between gauges- output and cracklength. The crack growth has to start at a known point for correct locating of the KRAK GAGE.

As a general rule, the installation of a KRAK-GAGE to a specimen is identical to the well established methods used for foil-type strain gauges. A successful test needs a proper, high quality gauge installation. A correct cleaning and degreasing is necessary to remove all surface contaminates, such as oils, greases, chemical residues, etc. Common degreasing methods include hot vapor, ultrasonic bath, aerosol spraying of chloroethene NU or Freon. It is recommended to degrease the entire test specimen, or a surface area somewhat larger in size than needed for the given KRAK-GAGE size.

Each KRAK-GAGE is provided with a suitable triangular alignment marks or notches to aid in precisely mounting the gauge onto the specimen. It is recommended to lay out a pair of cross reference marks onto the sample. The gauge can be seen in figures 5.26 and 5.27

Figure 5.26: Manufacturer of the strain gauge

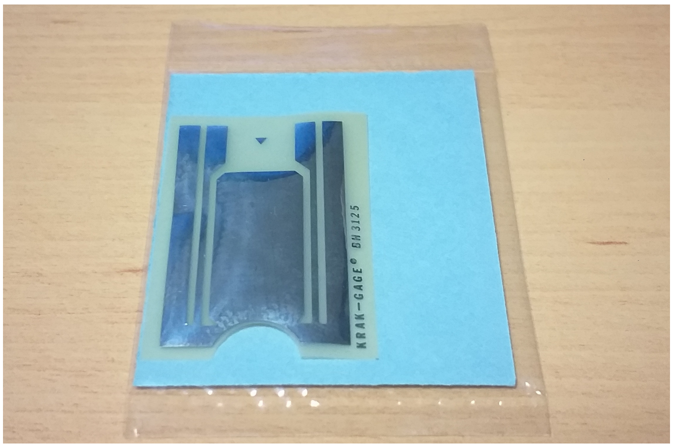

Figure 5.27: Strain gauge

Finally, the system is complete with the measuring system. The cracklength measuring system is commercially called FRACTOMAT, an image can be seen in figure 5.28.

The FRACTOMAT is a complete, self-contained, two channel cracklenth measuring system designed specifically for use with all the KRACK-GAGES. It is essential that the crack grows simultaneosluly in the test piece and the KRAK-GAGE. A digital panel meter shows the measuring values of cracklength.

The KRAK-GAGES are connected with a four wire cable to the FRACTOMAT intrument. The both constant sources excitate the KRACK-GAGES. The gauge outputs are processed in a two stage differential amplifiers. The output instrument is 10 V for 100 % nominal cracklentght. A "hold" circuit is provided to avoid possible reading errors because of crack closure effects during dynamic testing. This circuit stores the max. value of cracklenght.

Figure 5.28: FRACTOMAT measuring system [23]

For the calculus of the energy during this test the load-displacement evolution must be plotted. For this test the displacement is actually the separation of the two metallic cylinders minus their separation at the beginning, this is, the displacement of one of them multiplied by two.

The energy used by the machine for breaking the sample, or this is, the energy released by the sample, is the area below the curve. As it is intended to calculate the rate with the area of this energy, this is, the energy per-unit-area, the idea is to know the amount of this energy that has been released when the crack has advanced a certain amount and a new surface has been created. The method used is therefore the method of the area previously explained.

Unfortunately, due to the COVID-19 virus which was declared as a pandemic by the OMS the 11^{th} of march of 2020, all universities and research facilities were ordered to shutdown in France from the 13^{th} of march onwards and the experiment could not be conducted.

Results for the Gc_{fib} were expected to be around 0.01 $\frac{J}{mm^2}$, which in fact, as explained, is the value that has been used in all the simulations as is considered to be a good approach. However the samples are prepared and the experiment is well described here for anyone to continue it.

Next subsection will show the different models that were created in ABAQUS and the objective pursued with them.

5.3.5 ABAQUS models and results

Although the test was not conducted, two models were prepared in ABAQUS, in order to test the validity of the damage model by comparing results between them. To continue, it will be explained why this has been done.

Two ideas are pursued. First one is to input a desired value for G_{fib} in the two models and then calculated it with the results by the method of the area to see if the desired input value has been achieved. Second is to compare the results of the two models between them, as one of the methods (the one implemented in ABAQUS) is a proven method for this kind of analysis and it is useful to compare it with the results of the model in which the UMAT subroutine is used.

One of these models has been modelled with a cohesive contact property which includes cohesive behaviour and damage in the place through which the crack is going to propagate. Cohesive behaviour and this sort of failure damage modelling inside ABAQUS itself will be explained later but are typical and reliable forms of modeling these kind of fractures. In fact what is intended with the damage model of the UMAT subroutine is to include this kind of damage modeling, among others. For having a contact in the location of the crack, what has been done is creating first one half of the model and then making a mirror to have two different parts that can be put together through this contact. For understanding this, the first half of the model, and the whole model can be seen in figure 5.29. This model is run therefore without any subroutine.

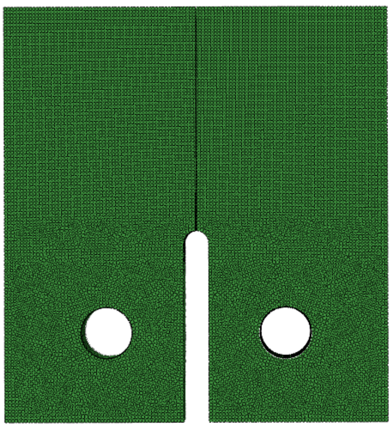

Figure 5.29: Model after performing a mirror in the crack zone

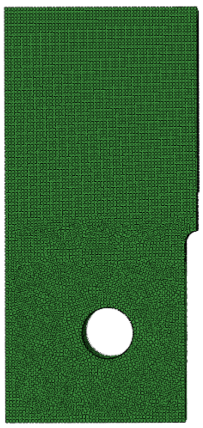

Figure 5.30: Original model realized

The second model will be a regular model which will be run together with the subroutine. However, as the only effects presented in the previous model are this sort of failure damage modelled inside ABAQUS together with a cohesive behaviour, the diffuse damage of the subroutine was deactivated for this second model. Actually, a model run with diffuse damage also would present very few diffuse damage through all the model and this would only be non deniable in the zone of the crack propagation, but it was deactivated i in order to have the most similar results between the two.

After extracting results for both models, it is possible to have through the method of the areas previously explained, the fibre energy released rates G_f and compare it with the ones used as an input. In case of coincidence for the subroutine's failure damage model, this will obviously mean that the damage model implemented is working correctly.

The first model is also used for compare results with this second one and see if the global behaviour is overall similar, which strengthens the reliability of our second model and therefore of the damage model implemented.

Although for this comparison between the two, the real value of fibre fibre energy rate G_f was not characterized yet, what is pursued here is yo have a first proof that the failure damage model implemented is working well.

Next step would have been the realization of the test in order to characterize G_f and a simulation of the ABAQUS model with the subroutine but this time with the diffuse damage activated too, as this damage is acting in the real life test. After that comparing results between the two in order to improve and implement the output- test value G_f would have been done. However, as explained, it was impossible to perform the test.

Cohesive contact and damage modelling inside ABAQUS

Cohesive contact is one of the capabilities offered by ABAQUS which can be used to model a bonded interface, with or without the possibility of damage and failure of the bond. The following has been extracted directly from ABAQUS reference guide, [11]. This capability has similarities to other features that could be considered for a bonded interface, including cohesive elements. Cohesive contact behaviour is typically easier to define than modeling the interface using cohesive elements and is primarily intended for situations in which the interface thickness is negligibly small. If the interface adhesive layer has a finite thickness and macroscopic properties of the adhesive material are available, it may be more appropriate to model the response using conventional cohesive elements.

In ABAQUS/Explicit the surface-based cohesive behaviour framework can also be used to model crack propagation in initially partially bonded surfaces via linear elastic fracture mechanics principles (LEFM).

In general contact cohesive behavior:

- Is defined as surface interaction property.
- Allows specification of cohesive data such as the fracture energy as a function of the ratio of normal to shear displacements (mode mix) at the interface;
- Assumes a linear elastic traction-separation law prior to damage;
- Assumes that failure of the cohesive bond is characterized by progressive degradation of the cohesive stiffness, which is driven by a damage process.

The available traction-separation model in ABAQUS assumes initially linear elastic behavior followed by the initiation and evolution of damage. The elastic behavior is written in terms of an elastic constitutive matrix that relates the normal and shear stresses to the normal and shear separations across the interface.

The nominal traction stress vector, t consists of three components (two components in two-dimensional problems): t_n,t_s, and (in three-dimensional problems) t_t, which represent the normal (along the local 3-direction in three dimensions and along the local 2-direction in two dimensions) and the two shear tractions (along the local 1- and 2-directions in three dimensions and along the local 1-direction in two dimensions), respectively. The corresponding separations are denoted by δ_n, δ_s, and δ_t. The elastic behavior can then be written as:

$$\mathbf{t} = \begin{bmatrix} t_n \\ t_s \\ t_t \end{bmatrix} = \begin{bmatrix} k_{nn} & k_{ns} & k_{nt} \\ k_{ns} & k_{ss} & k_{st} \\ k_{nt} & k_{st} & k_{tt} \end{bmatrix} \begin{bmatrix} \delta_n \\ \delta_s \\ \delta_t \end{bmatrix} = \mathbf{k}\delta$$

Uncoupled traction-separation behavior is marked.The simplest specification of cohesive behavior generates contact penalties that enforce the cohesive constraint in both normal and tangential directions. By default, the normal and tangential stiffness components will not be coupled: pure normal separation by itself does not give rise to cohesive forces in the shear directions, and pure shear slip with zero normal separation does not give rise to any cohesive forces in the normal direction. For uncoupled traction-separation behavior, the terms K_{nn}, K_{ss} and K_{tt} must be defined. The table with the values used can be seen in table 5.7. A typical traction-separation behaviour can be seen in figure 4.5.

$\boldsymbol{K_{nn}}\ \frac{\boldsymbol{N}}{\boldsymbol{mm^3}}$	$\boldsymbol{K_{ss}}\ \frac{\boldsymbol{N}}{\boldsymbol{mm^3}}$	$\boldsymbol{K_{tt}}\ \frac{\boldsymbol{N}}{\boldsymbol{mm^3}}$
100000	100000	100000

Table 5.7: Values for the cohesive property

These values have been selected according to (Turon et al., 2007) [24], which proposed them as default values for the interface stiffness. In any case, as the only G_f intended to know is the one of the fibre (perpendicular to the surface of the crack), the only value of interest is K_{nn}.

Finally, damage modeling has also been implemented. Damage modeling allows you to simulate the degradation and eventual failure of the bond between two cohesive surfaces. The failure mechanism consists of two ingredients: a damage initiation criterion and a damage evolution law. The initial response is assumed to be linear as discussed above. However, once a damage initiation criterion is met, damage can occur according to a user-defined damage evolution law. This evolution can be select as linear, figure 5.31 (the one selected here), or exponential, which can be seen in figure 5.32. Although the model of the subroutine is exponential results do not vary barely. If the damage initiation criterion is specified without a corresponding damage evolution model, ABAQUS evaluates the damage initiation criterion for output purposes only; there is no effect on the response of the cohesive surfaces (i.e., no damage will occur). Table 5.8 below shows the values of initiation criteria introduced. Once again the important one is the "normal only" as this is the direction in which it is desired to calculate the G_f. For writing this value, the stress strain of an element of the crack was plotted in the model run with the subroutine, in order to try to adjust this model to that one.

Normal only MPa	Shear-1 only MPa	Shear-2 only MPa
150	50	50

Table 5.8: Values for the damage law

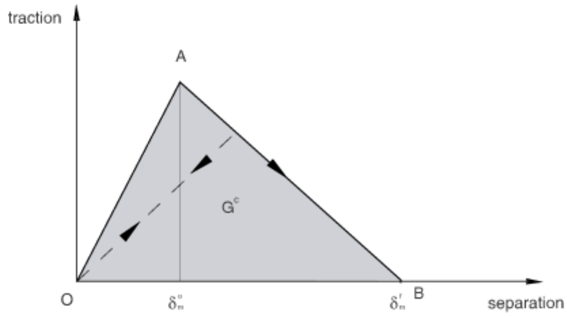

Figure 5.31: Traction separation with linear drop of the curve [11]

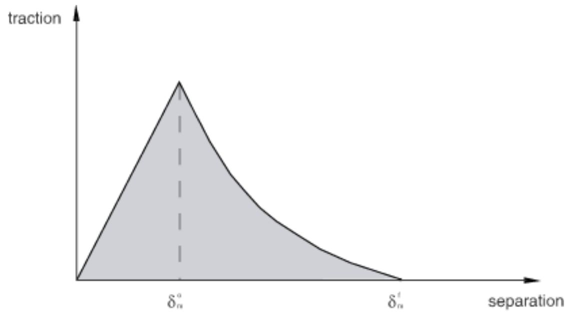

Figure 5.32: Traction separation with exponential drop of the curve [11]

Results

Results are presented in this section, for the model made up with cohesive elements and the one run with the routine jsut with failure model. It must be recalled that the first objective is that the G_f calculated in the second one is equal to the one input through the properties, this is $G_f = 0.01\frac{J}{mm^2}$, and the second one is to obtain a similar general beheviour when comparing the two models.

To extract results, load is plotted with the separation between the two points from which load is applied (separation between the center of the two drilled holes). After that, the method of areas is applied. For applying this method, first thing done is to locate the maximum load. After locating this maximum load, and through the damage parameter, the amount of separation needed for the failure of one element can be known. Two lines are drawn from origin to the instant 1 (when damage arrives the element, figure 5.33) and instant two (where the whole element is damaged, figure 5.34) and the area between the two points in the plot is calculated. After that, it is divided by the new surface created (which will be the element length multiplied by the thickness of the sample).

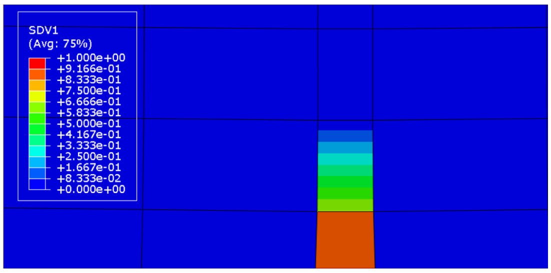

Figure 5.33: Instant one, damage arrives to the element.

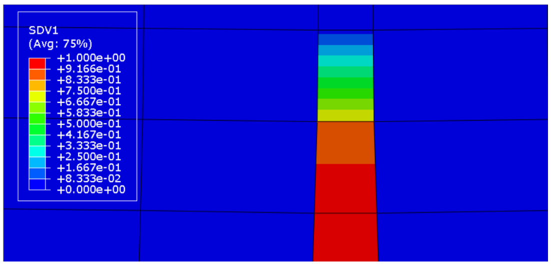

Figure 5.34: Instant two, the whole element is damaged

Finally, results are given below. In figure 5.35 the results for the model run with the subroutine UMAT without the diffuse damage can be seen, and below, in table 5.9 main values of the results are shown. In figure 5.36 and table 5.11 same results but for the model run with cohesive property are shown. Remark that the straight lines in figures 5.35 and 5.36 are not representing anything, but just joining the origin with the points in which the first, second and third elements are failing (after the maximum laod). They have been drawn in order to let clear that G_f is calculated with the area between the first and the second, and the second and the third, dividing by the surface created as told. Results for this energy can be shown in tables 5.10 and 5.12.

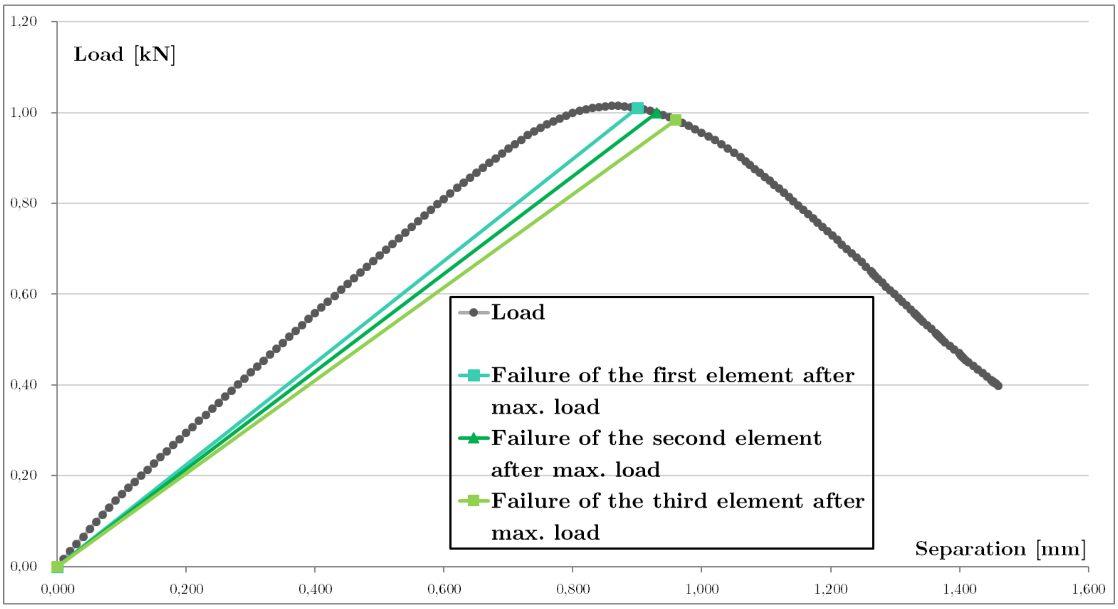

Figure 5.35: Load- separation plot for the model run with the UMAT subroutine

Instant	**Load [kN]**	**Separation [mm]**
Max. load	1.015	0.87
Failure of 1st element	1.010	0.90
Failure of 2nd element	0.9993	0.93
Failure of 3rd element	0.9834	0.96

Table 5.9: Main values for the model run with UMAT routine

In table 5.10 the values obtained for G_f through area's method are shown. As the input value was 10 $\frac{J}{mm^2}$ results are considered coherent.

Instant	G_f $[\frac{N}{mm}]$
From 1^{st} to 2^{nd} element	9.978
From 2^{nd} to 3^{rd} element	11.143

Table 5.10: G_f values obtained for the model run with UMAT routine

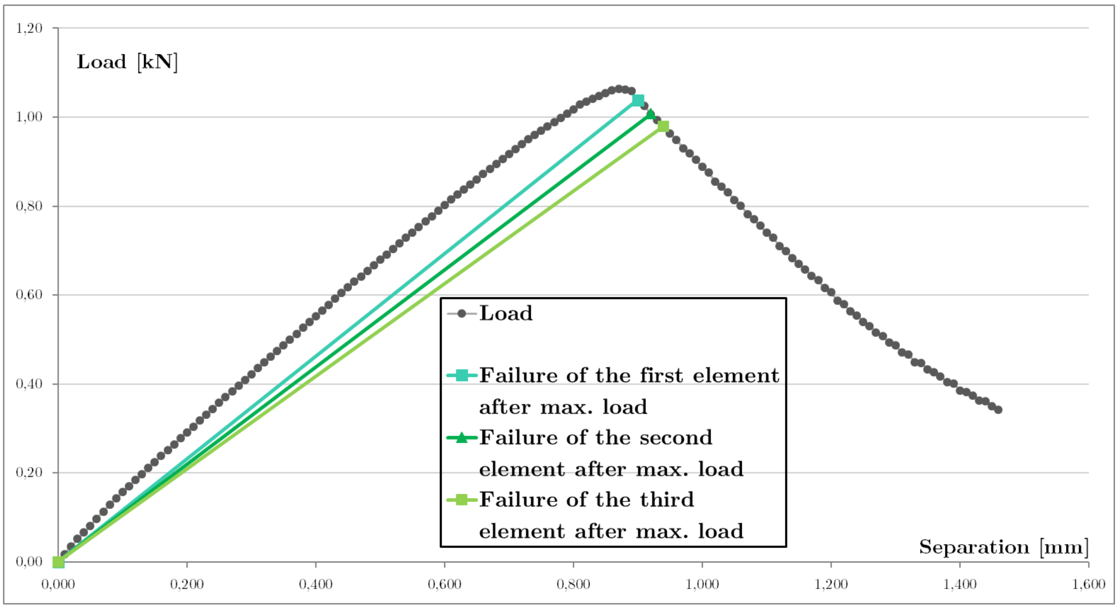

Figure 5.36: Load separation plot for the model run with the cohesive property

Instant	**Load [kN]**	**Separation [mm]**
Max load	1.061	0.88
Failure of 1st element	1.038	0.90
Failure of 2nd element	1.007	0.92
Failure of 3rd element	0.979	0.94

Table 5.11: Main values for the model run with cohesive property

In table 5.12 the values obtained through area's method for this model are shown. Once again, as the input for G_f value was 10 $\frac{J}{mm^2}$ results are considered coherent.

Instant	G_f $[\frac{N}{mm}]$
From 1^{st} to 2^{nd} element	12.264
From 2^{nd} to 3^{rd} element	11.138

Table 5.12: G_f values obtained for the model run with cohesive property

To conclude, a comparison of the results of the two models can be seen in figure 5.37.

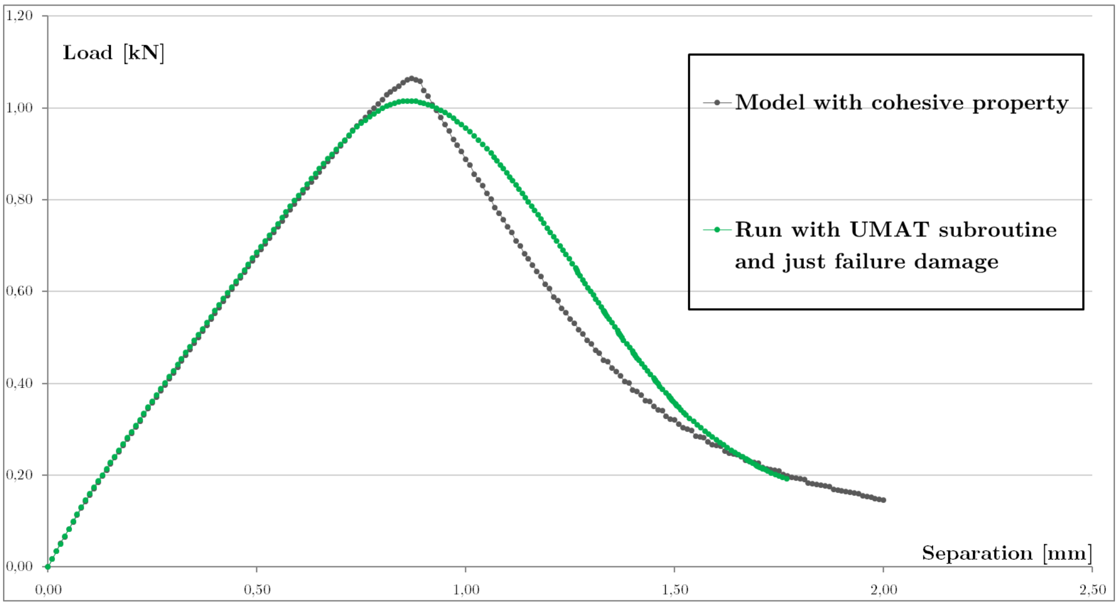

Figure 5.37: Comparison of results

It can be seen how the two follow exactly the same path during the loading phase. After that, the model with cohesive property presents a higher maximum in load, and finally they differ in the second part of the curve. The one run with UMAT presents an smoother slope even though it has an exponential modeling, while the one with cohesive property has a more pronounced slope. To conclude it can be said that the results of the UMAT routine are excellent as the two objectives have been achieved:

- To extract from the load- separation plot the same fibre released energy rate than the one used as input.
- To have a very similar behaviour under the same conditions than a common way to model this kind of experiments in ABAQUS such as it is the modeling with cohesive property.

Next step in order to characterize the G_f would be to conduct the real test. With the G_f obtained now an ABAQUS simulation can be run including also diffuse damage and behavior can be compared with the one in the test in order to improve the model.

Chapter 6

Dynamic analysis

This chapter is intended to explain the dynamic analysis carried out, necessary in order to model the behaviour and damage when the flax fibre panels are submitted to dynamic loads.

To begin with, a brief explanation about the functioning of the VUMAT subroutine, the subroutine proportioned by ABAQUS to perform explicit analysis, will be given.

To continue, the impact test will be introduced. It is clear that in order to perform a dynamic test with the bio composite there are not a lot of options apart from an impact test, so this is why it was the chosen for comparing results between real model and the model prepared in ABAQUS. The real experiment together with the one carried out in ABAQUS will be explained. Finally, once again the results of the two will be compared in order to evaluate the degree of compliance with reality of the model.

6.1 VUMAT routine

VUMAT is the equivalent to the subroutine UMAT used when the simulation has an explicit step. Explicit simulation is used as it is the most appropriate for a dynamic test such as the impact test developed. As UMAT, VUMAT allows the user to define the mechanical behavior of the material for materials whose properties can not be accurately represented by the ABAQUS material library, by allowing to define the stiffness matrix in each iteration, in order to perform non linear analysis. As UMAT, it has been written in FORTRAN.

There are, however, some differences with UMAT that come from the fact that an explicit analysis is being performed, this is, with an explicit solver, normally a forward Euler.

Explicit methods differ from implicit methods in the fact that they do not need to calculate an extra equation in each iteration. In the case of an static load analysis this equation would be the equilibrium of loads. For explicit methods it is verified that:

$$Y(t + \triangle t) = F(Y(t))$$

But as it has been seen, all explicit methods are not unconditionally stable but have a stability limit.

$$|\triangle\epsilon| < \triangle\epsilon_{stab}$$

In the equation above, $\triangle\epsilon_{stab}$ is usually less than the elastic strain magnitude. This means that for explicit integration the time increment must be controlled. To do this, system of units is changed respect to the one used for the implicit analysis. This is because some magnitudes like the density are involved in the calculus of the time step in explicit analysis, and using the same system of units as in implicit forces to run the simulation in double precision, bringing some undesirable numerical effects. In general the system of units used here is more recommended for explicit analysis. Remind once again that the parameters that must be read from VUMAT from ABAQUS, which were discussed at the end of chapter 4, must respect the chosen system of units. In table 6.1 the system of units used for the explicit analysis is shown.

As a positive aspect, the Jacobian has not to be programmed since the equilibrium equation is not solved as in the case of UMAT, so the coding of VUMAT is in general much more easy.

Two additional new characteristics with respect to UMAT should be introduced. The first one is that diffuse and failure damage are introduced in explicit analysis for out-ply shear directions 13 and 23. The reason for doing this is that in the first tests it was observed that stresses in these directions were at the same level than the ones in the in-ply direction 12 (τ_{12}). Failure and diffuse damage are identically reproduced to the ones in the other directions. For diffuse damage the strain threshold of activation used is exactly the same value than the used for in-ply diffuse damage. Mean while, the strain limit (from which no more diffuse damage is applied and failure damage starts) has been chosen as 3 times bigger than the one used for in-ply failure, this is, around $\tilde{\gamma_{13}} = \tilde{\gamma_{23}} = 0.18$, as experience shows that this value is around 2-3 times bigger in this direction when compared with in-ply shear direction for composite elements form by the stacking of plies. The logarithmic function is done to have therefore the same shape but with a different upper limit.

$$FD_i = \frac{1}{2}\gamma jk^2 G_{jk} > FD_{0i}$$

$$D_{di} = c_4 + c_5\, ln(\sqrt{FD_i})$$

For the failure damage criteria is the same as in-ply failure damage, changing the corresponding elements associated with each direction.

$$FF_i = \frac{\gamma_{jk}}{\tilde{\gamma_{jk}}} > 1$$

$$D_{fi} = 1 - \frac{e^{(1-FF_i)\frac{G_{jk}\tilde{\gamma_{jk}}^2 CELENT}{G_{mat}}}}{FF_i}$$

It must be remembered that now there is damage in all directions except in the stacking direction (ϵ_{33} & σ_{33}). After starting to consider damage in this shear directions, elements $C_{d_{55}}$ and $C_{d_{66}}$ result affected and damaged stiffness matrix is now:

$$\begin{bmatrix} (1-D_{f1})(1-D_{d1})C_{11} & \cdots & 0 & 0 \\ \vdots & \ddots & \vdots & \vdots \\ 0 & \cdots & C_{55}(1-D_{f1})(1-D_{f1})(1-D_{f4})(1-D_{d4}) & 0 \\ 0 & \cdots & 0 & C_{66}(1-D_{f1})(1-D_{f2})(1-D_{f5})(1-D_{d5}) \end{bmatrix}$$

The other thing to talk about is the deletion of elements. ABAQUS offers an extra SDV (solution dependent state variable) in order to manually control the deletion of elements. In dynamic analysis it is common that when there is an impact some elements undergo what is called "excessive distortion". Basically in real life what is happening is that there is being necking and fracture (in any case normal materials suffer from deformations of several times their original length). This is not a matter in static analysis since as told before, in a static analysis equilibrium is calculated after each iteration, so computation will stop way sooner some element is undergoing excessive distortion, plus the appearance of elements under this situation is much more harder, probably due to a bad posed problem. Dynamic computation do also stop due to the presence of excessive distorted elements but since equilibrium is not calculated it is easy to reach this situation. In order to control the appearance of excessive distortion, element deletion is included. It is possible to define a condition which, if accomplished, changes the value of the SDV associated to deletion. This causes that the element is deleted. For this case the deletion variable is activated if any of the following conditions is given:

$$|\epsilon_{11}| > 2 \quad |\epsilon_{22}| > 2 \quad |\epsilon_{33}| > 2 \quad |\epsilon 12| > 2 \quad |\epsilon 13| > 2 \quad |\epsilon_{23}| > 2$$

This will delete any element before it can undergo a situation of excessive distortion, and at the same time it is ensured that no element which is still offering some resistance is deleted, since any element which is above an strain of 2 in some direction has passed way long ago fracture in that direction.

The criteria for the stress and strain vector is changed from UMAT to VUMAT. Stress and strain vector are left below. This must be kept in mind when coding, as stiffness matrix changes and criteria for damage shall also be changed. Keep in mind that $\gamma_{ij=2\epsilon_{ij}}$. See also in the stress vector that here τ_{13} and τ_{23} have flipped with respect to the convention in UMAT routine.

$$\vec{\epsilon} = [\epsilon_{11} \quad \epsilon_{22} \quad \epsilon_{33} \quad \epsilon_{12} \quad \epsilon_{13} \quad \epsilon_{23}]$$

$$\vec{\sigma} = [\sigma_{11} \quad \sigma_{22} \quad \sigma_{33} \quad \tau_{12} \quad \tau_{23} \quad \tau_{13}]$$

In general, the some variables are available from ABAQUS (their units should be changed as another system of units is used here), and once again is necessary to code to define the stress through the stiffness matrix and to define the solution-dependent strain variables, or SDVs.

Finally the scheme shown in figure 5.1 is also useful in order to understand the behaviour of the VUMAT routine.

Quantity	**Unit**
Length	mm
Force	kN
Mass	Kg
Time	ms
Stress	GPa
Energy	kN · mm (J)
Density	Kg/mm^3

Table 6.1: System of units used for implicit analysis

6.2 Impact test

6.2.1 Introduction

An impact test is conducted to analysed the mechanic behaviour that a material shows when it suffers a collision loading that causes an instant deformation or rupture of the sample. Sample must be fixed with a particular orientation and geometrical features, that will depend on the type of test. After that, an established weight is released from a specific height. As a result it collides with the sample with a shock load. During the collision between the weight and sample occurs an energy transfer that provides the fracture mechanics of the tested material. In general, the collision causes the destruction of the sample.

An impact test objective is to measure the capacity of a material to absorb the energy transfer from the weight to the sample occurred in the crash. These tests are useful to select materials for applications in which they may have to suffer a very quick loading, like a collision, and they need to present impacts capacities. A good example of this is any motorized vehicle.

Impact testing may be useful for almost all kinds of materials, but is it more common for plastics, composites, metals, ceramics and woods, which are generally configured with several plies of different thicknesses. It has been chosen for comparing the compliance of the damage model implemented in VUMAT with the results, due to its relative simplicity and generality among other dynamic tests.

6.2.2 Impact Test

Impact test was conducted according to STM D7136 / D7136M-15, Standard Test Method for Measuring the Damage Resistance of a Fiber-Reinforced Polymer Matrix Composite to a Drop-Weight Impact Event, [25]. To perform this test a drop tower machine was used. This tower can be seen in figure 6.1. As a weight for the impact a cylinder with an 16 mm hemispherical head is used. The weight drops guided as it runs over two guiding rails. Above the cylinder a mass is placed. Varying between several masses and heights allows to have different potential energies and so happens with the kinetic energy at impact. A piezoelectric load cell acts as accelerometer and its placed inside the cylindrical head in order to record data. Most important characteristics can bee seen in table 6.2.

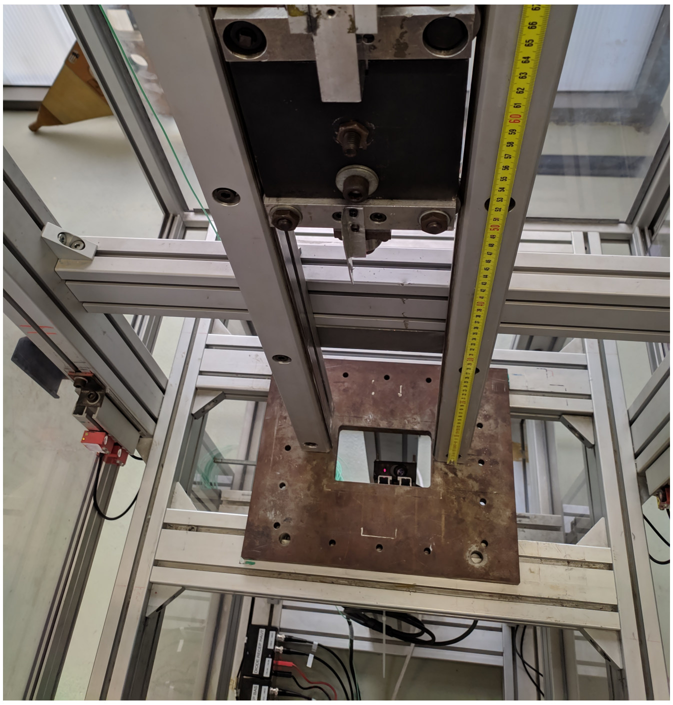

Figure 6.1: Drop tower used for the impact test

Sensitivity	224.8 (mV/kN)
Measurement Range (Comprex)	22.24 [kN]
Maximum static Force (Comprex)	44.48 [kN]
Upper frequency limit	25 kHz
Full scale output	5 [V]

Table 6.2: Main parameters of the accelerometer

There are two lasers (which can be seen in the figure as red rectangles) which are positioned a few centimeters above the plate at a known height. These lasers have a double mission, as they are in charge of recording the slide speed, but they also activate the recording system when the signal between the two is interrupted. There is another laser under the plate which is used for recording the deep dent of the sample, whether there is fracture or a elastic deformation. There is a blocking system that avoids the mass to go down after the impact bouncing. Through this way a second crash is avoided, avoiding additional damage, and moreover, with the difference between kinetic and potential energy is possible to know the amount of energy that has been absorbed by the sample. The sampling frequency was set to 40 kHz for a 2 seconds period, and an amplifier was used to increase the piezoelectric tension signal.

The tests performed can be considered as low energy impact due to the low speed of the weight at the moment of the impact. Parameters can be seen in table 6.3

Drop Height [m]	**Impact velocity** [$\frac{m}{s}$]	**Impact energy** [J]
0.215	2.054	5
0.322	2.516	7.5
0.43	2.906	10

Table 6.3: Parameters of the tests

Although geometry will be presented next, it is important to observe figures 6.6 and 6.5 that show the cross-section to understand that results are not the same if impact occurs in one side, rather than in the other, as in figure 6.6 the cross-section provides an extra thickness that increases resistance to impact. This is why the panel was tested in the two sides.

The corrugated panel in which the impact occurs in the side with just one skin (figure 6.5) is going to called from now on BC-1, and the upside down one, where there is skin and corrugated cross- section in the impact zone will be called BC-2 (figure 6.6).

The BC-1 panel was tested only with 5 J, while the BC-2 was tested with 5, 7.5 and 10 J. The reason is that configuration BC-1 show less resistance and suffers from a full penetration just with 5J. The configuration BC-2 can withstand more and this is the reason why it was tested with highers speeds. Results for the panel tested at 5, 7.5 and 10 jules will be given, but just plots for the 5 jules will be given as the simulations were just run with this value.

6.2.3 FEM model

This subsection aim is to present the model prepared in ABAQUS in order to simulate the impact test carried out. By showing the FEM model geometry and configuration the characteristics of the real model will also be presented. As with the three point bending test model, the real model here is similar and was built with some similar measure specifications, regarding the length, width and the geometry and measures of the cross section and those have been the pattern to follow when creating the FEM model. This model has been meshed with C3D8R brick elements.

The model consists on a corrugated panel, with a cross-section "W" shape, which can also be called omega panel. Here the sample of the test has a four omega cross-section (one more than in the case of the three point bending test), between two flat plates or skins of 0.5 mm, and is made off with the composite that has been used through all this dissertation, compound of flax fibre and epoxy resin with the seen properties.

Some images of the model can be seen in figures 5.3, 5.4 and 5.4. Figure 5.3 shows a general view in order to have and idea of the configuration, while 5.4 shows again a general view but without the upper skin, and figure 5.5 shown a lateral view in order to see better the cross- section. Real model cross section can be seen in figure 6.7.

Main measures of the model are shown in table 6.4.

Measure	**Value [mm]**
Length	100
Width	100
Height	10
Skin thickness	0.5
Corrugated panel thickness	0.6

Table 6.4: Main measures of the three point bending test model

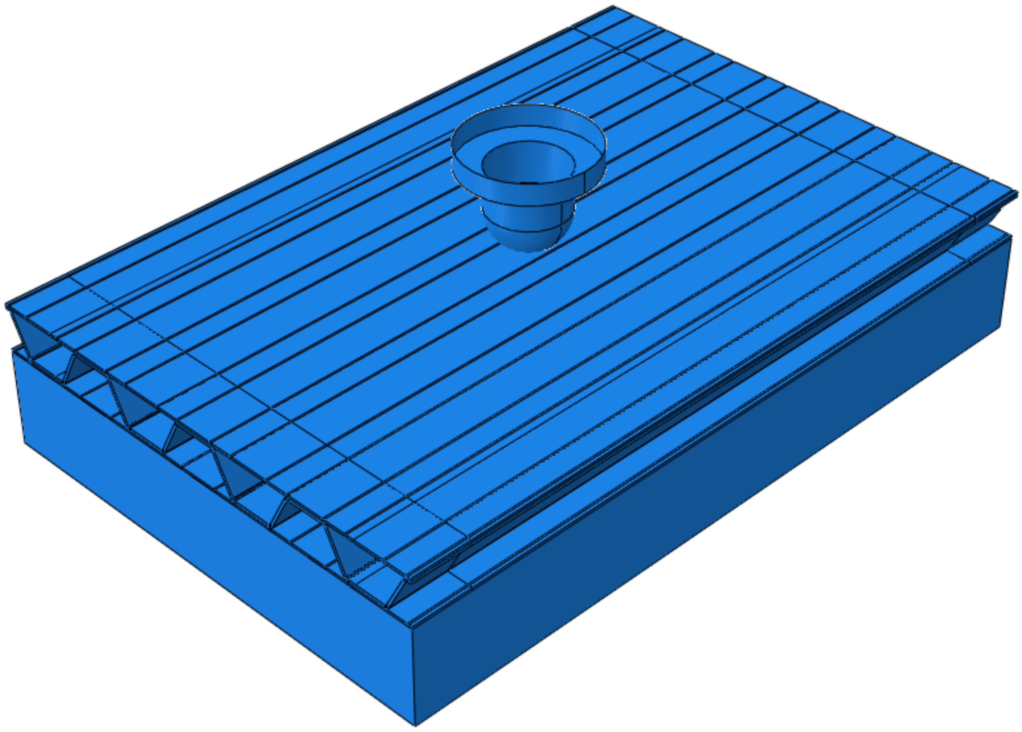

Figure 6.2: General view of the whole test setup FEM model for impact test, panel BC-2

Figure 6.2 can be used to see also the setup of the experiment. The omega panel (which can be seen alone in figure 6.3, in this case the BC-2 case) is placed on a base which acts as support, but which at the same time has all the interior hollow, in order not to interfere with the impact and allow the displacement of the inferior surface of the panel. All the panels test are mounted on this "base", which can be seen in figure 6.4. Image shows also the head of the weight used as an impactor. In the real test a mass is placed over this head in order to give it the total weight of 2.368 Kg, in ABAQUS it is possible to just mesh this head and give it the total mass. These too elements, the base and the impactor, are model as rigid since they are metallic and their stiffness is several times the one of the panel.

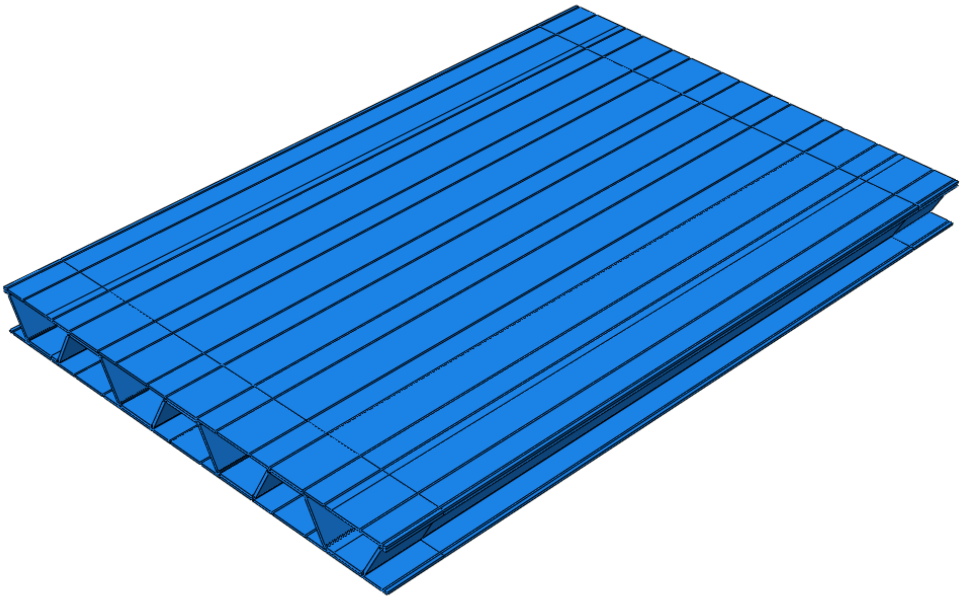

Figure 6.3: View of FEM panel for impact test ,panel BC-2

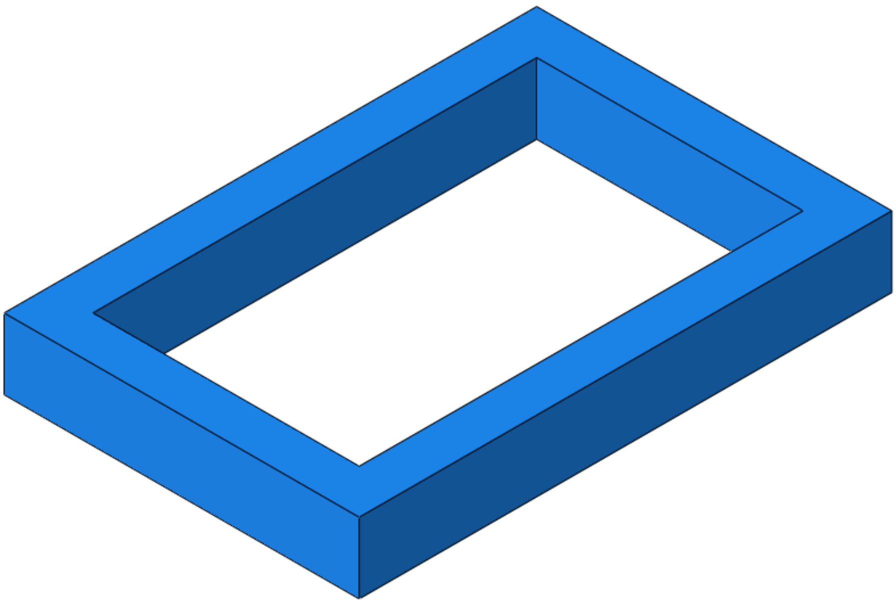

Figure 6.4: View of the FEM model of the base for the impact test

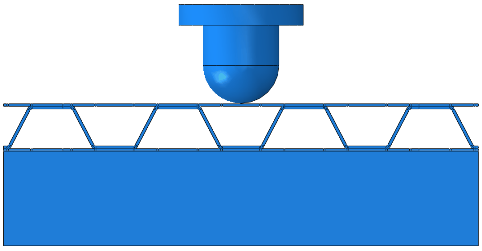

Figure 6.5: View of the cross- section of the whole test setup FEM model for impact test, panel BC-1

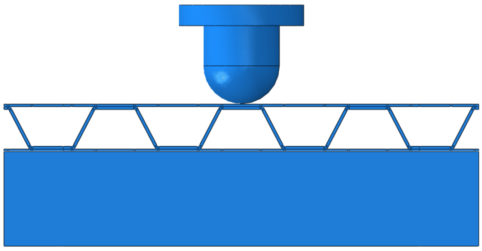

Figure 6.6: View of the cross- section of the whole test setup FEM model for impact test, panel BC-2

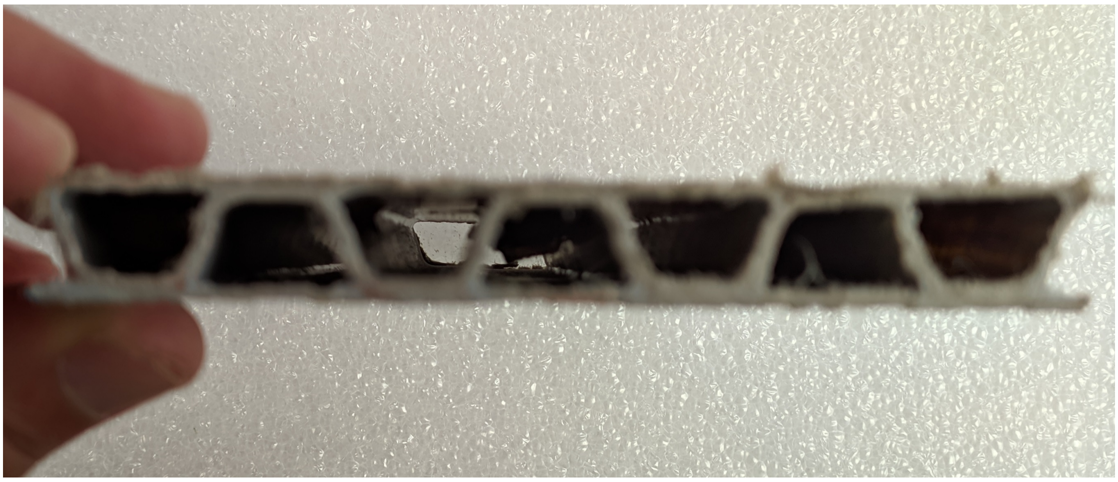

Figure 6.7: View of the cross section in real panel

The previous images, figures 6.6 and 6.5, serve to clear up what has been said before. Model BC-2, due to the configuration of the omega cross section, is provided with an extra thickness section that increases resistance to impact. This will be useful to explain the different results between the two configurations that will be presented in the next chapter.

6.2.4 Results

This section goal will be to present the different results for the 5 joules impact case with the panel with single-skin in the impact zone (BC-1) and the panel with double skin in the impact zone (BC-2). All results, both from the real tests and from ABAQUS simulations will be presented here. First, the ones from the real tests, then a series of plots comparing the results from real tests and ABAQUS (these plots will be the total reaction force in the impact weight and the displacement of the inferior face of the panel), and finally some images from the results from ABAQUS models will be shown.

In order to present the results, a classification is going to be set , depending on the degree of penetration of the lower skin. An image representing the four cases can be seen in figure 6.8

- Grade A: complete rupture and perforation
- Grade B: partial perforation, large crack (> 10 mm)
- Grade C: no perforation, small cracks (< 10 mm)
- Grade D: no perforation, no visible cracks

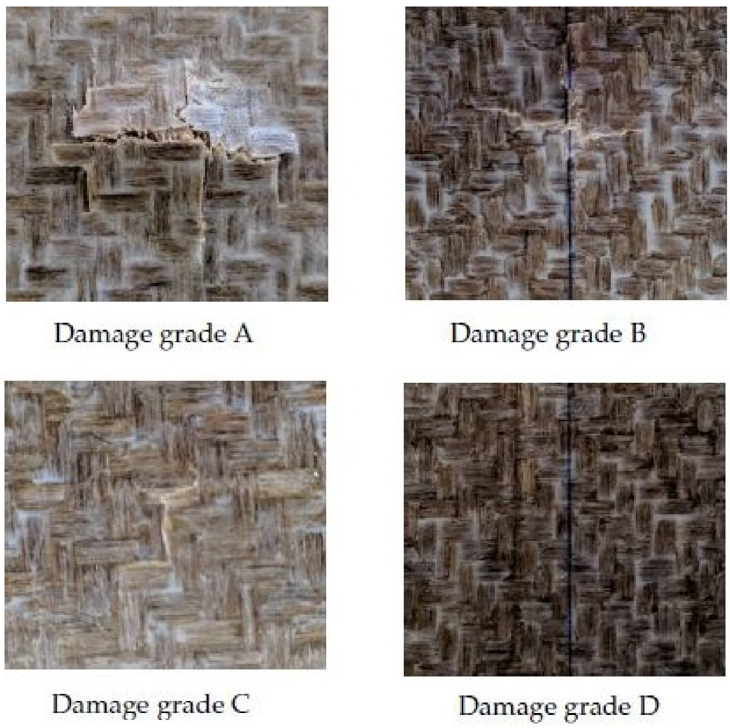

Figure 6.8: Damage classification

A table with the configurations, the kinetic energy at the impact, the residual energy based on the height achieved by the mass after the impact, and the absorbed one (the difference) and the degree of damage (based on the previous classification) of the real tests is shown below.

Experiment	**Impact velocity** $[\frac{m}{s}]$	**Impact energy [J]**	**Residual energy**	**Absorbed energy**	**Damage**
BC-1 5J	2.05	4.93	0	4.93	B
BC-2 5J	2.02	4.80	0.53	4.27	D
BC-2 7.5J	2.50	7.38	0.28	7.1	D
BC-2 10J	2.91	10	0.11	9.89	B

Table 6.5: Results of the tests

It can be seen how due to the fact that panel BC-1 is perforated by the mass, the residual energy is null, and all of it is transferred to the panel, meaning that the impact mass does not recover any energy and does not come back up. In panels BC-2 there is some residual energy. As it can be seen it is necessary to raise the energy of the impact until 10 jules for having again some perforation in the panel BC-2. In this case residual energy is very low but there is still some recover.

Al told before, the results which are going to be given are of two kinds. First one is the reaction force in the impactor (or in the panel, it is the same) as a function of time. In both cases, real test and ABAQUS, this reaction force is calculated as the acceleration of the impact weight multiplied by its mass. The other result plotted will be the displacement of the inferior skin of the panel. This combination gives a lot of information and is easily measured in the real test so data can be compared with the ABAQUS model to know if the rest of information given by ABAQUS is reliable.

Figures 6.9 and 6.10 show the results for the panel configuration BC-2. In all cases the blue curve represents the results given by ABAQUS while the green one represents the results from the test.

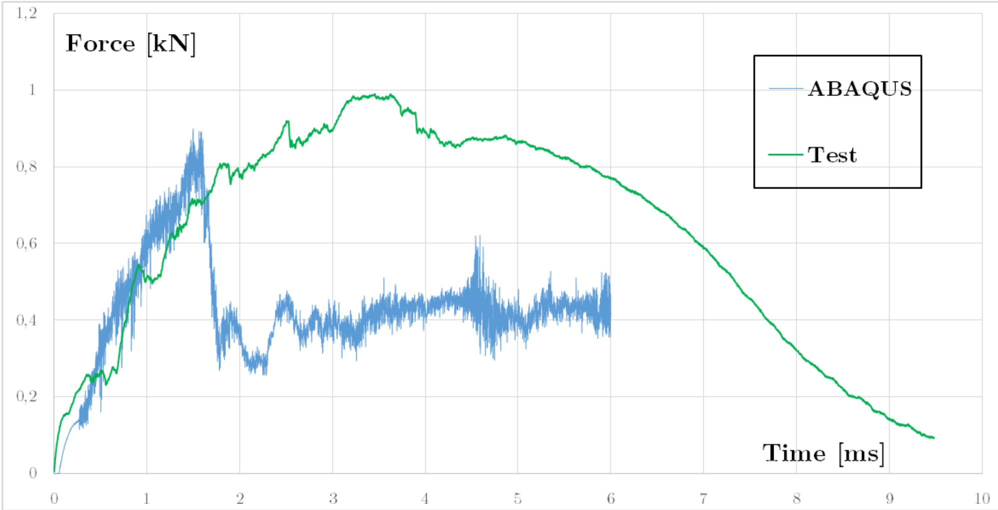

Figure 6.9: Reaction load vs Time results, BC-2 case

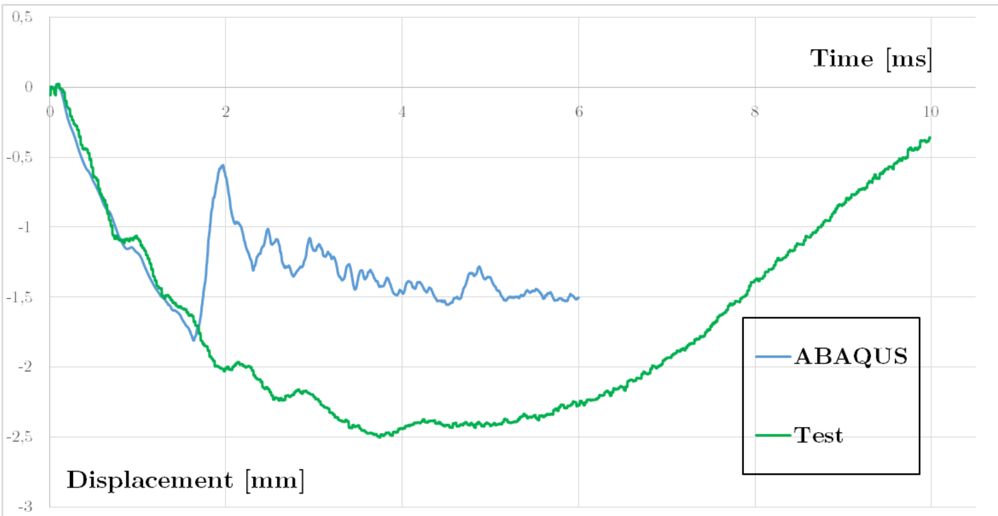

Figure 6.10: Displacement of lower skin vs time results, BC-2 case

For this case of panel, results seem to be pretty good as behaviour is very similar both for force and displacement and curves follow very well the ones of the real test until the point in which perforation of the sample occurs, at around 1.6 ms after impact.

Is at this point where results from ABAQUS diverge sharply from those of real test. Failure development seems to star at similar levels in both cases (around 900 N in ABAQUS and around 1000 N in the real test) however the failure development seems to be faster in the ABAQUS model.

As will be shown later, even though there were clear surface contact established between all the surfaces, there is some penetration between the surfaces that form the upper skin and the ones that form the cross section of the panel. Correcting this will improve results and delay the appearance of the failure damage. A parametric study seems to be a good option to improve results too. It obviously implies a lot of time, since computation time for a single analysis is around 6-7 hours, but is a reasonable way to achieve better results. Variables which may be studied are those directly related with the fracture of the elements. Should generally be studied the released fibre energy rate "G_{fib}" (a grater value would be search as a slower failure is intended), the friction coefficient of the contact between the impactor and the panel (increased value once again for the same reason). The strain at failure could also be object of the study, but the value used seem to be a good approach to reality. And finally the equation of deletion can also be modified.

Results for the VC-1 panel case are shown below, in figures 6.11 and 6.12.

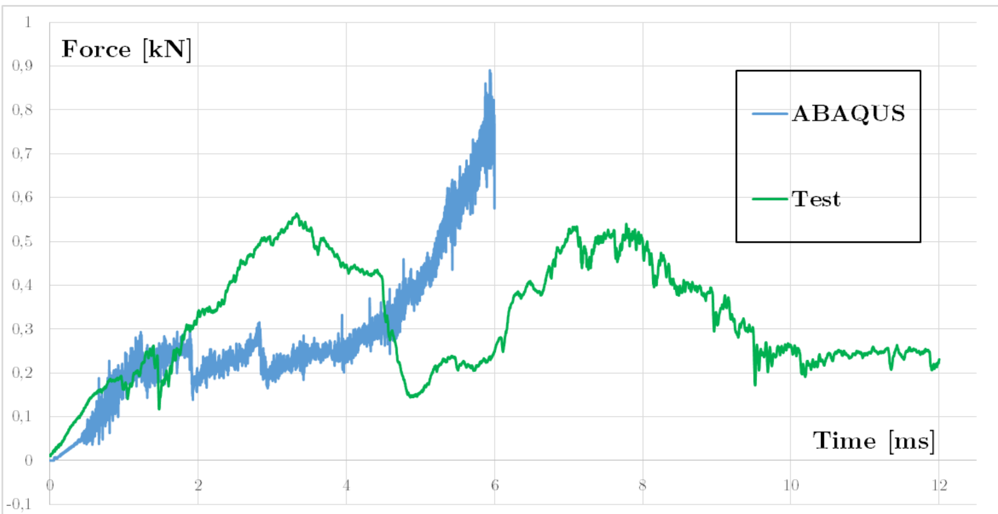

Figure 6.11: Reaction load vs Time results, BC-1 case

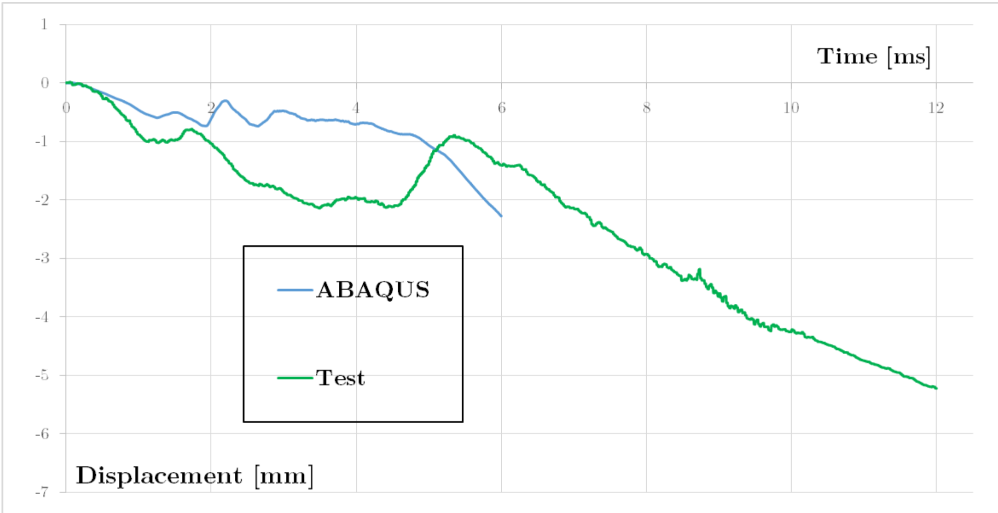

Figure 6.12: Displacement of lower skin vs time results, BC-1 case

For this case results are not as good as in the previous one. Force seem to reach the same value, around 900 N (although as would be logic, this happens in a higher time as the impact head does not find so soon the additional resistance that implies the double skin from the previous case). However maximum load in the real test is around 600 N so there is great difference. In this case it should only be taken as important the first maximum, which appears because of the failure of the first ply. The second maximum appears when the cylindrical part of the impactor arrives (this part does not belong to the impact head and it is not considered in the FEM model). The reason why this maximum appears here is that there is penetration in the inferior panel, and there is not elastic comeback as in the previous case, where the impactor "bounces" and recover some energy, so the part above the impactor crashes with the panel.

Once again here a parametric study involving the different variables which are directly related with the failure damage can help to improve the results. Variables which can be object of the study are the same as in the previous case. The duration of the time in the step of the ABAQUS tests should also be slightly increased, for both cases, in order to represent the drop of the load curve after the maximum.

To continue images from the real tests will be shown. Figures 6.13 and 6.14 show the BC-2 panel case. In figure 6.13 it is seen how the impactor has perforated the upper skin, but figure 6.14 show how the lower skin is almost intact. Meanwhile figures 6.15 and 6.16 show the BC-1 panel case. For this case it can be seen in this last figure how the impactor has perforated the lower skin. In both cases the samples had undergone the 5 joules test.

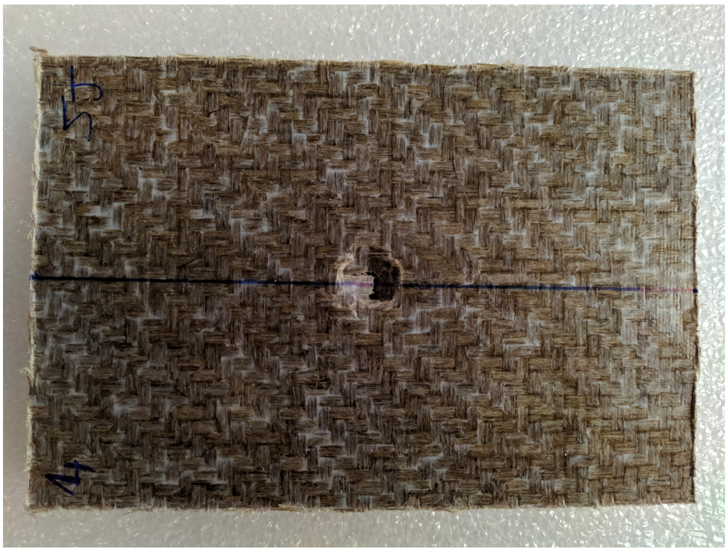

Figure 6.13: View of the upper skin after impact, BC-2 panel

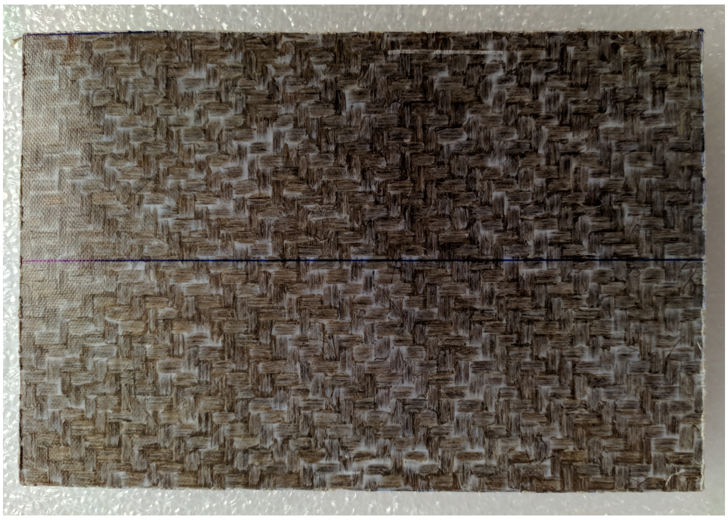

Figure 6.14: View of the lower skin after impact, BC-2 panel

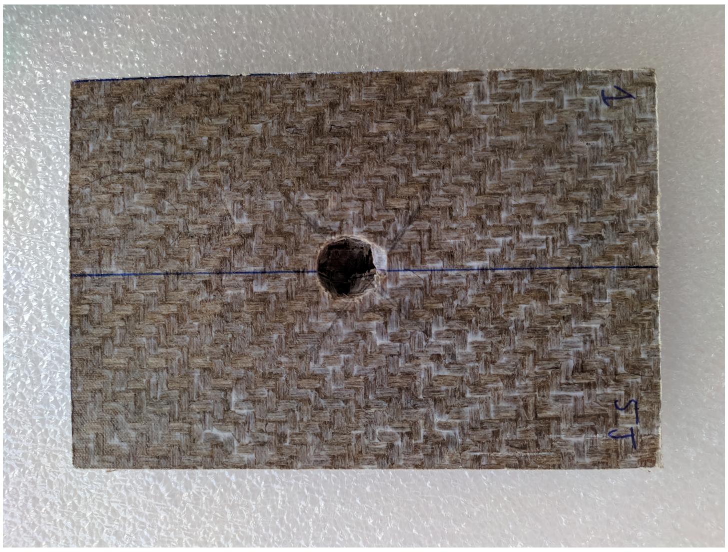

Figure 6.15: View of the upper skin after impact, BC-1 panel

Figure 6.16: View of the lower skin after impact, BC-1 panel

To conclude this chapter, images of the ABAQUS simulations will be shown.

ABAQUS prints, BC-2 case

Figure 6.17 shows a general upper view of the impact, without the impactor. Figure 6.18 shows the final instant with the impactor (which appears in white due to its rigid condition). Von misses stress is shown in some of the following images although it is inappropriate to show this kind of criteria since the material is a composite. Anyway with these images it is not intended to show results in stress but just a general idea of the simulation.

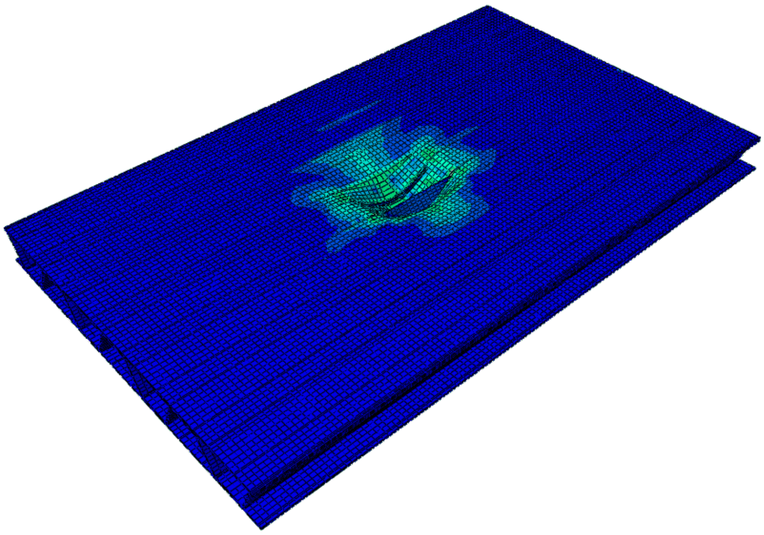

Figure 6.17: General view of the impact, BC-2

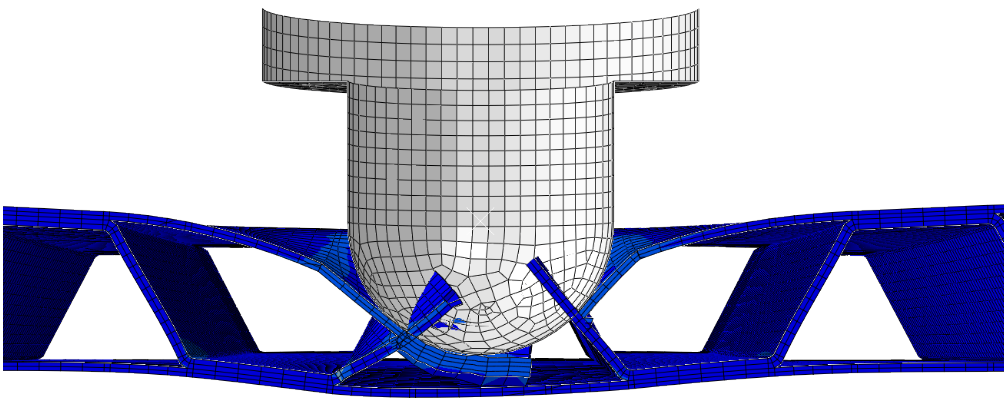

Figure 6.18: Cut view of impact, final time, BC2-case

Figures 6.19 to 6.21 show a cut view of the panel, just in the impact zone. In figures 6.19, 6.20 and 6.21 the impactor has been removed in order to show better the impact zone. These images are from instants $t = 0.6\ ms$, $t = 2.1\ ms$ and $t = 6\ ms$ and they let to see the sinking of the panel as the impactor advances. It is seen in 6.21 how the omega cross section crosses the upper skin, even a contact condition was defined between the two surfaces.

This cross of the two surfaces is important as it is from the penetration when results are being affected. Had it not been so, panel would show a higher resistance and failure would not be so fast, so results would be better. Model shall be improved in the future to avoid this. Unfortunately the shutdown of research facilities caused the author to run out of time to perform more simulations.

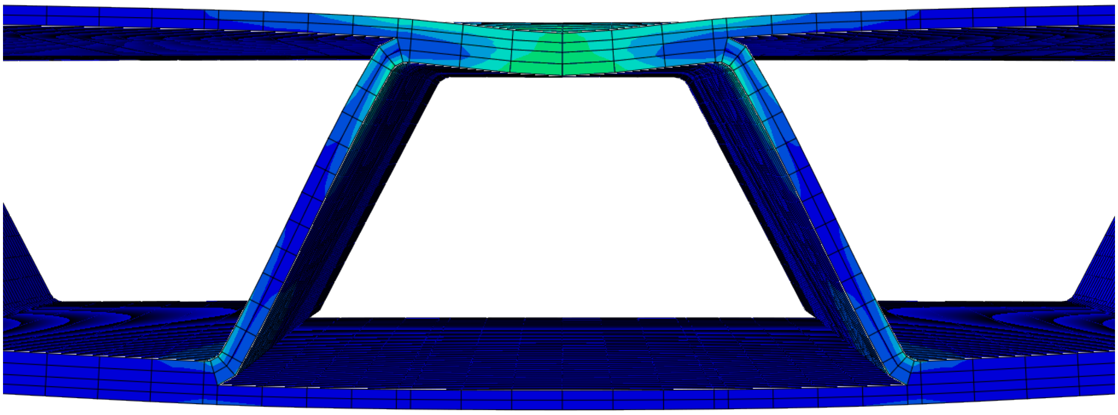

Figure 6.19: Cut view of impact, time =0.6 ms, BC-2 case

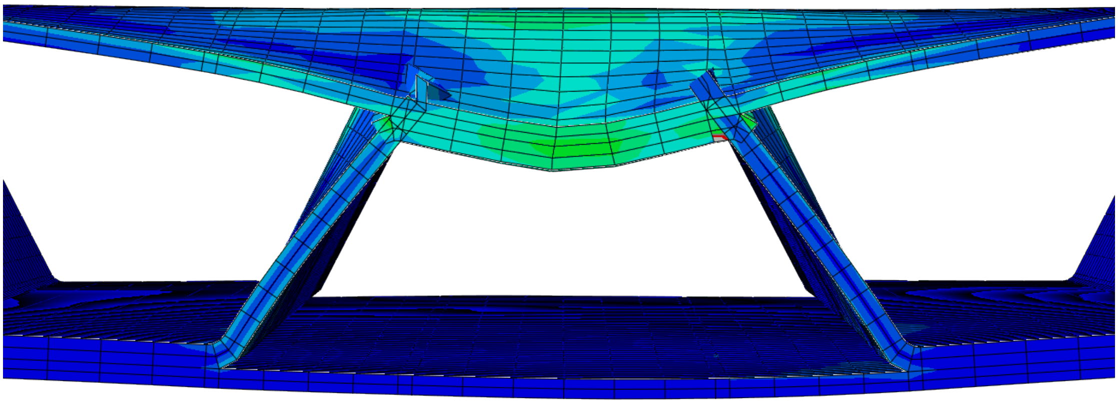

Figure 6.20: Cut view of impact, time =2.1 ms, BC-2 case

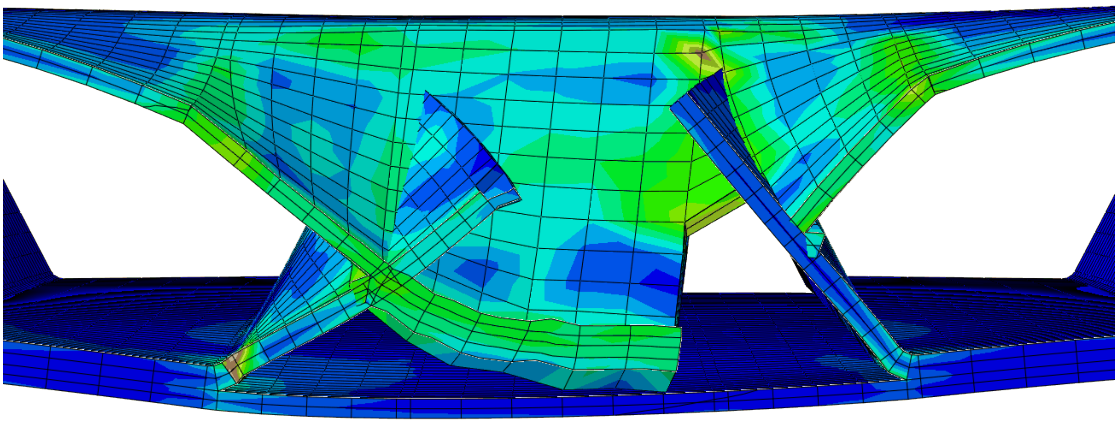

Figure 6.21: Cut view of impact, time =6 ms, BC-2 case

Figure 6.20 shows penetration of the cross section into the upper skin. This penetration begins around $time = 1.7\,ms$, just when results start to diverge from the ones from real test, so it seems very clear that this fact has affect the results.

Figures 6.22 to 6.31 will show the SDV value associated to each one of the ten existing damages (five for diffuse and five for failure). The images are once again from the impact zone and model has been cut. Table 6.6 indicates the different damages that have been associated with each SDV. For identifying damages through the SDV, the images captions should be payed attention, but not the images legends.

SDV	Magnitude
SDV 1	Failure fibre damage, 11 direction
SDV 2	Failure fibre damage, 22 direction
SDV 3	Failure matrix damage, 12 direction
SDV 4	Failure matrix damage, 23 direction
SDV 5	Failure matrix damage, 13 direction
SDV 6	Diffuse fibre damage, 11 direction
SDV 7	Diffuse fibre damage, 22 direction
SDV 8	Diffuse matrix damage, 12 direction
SDV 9	Diffuse matrix damage, 23 direction
SDV 10	Diffuse matrix damage, 13 direction

Table 6.6: SDV association

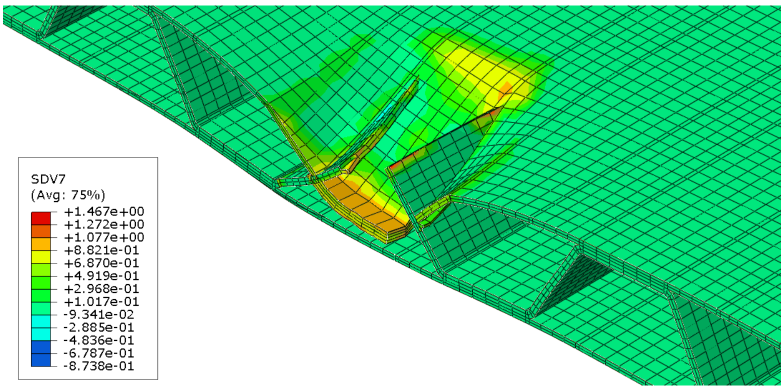

Figure 6.22: Cut view, SDV 1, BC-2 case

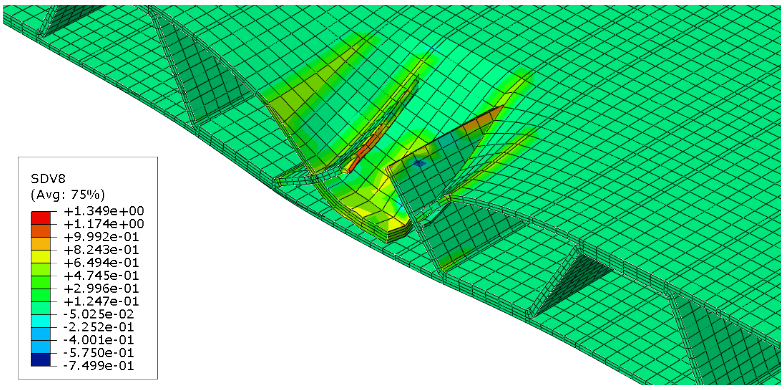

Figure 6.23: Cut view, SDV 2, BC-2 case

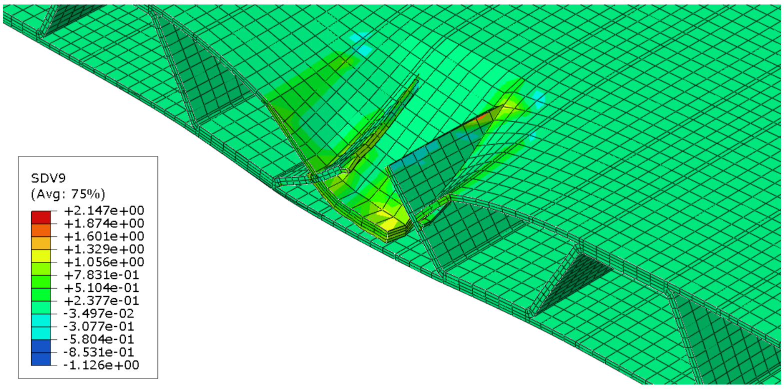

Figure 6.24: Cut view, SDV 3, BC-2 case

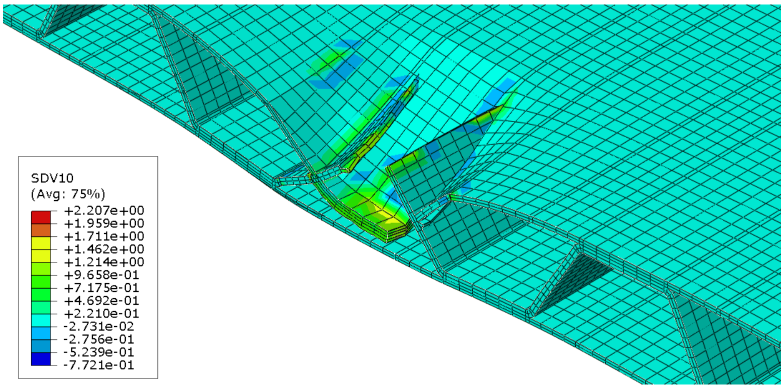

Figure 6.25: Cut view, SDV 4, BC-2 case

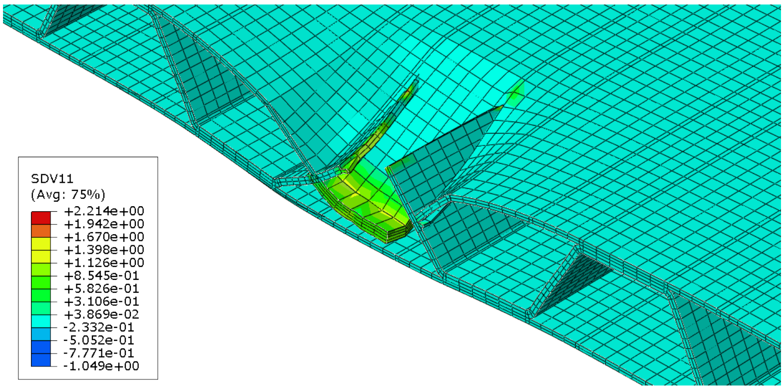

Figure 6.26: Cut view, SDV 5, BC-2 case

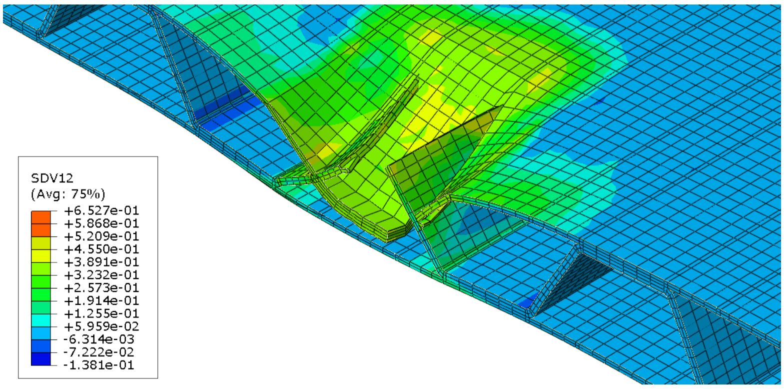

Figure 6.27: Cut view, SDV 6, BC-2 case

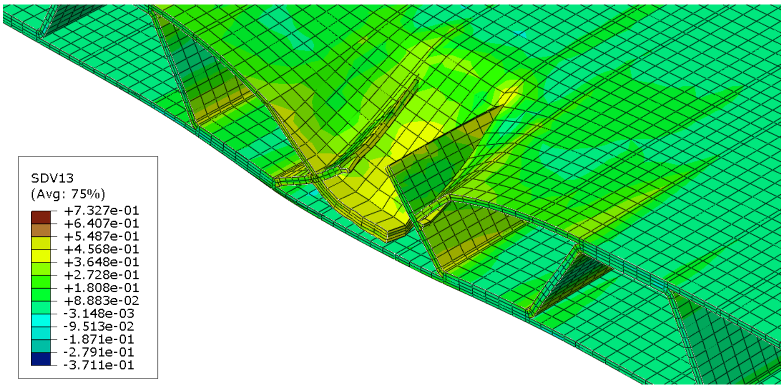

Figure 6.28: Cut view, SDV 7, BC-2 case

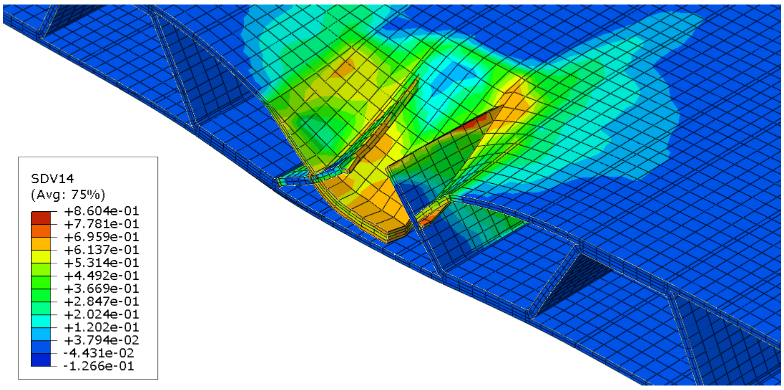

Figure 6.29: Cut view, SDV 8, BC-2 case

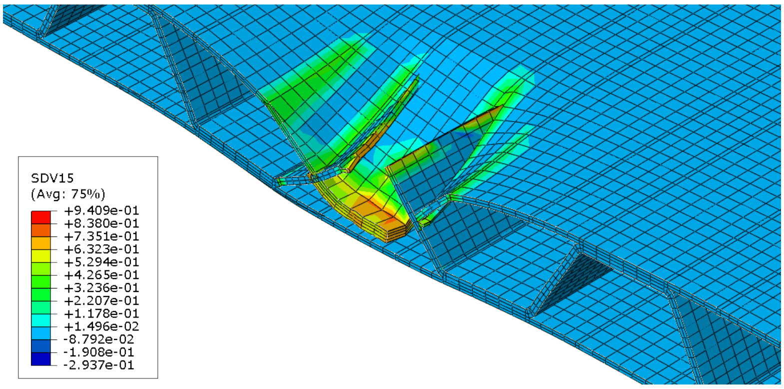

Figure 6.30: Cut view, SDV 9, BC-2 case

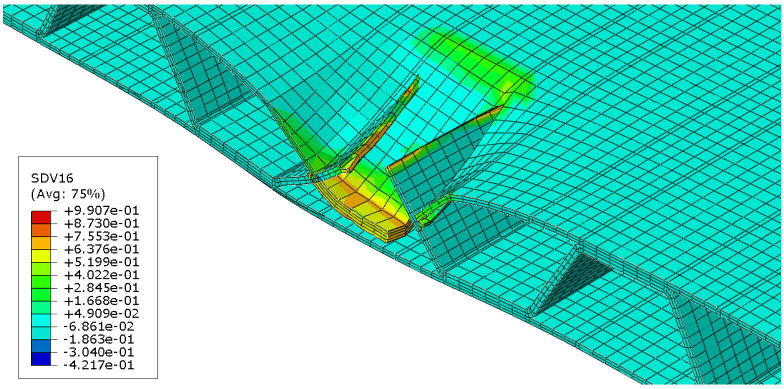

Figure 6.31: Cut view, SDV 10, BC-2 case

ABAQUS prints, BC-1 case

Printed images from ABAQUS will be now shown for the BC-1 panel case. Figure 6.32 shows a general upper view of the impact, with the impactor (which appears in white due to its rigid condition). Figure 6.33 shows a cut view of the impact zone at the final instant without the impactor.

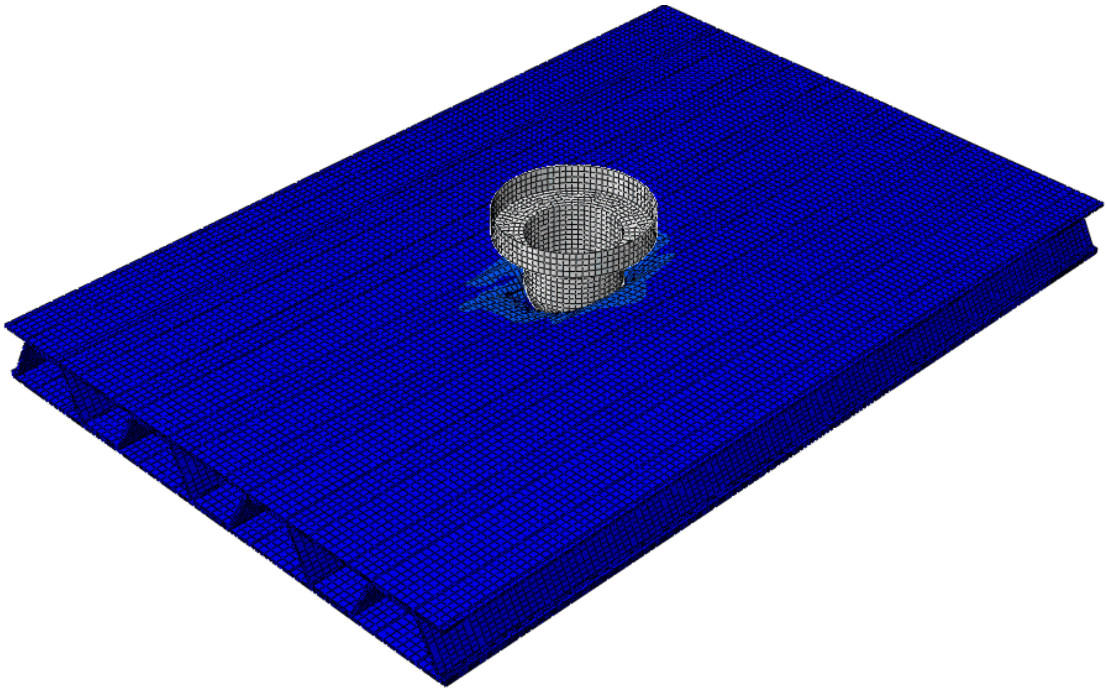

Figure 6.32: General view of the impact, BC-1 case

Figures 6.33 to 6.35 show cut views of the panel for different instants. As before, impactor has been removed in order to show better the impact zone. These images are from instants $t = 1.2\,ms$, $t = 3\,ms$ and $t = 6\,ms$ and they let to see the evolution of the bending and sinking of the panel. Here there is no the same problem as before, sections crossing between them, as it is not possible due to the geometric configuration. It is seen in figure 6.34 the first instant in which there occurs deletion of elements, which coincides approximately in time with the real penetration of the upper skin.

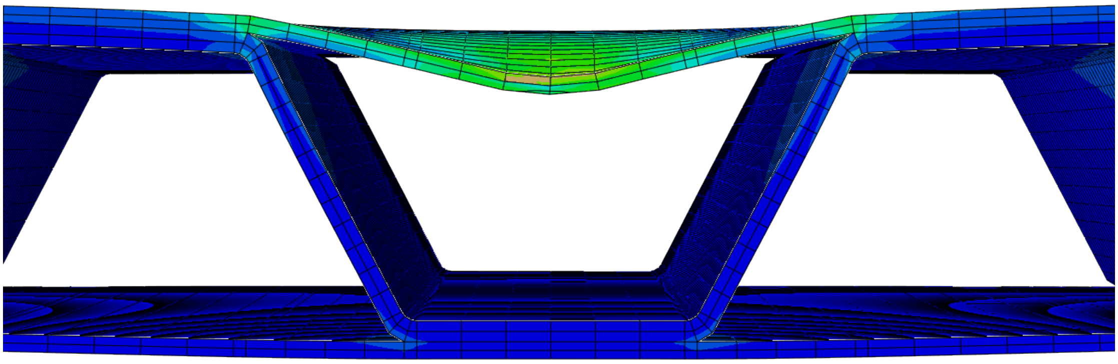

Figure 6.33: Cut view of impact, time =1.2 ms, BC1 case

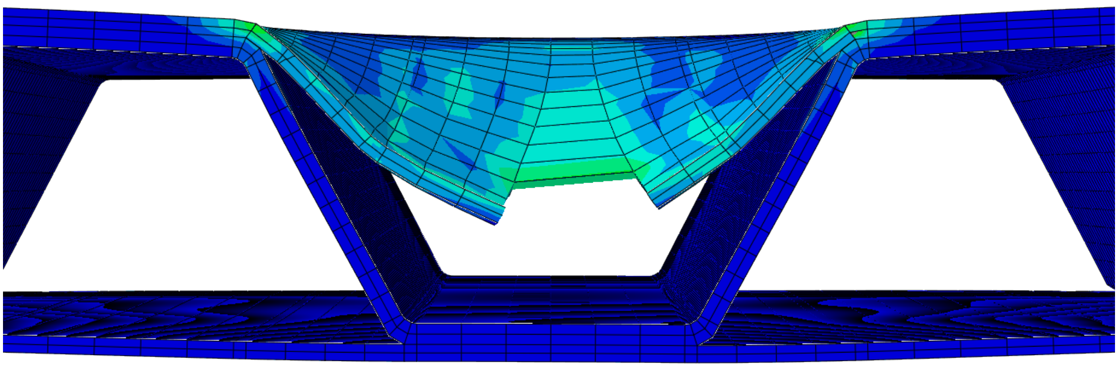

Figure 6.34: Cut view of impact, time =3 ms, BC1 case

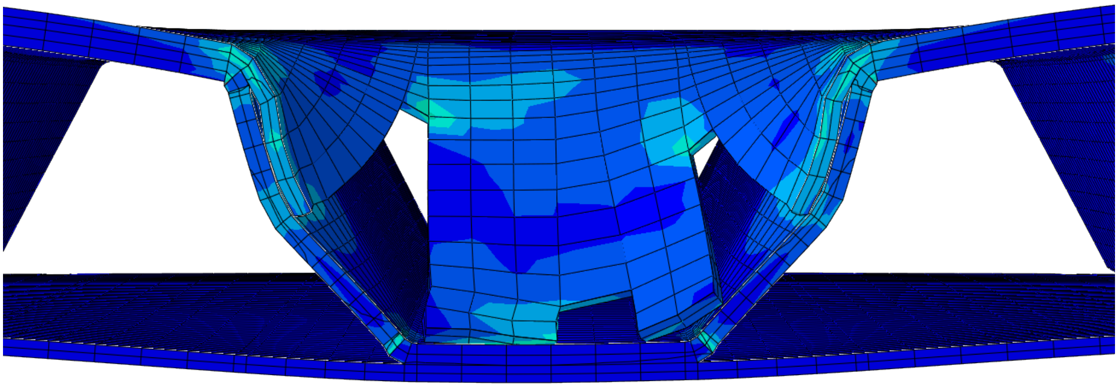

Figure 6.35: Cut view of impact, time =6 ms, BC1 case

Figures 6.36 to 6.45 will show the SDV value associated to each one of the ten existing damages (five for diffuse and five for failure). The images are once again from the impact zone and model has been cut. The same table used in the previous case, table 6.6, is valid for indicating the different damages that have been associated with each SDV. For identifying damages through the SDV, the images captions should be payed attention, but not the images legends.

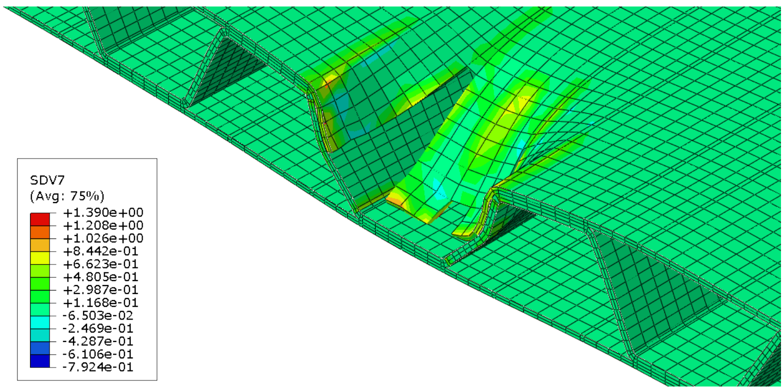

Figure 6.36: Cut view, SDV 1, BC-1 case

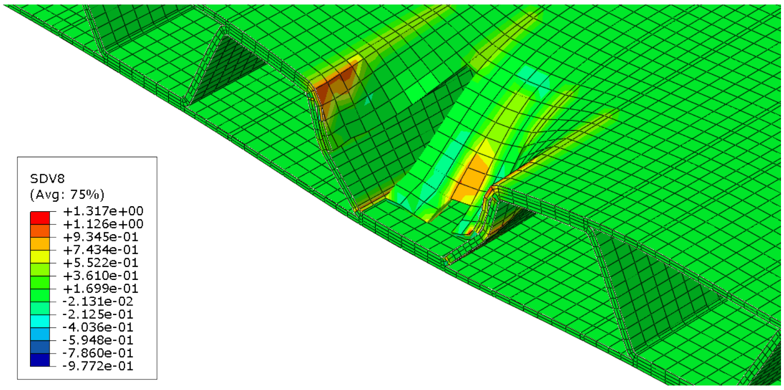

Figure 6.37: Cut view, SDV 2, BC-1 case

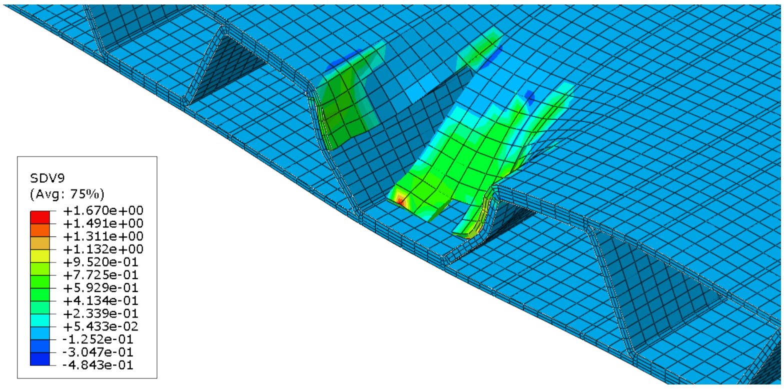

Figure 6.38: Cut view, SDV 3, BC-1 casek

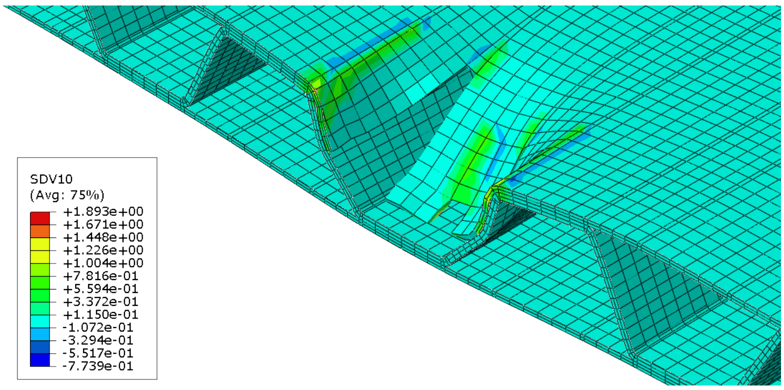

Figure 6.39: Cut view, SDV 4, BC-1 case

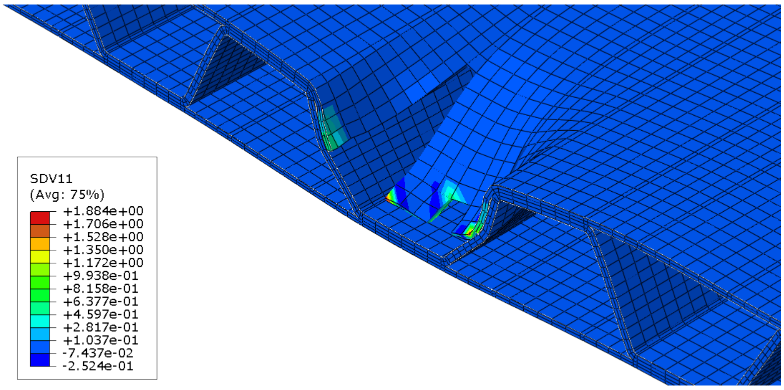

Figure 6.40: Cut view, SDV 5, BC-1 case

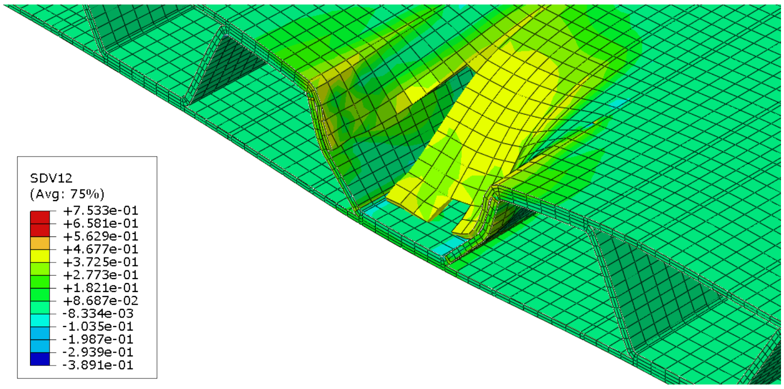

Figure 6.41: Cut view, SDV 6, BC-1 case

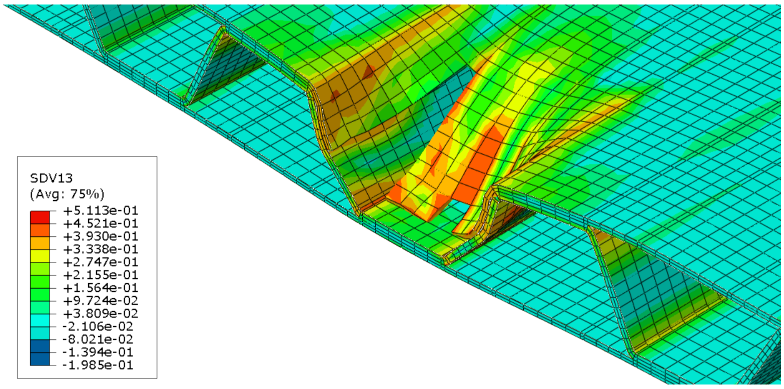

Figure 6.42: Cut view, SDV 7, BC-1 case

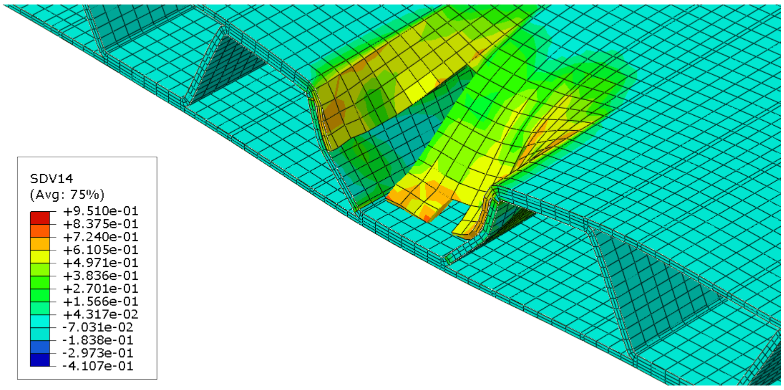

Figure 6.43: Cut view, SDV 8, BC-1 case

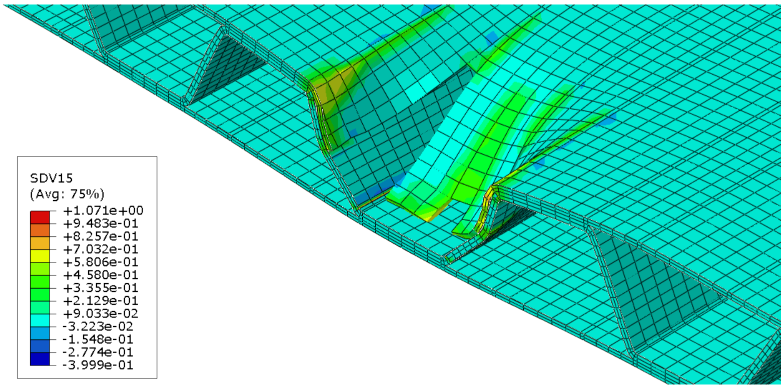

Figure 6.44: Cut view, SDV 9, BC-1 case

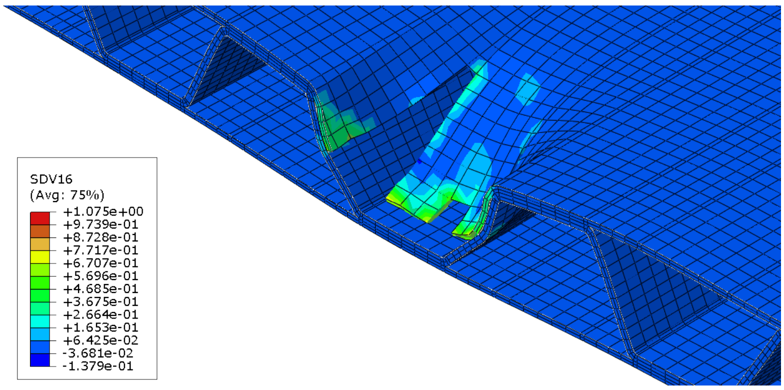

Figure 6.45: Cut view, SDV 10, BC-1 case

Chapter 7

Conclusions

The main objective of this thesis was the characterization of properties and the creation and testing of damage models able to reproduce the behaviour and mechanics exhibit by panels made from natural fibres, particularly the flax fibre. Understanding the behaviour of these materials and being able to predict how are they going to react under different types of loads is a key aspect in order to delve into in their knowledge. This will allow an spread, commercialization and in the end, an increased use with the time. In this sense the creation of models to reproduce this behaviour has become even more logical with the popularisation and improvement of current FEM programs. If a good model is used, simulations run with these tools can predict very well the global behaviour and help in the comprehension, saving a lot of time and resources, and ultimately, money.

Damage models created were tested through two real tests, one static (3PBT), and one dynamic (impact test), that were compared with the simulations done with ABAQUS. In addition, one property, the fibre energy released rate, was aimed to characterize, due to its great importance for this damage model. Therefore conclusion will deep into these three aspects.

Regarding the three points bending test, results are, overall, very positive. Real results show a relatively big non linear response. The reason to these non linearities has been explained in chapter three. A model was prepared in ABAQUS and the subroutine UMAT, which was partially written at the beginning, was corrected and finished, implementing the Jacobian, instead of an approximation. Model implemented has proven to be able to replicate the non linear behaviour pretty good. In addition, mechanism of failure has been the same in both the tests and the simulation, the failure due to the buckling of the upper skin. Results could improve if a better way to calculate the *celent* were implemented, something in which a lot of time was spent but that could not be achieved in the end. Another way to have more accurate results would be to use more accurate values of the main properties that affect the damage models and the stiffness matrix. These parameters are those of table 2.1 and table 4.3. However it makes more sense to do this for a real application where a simulation would be run beforehand and would help to predict some results. In this stage of validating a model this does not seem so necessary.

Regarding the impact test results are not that positive. The VUMAT routine was written from zero. Having already a good version of UMAT is helpful, but this is anyway a very time consuming task. A model was prepared in ABAQUS too. Results have shown to be good until a degree of penetration of the impactor. More was discussed on chapter 6, but failure seems to be faster in the simulations than in reality. As told in there, model has some contact issues that need to be solved. Regarding the damage model, a parametric study could help too in order to try to approach both results. Unfortunately, once the model and the routine were prepared, shutdown of universities and research facilities occurred due to the spread of Covid-19. Two simulations were launch from home in order to have some results but there was not time for more.

Regarding the characterization of the fibre energy released, results are positive but Covid-19 emergency once again did not allow to complete all the work intended. Simulations with ABAQUS show that the UMAT model did work and show results according with the value for G_{fib} used. Moreover, comparisons between the UMAT subroutine (with just failure damage model) and the ABAQUS implemented tool "Cohesive property" show great similarity between the two ways of modeling the failure, with very similar curves. Test would have helped to have a correct value of G_{fib} and results could have been compared with an ABAQUS simulation using the routine with both failure and diffuse damage activated. Unfortunately, as told, test was left for mid- march and once again due to Covid-19 emergency it could not be conducted.

7.1 Future perspectives

Now that all the models are done and the two subroutines UMAT and VUMAT are fully written future perspectives are good. Work could focus on trying to improve the models through the commented means. An internal subroutine in order to correct the *celent* of each element is a good way of improving the model. Parametric study will also help improving the results in both the static and dynamic simulations. Conducting the released fibre energy rate will characterise this value, something that will improve the failure model too and help to obtain better results.

Appendix A

Subroutine Orient

This appendix is intended to explain the functioning of the small routine orient created.

As explained in the main text, the objective is to get from ABAQUS what will be called here *FLENGTH*, this is, the dimension of the element perpendicular to the fibre and that is contained in the ply (or the dimension of the element that is perpendicular to the fibre and perpendicular to the stacking direction). ABAQUS routines UMAT and VUMAT give a magnitude that is called *CELENT* (stands for characteristic element length). However this magnitude is not the one desired, as this magnitude is calculated by ABAQUS as the cubic root of the volume for a volumetric element, and as the square root of the area in a surface element. So this would match with the desired length (*FLENGTH*) just in the case in which all the model of ABAQUS were meshed with perfect cube elements. This is normally impossible as it has been already told.

When looking of ways to calculated the desired length, through the means proportioned by ABAQUS, the most clear one seems to get something from ABAQUS that allows to compute this dimension, ideally the coordinates of the nodes of the element. Unfortunately, coordinates of the nodes are not a magnitude use as an input in the UMAT or VUMAT subroutine. However, it is a magnitude which can be used as an input in the subroutine ORIENT, so this is the reason why this subroutine has been the chosen one.

First thing to say is that if the ABAQUS .inp file is ran with this routine, with just one core, this routine will be executed as many times as the number of existent Gauss points of each element. This is, if there are three C3D8R elements, routine will be executed first for Gauss point 1 of element 1, then Gauss point 2 of element 1, Gauss point 3 of element 1... when it has finished with element 1 it will pass to element 2, and later to element 3. In this case it will be executed a total of 24 times (3 elements and 8 Gauss points per element). Routine is executed in this order, from Gauss point 1 to 8 and from the lowest numbered element to the highest numbered one. Ideally, it would be desired that the routine were executed just one time for each element, as the *FLENGTH* is associated to all the element, there is not a different *FLENGTH* for each Gauss point inside the same element. Anyway this will be controlled in the subroutine. However, passing the *FLENGTH* value obtained in this subroutine to the main one, UMAT or VUMAT, has been found to be troublesome. The method used here writes this value in a .txt file. In this .txt file they are written in two columns the number of element and the value for the *FLENGTH*. After this, the main routine (UMAT or VUMAT) would open the .txt file to read it and pick the value for each element. Obviously the writing must be done ordered so that the reading is done ordered too. This has been found to be done correctly when the computation is just done with one core, but there have appeared problems when computation is done with more than one. Basically what is happening here is that the several computers are executing the subroutine and routine at the same time (as each core has associated a series of elements, this is basically what parallel computation does to be faster, dividing the problem). As the subroutine is now execute several times at the same time, the same happens with the writing of the file (so this writing is not anymore in order) and the same happens when UMAT or VUMAT read this file with the *FLENGTH* values. All this is very troublesome and could not be solved, so this subroutine was just used for the released fibre energy rate model, as this model could be run with just one core due to its greater simplicity and reduced computation time when compared with the 3PBT and impact test models.

First thing to do is to define the matrix called T. T is defined in ABAQUS documentation as "An array containing the direction cosines of the preferred orientation in terms of the default basis directions. T(1,1), T(2,1), T(3,1) give the (1, 2, 3) components of the first direction; T(1,2), T(2,2), T(3,2) give the second direction; etc. For shell and membrane elements only the first and second directions are used. The directions do not have to be normalized. If the second direction is not orthogonal to the first direction, ABAQUS/Standard will orthogonalize and normalize the second direction with respect to the first. The third direction is then determined by taking the cross product of the first and second directions. For planar elements the first two directions must lie in the plane of the element". This basically means that if T is defined as a unit matrix, the fibre direction will be the x direction of the global coordinates, the in-ply 90º direction will be the y direction of the global coordinates and the stacking direction will be the one of z in the global coordinates.

In order to understand what has been done the routine will be explained together with the model prepared for the released fibre energy rate, to understand the limitations of the routine, which are several.

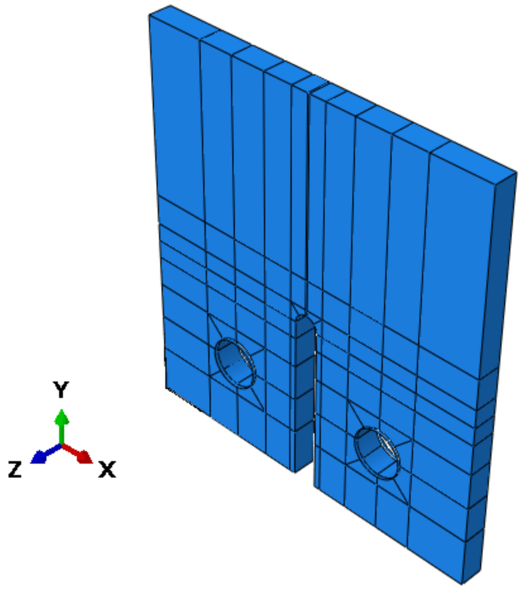

Figure A.1: Model used

As can be seen in the image, the model has been placed and oriented inside the assembly so that the fibre warp direction points towards the global x global, the fibre weft direction points towards the global y direction, and the stack direction points towards the z global direction. Knowing this, in clear that for this *specific* case the T matrix has to be defined as a unit matrix.

$$T = \begin{pmatrix} 1 & 0 & 0 \\ 0 & 1 & 0 \\ 0 & 0 & 1 \end{pmatrix}$$

Two variables are after given a value. These variables where called in the routine "CAS" and "VAR". CAS represent the *FLENGTH*, while VAR is just used for control. CAS is given an impossible random value (in this case a negative value, as it is a length), while VAR is given a 0 value.

```
CAS=-10

VAR=0


DO I=2,NNODES
  IF (VAR .EQ. 0) THEN

              IF (((T(1,1) .NE. 0 ) .AND. (T(2,2) .NE. 0))   .OR.  ((T(3,1) .NE. 0 ) .AND. (T(2,2) .NE. 0))) THEN

                         IF   ((ABS(CNODES(1,1)-CNODES(1,I)) .LT. 0.001 )   .AND.  (ABS(CNODES(3,1)-CNODES(3,I))  .LT. 0.001 )) THEN

                                CAS=((CNODES(1,1)-CNODES(1,I))**TWO+(CNODES(2,1)-CNODES(2,I))**TWO+(CNODES(3,1)-CNODES(3,I))**TWO)**HALF
                                VAR=1

                         END IF


              ELSE IF  (((T(1,1) .NE. 0 ) .AND. (T(3,2) .NE. 0))   .OR.  ((T(2,1) .NE. 0 ) .AND. (T(3,2) .NE. 0))) THEN

                         IF   ((ABS(CNODES(1,1)-CNODES(1,I)) .LT. 0.001 )   .AND.  (ABS(CNODES(2,1)-CNODES(2,I))  .LT. 0.001 )) THEN

                                CAS=((CNODES(1,1)-CNODES(1,I))**TWO+(CNODES(2,1)-CNODES(2,I))**TWO+(CNODES(3,1)-CNODES(3,I))**TWO)**HALF
                                VAR=2

                         END IF


              ELSE IF  (((T(2,1) .NE. 0 ) .AND. (T(1,2) .NE. 0))   .OR.  ((T(3,1) .NE. 0 ) .AND. (T(1,2) .NE. 0))) THEN

                         IF   ((ABS(CNODES(2,1)-CNODES(2,I)) .LT. 0.001 )   .AND.  (ABS(CNODES(3,1)-CNODES(3,I))  .LT. 0.001 )) THEN

                                CAS=((CNODES(1,1)-CNODES(1,I))**TWO+(CNODES(2,1)-CNODES(2,I))**TWO+(CNODES(3,1)-CNODES(3,I))**TWO)**HALF
                                VAR=3
                         END IF

              END IF

  END IF
END DO
```

Figure A.2: Code

After this, the routine has a loop that is going to calculate this *FLENGTH* distance. An image above shows the code.

The loop goes from 2 to the number of nodal points of the element that contains the Gauss point that is being executed in that moment. After it there is one "if" for checking if the value of "VAR" is equal to zero. If it is not zero this basically means that loop has already been gone across and a value for "CAS" has already been given.

Taking into account that if a coordinate system is rotated (that would be the one pointing warp, weft and stacking directions) around another one (that would be the general one), but keeping always the axis pointing towards the directions of the axis of the general one (or the oppose direction), it can be proven that for calculating *FLENGTH* there are just three cases, that can be separated according to three different conditions for the T matrix, that are specified in each of the three "IF" conditions. If any of these "IF" conditions is true the value "CAS" is calculated (this "CAS" represents *FLENGTH* as told) and the value of "VAR" is changed so the loop is interrupted and computation exits from it.

The "IF" condition inside is just for ensuring that the *FLENGTH* calculated is the correct one and is here where the loop for the number of nodes is used. This condition and the calculus varies depending of the case among the three ones told.

Control of assignation could have been done with just one variable "CAS", instead of including "VAR" too but inserting an external variable for this control allows more flexibility in case of any change.

After this, "CAS" and "NOEL" are written in a .tex file that is later opened by UMAT or VUMAT. If the element is not a cuboid (each of the faces is a rectangle and each pair of adjacent faces meets in a right angle) and its edges are not contained in the x, y and z global axes, then the loop is done without entering in any "if" condition and "VAR" remains with value 0, while "CAS" remains with its negative random value given at the beginning. If this happens, this random value is written and read after by UMAT or VUMAT. UMAT or VUMAT have an "if" condition by which they have to use the approximation given by *CELENT* if they read this random negative (and therefore impossible) value for an element in the .txt file.

As a summary, this subroutine cannot be used if elements are not a cuboid and their edges are not contained in the x, y and z global axes. It is responsibility of the user to define matrix T according to how has he placed the part in the assembly. If there were more than two parts with different orientations, more than one subroutine ORIENT should be used (procedure is similar to using more than one UMAT or VUMAT when there are several different materials that required it). Finally it also cannot be used if parallel computation is going to be used, computation is restricted to one core.

Appendix B

Jacobian

This appendix is intended to explain the mathematical background behind the calculus of the Jacobian matrix.

As it has been seen the equation that relates the stresses and the strains is, as seen in equation 2.1:

$$\vec{\sigma} = \overline{\overline{C}} : \vec{\epsilon} \tag{B.1}$$

For the 3D case of stresses this can be developed as:

$$\begin{bmatrix} \sigma_1 \\ \sigma_2 \\ \sigma_3 \\ \sigma_4 \\ \sigma_5 \\ \sigma_6 \end{bmatrix} = \begin{bmatrix} C_{D11} & C_{D12} & C_{D13} & 0 & 0 & 0 \\ C_{D21} & C_{D22} & C_{D23} & 0 & 0 & 0 \\ C_{D31} & C_{D32} & C_{D33} & 0 & 0 & 0 \\ 0 & 0 & 0 & C_{D44} & 0 & 0 \\ 0 & 0 & 0 & 0 & C_{D55} & 0 \\ 0 & 0 & 0 & 0 & 0 & C_{D66} \end{bmatrix} \begin{bmatrix} \epsilon_1 \\ \epsilon_2 \\ \epsilon_3 \\ \epsilon_4 \\ \epsilon_5 \\ \epsilon_6 \end{bmatrix} \tag{B.2}$$

Stress and strain vector can be expressed with several notations.

$$\vec{\sigma} = \{\sigma_1 \;\; \sigma_2 \;\; \sigma_3 \;\; \sigma_4 \;\; \sigma_5 \;\; \sigma_6\}^T = \{\sigma_{11} \;\; \sigma_{22} \;\; \sigma_{33} \;\; \tau_{12} \;\; \tau_{13} \;\; \tau_{23}\}^T \tag{B.3}$$

$$\vec{\epsilon} = \{\epsilon_1 \;\; \epsilon_2 \;\; \epsilon_3 \;\; \epsilon_4 \;\; \epsilon_5 \;\; \epsilon_6\}^T = \{\epsilon_{11} \;\; \epsilon_{22} \;\; \epsilon_{33} \;\; \gamma_{12} \;\; \gamma_{13} \;\; \gamma_{23}\}^T \tag{B.4}$$

Below it is seen the variable dependence of each term with the different strains, necessary in order to differentiate.

$$
\begin{gathered}
\sigma_{11} = C_{D11}(\epsilon_1)\ \epsilon_1 + C_{D12}(\epsilon_1, \epsilon_2)\ \epsilon_2 + C_{D13}(\epsilon_1, \epsilon_2)\ \epsilon_3 \\
\sigma_{12} = C_{D12}(\epsilon_1, \epsilon_2)\ \epsilon_1 + C_{D22}(\epsilon_2)\ \epsilon_2 + C_{D23}(\epsilon_2, \epsilon_4)\ \epsilon_3 \\
\sigma_{33} = C_{D13}(\epsilon_1, \epsilon_2)\ \epsilon_1 + C_{D23}(\epsilon_2, \epsilon_4)\ \epsilon_2 + C_{D33}(\epsilon_1)\ \epsilon_3 \\
\sigma_{44} = C_{D44}(\epsilon_1, \epsilon_2, \epsilon_4)\ \epsilon_4 \\
\sigma_{55} = C_{D55}\ \epsilon_5 \\
\sigma_{66} = C_{D66}\ \epsilon_6
\end{gathered}
\tag{B.5}
$$

And each term of the matrix is:

$$
\begin{gathered}
C_{D11} = (1 - D_{f1})(1 - D_{d1})C_{11} \\
C_{D12} = (1 - D_{f1})(1 - D_{f2})(1 - D_{d2})C_{12} \\
C_{D13} = (1 - D_{f1})(1 - D_{d2})C_{13} \\
\\
C_{D21} = C_{21} \\
C_{D22} = (1 - D_{f2})(1 - D_{d2})C_{22} \\
C_{D23} = (1 - D_{f3})(1 - D_{d2})C_{23} \\
\\
C_{D31} = C_{31} \\
C_{D32} = C_{32} \\
C_{D33} = C_{33} \\
\\
C_{D44} = (1 - D_{f1})(1 - D_{f2})(1 - D_{f3})(1 - D_{d3})C_{44} \\
C_{D55} = C_{55} \\
C_{D66} = C_{66}
\end{gathered}
\tag{B.6}
$$

By definition, the Jacobian matrix is:

$$J = \frac{\partial \boldsymbol{\sigma}}{\partial \boldsymbol{\epsilon}} = \begin{bmatrix} \frac{\partial\sigma_1}{\partial\epsilon_1} & \frac{\partial\sigma_1}{\partial\epsilon_2} & \frac{\partial\sigma_1}{\partial\epsilon_3} & 0 & 0 & 0 \\ \frac{\partial\sigma_2}{\partial\epsilon_1} & \frac{\partial\sigma_2}{\partial\epsilon_2} & \frac{\partial\sigma_2}{\partial\epsilon_3} & \frac{\partial\sigma_2}{\partial\epsilon_4} & 0 & 0 \\ \frac{\partial\sigma_3}{\partial\epsilon_1} & \frac{\partial\sigma_3}{\partial\epsilon_2} & \frac{\partial\sigma_3}{\partial\epsilon_3} & \frac{\partial\sigma_3}{\partial\epsilon_4} & 0 & 0 \\ \frac{\partial\sigma_4}{\partial\epsilon_1} & \frac{\partial\sigma_4}{\partial\epsilon_2} & 0 & \frac{\partial\sigma_4}{\partial\epsilon_4} & 0 & 0 \\ 0 & 0 & 0 & 0 & \frac{\partial\sigma_5}{\partial\epsilon_5} & 0 \\ 0 & 0 & 0 & 0 & 0 & \frac{\partial\sigma_6}{\partial\epsilon_6} \end{bmatrix} \tag{B.7}$$

So what is left now is differentiating each term one by one. As an example, the derivative $\frac{\partial\sigma_2}{\partial\epsilon_2}$ has been done:

$$\frac{\partial\sigma_2}{\partial\epsilon_2} = \epsilon_1 \frac{\partial C_{D12}}{\partial\epsilon_2} + C_{D22} + \epsilon_2 \frac{\partial C_{D22}}{\partial\epsilon_2} + \epsilon_3 \frac{\partial C_{D23}}{\partial\epsilon_2}$$

And each of the terms is expanded below:

$$\epsilon_1 \frac{\partial C_{D12}}{\partial\epsilon_2} = -\epsilon_1(1 - D_{f1})(1 - D_{d2})C_{12}(\frac{\partial D_{f2}}{\partial\epsilon_2} + \frac{\partial D_{d2}}{\partial\epsilon_2})$$

$$C_{D22} = (1 - D_{f2})(1 - D_{d2})C_{22}$$

$$\epsilon_2 \frac{\partial C_{D22}}{\partial\epsilon_2} = -\epsilon_2(1 - D_{f2})C_{22}(\frac{\partial D_{d2}}{\partial\epsilon_2} + \frac{\partial D_{f2}}{\partial\epsilon_2})$$

$$\epsilon_3 \frac{\partial C_{D23}}{\partial\epsilon_2} = -\epsilon_3(1 - D_{f3})C_{23}\frac{\partial D_{d2}}{\partial\epsilon_2}$$

The final derivatives are $\frac{\partial D_{f1}}{\partial \epsilon_1}$, $\frac{\partial D_{f2}}{\partial \epsilon_2}$, $\frac{\partial D_{f3}}{\partial \epsilon_4}$, $\frac{\partial D_{d1}}{\partial \epsilon_1}$, $\frac{\partial D_{d2}}{\partial \epsilon_2}$, $\frac{\partial D_{d3}}{\partial \epsilon_4}$. Their calculus has to be done according to the expressions of damage 4.7 and 4.9, seen in chapter two. Derivatives are shown below:

For failure damage in warp direction:

$$\begin{gathered}
\frac{\partial D_{f1}}{\partial \epsilon_1} = \frac{1}{2} e^{(1-FF_1)a} \left(\frac{1 + a\, FF_1}{FF_1^3} \right) \left(\frac{2\epsilon_1 + \tilde{\epsilon}_{T1} - \tilde{\epsilon}_{T1}}{\tilde{\epsilon}_{C1}\tilde{\epsilon}_{T1}} \right) \\
FF_1 = \sqrt{\frac{\epsilon_1^2}{\tilde{\epsilon}_{T1}\tilde{\epsilon}_{C1}} + \frac{\epsilon_1(\tilde{\epsilon}_{C1} - \tilde{\epsilon}_{T1})}{\tilde{\epsilon}_{T1}\tilde{\epsilon}_{C1}}} \\
a = \frac{C_{11}\tilde{\epsilon}_{T1}^2 CELENT}{G_{fib}}
\end{gathered} \tag{B.8}$$

For failure damage in waft direction:

$$\begin{gathered}
\frac{\partial D_{f2}}{\partial \epsilon_2} = \frac{1}{2} e^{(1-FF_2)b} \left(\frac{1 + b\, FF_2}{FF_2^3} \right) \left(\frac{2\epsilon_2 + \tilde{\epsilon}_{T2} - \tilde{\epsilon}_{T2}}{\tilde{\epsilon}_{C2}\tilde{\epsilon}_{T2}} \right) \\
FF_2 = \sqrt{\frac{\epsilon_2^2}{\tilde{\epsilon}_{T2}\tilde{\epsilon}_{C2}} + \frac{\epsilon_2(\tilde{\epsilon}_{C2} - \tilde{\epsilon}_{T2})}{\tilde{\epsilon}_{T2}\tilde{\epsilon}_{C2}}} \\
b = \frac{C_{22}\tilde{\epsilon}_{T2}^2 CELENT}{G_{fib}}
\end{gathered} \tag{B.9}$$

For failure damage in in-ply shear direction:

$$\begin{gathered}
\frac{\partial D_{f3}}{\partial \epsilon_4} = \frac{\partial D_{f3}}{\partial \gamma_{12}} = e^{(1-FF_3)c} \left(\frac{1 + c\, FF_3}{FF_3^2} \right) \frac{1}{\tilde{\gamma}} \\
FF_3 = \frac{\gamma}{\tilde{\gamma}} \\
c = \frac{C_{44}\tilde{\gamma}^2 CELENT}{G_{mat}}
\end{gathered} \tag{B.10}$$

For diffuse damage in warp direction:

$$
\begin{aligned}
D_{d1} &= c_0 + c_1 \ln \sqrt{\frac{1}{2}\epsilon_1^2 C_{11}} \\
\frac{\partial D_{d1}}{\partial \epsilon_1} &= \frac{c_1}{\epsilon_1}
\end{aligned}
\tag{B.11}
$$

For diffuse damage in weft direction

$$
\begin{aligned}
D_{d2} &= c_2 + c_3 \ln \sqrt{\frac{1}{2}\epsilon_2^2 C_{22}} \\
\frac{\partial D_{d2}}{\partial \epsilon_2} &= \frac{c_3}{\epsilon_2}
\end{aligned}
\tag{B.12}
$$

For diffuse damage in in-ply shear direction:

$$
\begin{aligned}
D_{d3} &= c_4 + c_5 \ln \sqrt{\frac{1}{2}\epsilon_4^2 C_{33}} \\
\frac{\partial D_{d3}}{\partial \epsilon_4} &= \frac{c_5}{\epsilon_4}
\end{aligned}
\tag{B.13}
$$

If derivatives of the damages are being calculated after the viscous regularization, calculus is very simple, as previous expressions just have to be multiplied by the factor:

$$
\frac{\triangle t}{\eta + \triangle t} \tag{B.14}
$$

It can be seen how for $\eta = 0$ the value of this factor is one, so derivatives would be exactly as if not viscous regularization would have been considered.

B.0.1 2D Plane stress case

For a plane case of stresses, this is, for a shell element, Jacobian would seem easier to calculate, but calculus is in fact harder, as resultant expressions are even longer. If a matrix condensation is performed for having the equation B.1 or B.2, but in this plane case, resultant system is:

$$\begin{bmatrix} \sigma_1 \\ \sigma_2 \\ \tau_{12} \end{bmatrix} = \begin{bmatrix} C_{D11} - \frac{C_{D13}^2}{C_{D33}} & C_{D22} - \frac{C_{D23}^2}{C_{D33}} & 0 \\ C_{D12} - \frac{C_{D13}C_{D23}}{C_{D33}} & C_{D11} - \frac{C_{D13}^2}{C_{D33}} & 0 \\ 0 & 0 & C_{D44} \end{bmatrix} \begin{bmatrix} \epsilon_1 \\ \epsilon_2 \\ \gamma_{12} \end{bmatrix} \tag{B.15}$$

It must be said that each term appeared through this development with the form C_{Dii} or C_{Dij} is the exact as in the 3D case, and its definition is shown in B.6. In addition, a C_{ii} or C_{ij} term comes from the original undamaged 3D stiffness matrix, shown in equation 2.13. To continue the same equation in B.15 is shown but with the stiffness matrix showing the functional dependence with the strains, necessary for differentiating.

$$\begin{bmatrix} \sigma_1 \\ \sigma_2 \\ \tau_{12} \end{bmatrix} = \begin{bmatrix} H_{D11}(\epsilon_1, \epsilon_2) & H_{D22}(\epsilon_1, \epsilon_2, \epsilon_3) & 0 \\ H_{D12}(\epsilon_1, \epsilon_2, \epsilon_3) & H_{D22}(\epsilon_1, \epsilon_2) & 0 \\ 0 & 0 & H_{D33}(\epsilon_1, \epsilon_2, \epsilon_3) \end{bmatrix} \begin{bmatrix} \epsilon_1 \\ \epsilon_2 \\ \gamma_{12} \end{bmatrix} \tag{B.16}$$

And the Jacobian matrix is the following:

$$J = \frac{\partial \boldsymbol{\sigma}}{\partial \boldsymbol{\epsilon}} = \begin{bmatrix} \frac{\partial \sigma_1}{\partial \epsilon_1} & \frac{\partial \sigma_1}{\partial \epsilon_2} & \frac{\partial \sigma_1}{\partial \epsilon_3} \\ \frac{\partial \sigma_2}{\partial \epsilon_1} & \frac{\partial \sigma_2}{\partial \epsilon_2} & \frac{\partial \sigma_2}{\partial \epsilon_3} \\ \frac{\partial \sigma_3}{\partial \epsilon_1} & \frac{\partial \sigma_3}{\partial \epsilon_2} & \frac{\partial \sigma_3}{\partial \epsilon_3} \end{bmatrix} \tag{B.17}$$

Once again, one of the derivatives is shown as example, in this case $\frac{\partial \sigma_2}{\partial \epsilon_2}$:

$$\frac{\partial \sigma_2}{\partial \epsilon_2} = \frac{\partial H_{D12}}{\partial \epsilon_2}\epsilon_1 + H_{D22} + \frac{\partial H_{D22}}{\partial \epsilon_2}\epsilon_2$$

An each of the terms is expanded below:

$$\begin{aligned}\frac{\partial H_{D12}}{\partial \epsilon_2}\epsilon_1 = \epsilon_1 \Bigg\{ &(1-D_{f1})C_{12}\left[(-1)(1-D_{d2})\frac{\partial D_{f2}}{\partial \epsilon_2} - \frac{\partial D_{d2}}{\partial \epsilon_2}\right] + \\ &+ \frac{2}{C_{33}}C_{13}C_{23}(1-D_{f1})(1-D_{f3})(1-D_{d2})\frac{\partial D_{d2}}{\partial \epsilon_2}\Bigg\}\end{aligned}$$

$$H_{D22} = C_{D11} - \frac{C_{D13}^2}{C_{D33}} = (1-D_{f1})(1-D_{d1})C_{11} - \frac{((1-D_{f1})(1-D_{d2})C_{13})^2}{C_{33}}$$

$$\begin{aligned}\frac{\partial H_{D22}}{\partial \epsilon_2}\epsilon_2 = \epsilon_2 \Bigg\{ &C_{12}\left[(-1)(1-D_{f2})\frac{\partial D_{d2}}{\partial \epsilon_2} - (1-D_{d2})\frac{\partial D_{f2}}{\partial \epsilon_2}\right] + \\ &+ \frac{2}{C_{33}}C_{23}^2(1-D_{d3})^2(1-D_{d2})\frac{\partial D_{d2}}{\partial \epsilon_2}\Bigg\}\end{aligned}$$

The final derivatives $\frac{\partial D_{f1}}{\partial \epsilon_1}$, $\frac{\partial D_{f2}}{\partial \epsilon_2}$, $\frac{\partial D_{f3}}{\partial \epsilon_4}$, $\frac{\partial D_{d1}}{\partial \epsilon_1}$, $\frac{\partial D_{d2}}{\partial \epsilon_2}$, $\frac{\partial D_{d3}}{\partial \epsilon_4}$ are exactly the same than in the 3D case.

Bibliography

[1] A. Guemes Gordo, A. Fernandez Lopez, and J.M. Pintado Sanjuan Benito, eds. *Ciencia de materiales para ingenieros*. Pearson, 2012. ISBN: 97884883227190 (cit. on p. 1).

[2] Airbus. *A350-XWB*. URL: `https://www.airbus.com/newsroom/galleries/photo-gallery.html`. (accessed: 10.04.2020) (cit. on p. 2).

[3] Unknown. *Warp and weft scheme*. URL: `http://blog.stephens.edu/arh101glossary/?glossary=warp`. (accessed: 10.04.2020) (cit. on p. 6).

[4] Unknown. *Linen (Flax)*. URL: `https://www.aestheticstories.com/linen-flax/`. (accessed: 10.04.2020) (cit. on p. 13).

[5] J. Mussig and C. Stevens, eds. *Industrial Applications of Natural Fibres - Structure, Properties and Technical Applications*. Wiley, 2010. ISBN: 9780470695081. DOI: `10.1002/9780470660324` (cit. on pp. 14–16).

[6] A. Amiri, A. Yu, D. Webster, and C. Ulven. «Bio-Based Resin Reinforced with Flax Fiber as Thermorheologically Complex Materials». In: *Polymers* 4 (Apr. 2016). ISSN: 2073-4360. DOI: `10.3390/polym8040153`. URL: `https://europepmc.org/articles/PMC6432415` (cit. on p. 14).

[7] P. Asokan, M. Firdoous, and W. Sonal. «PROPERTIES AND POTENTIAL OF BIO FIBRES, BIO BINDERS, AND BIO COMPOSITES». In: *Advance Materials science* 30.0 (Jan. 2012), pp. 254–262 (cit. on p. 15).

[8] P. Ladeveze and E. Le Dantec. «Damage modelling of the elementary ply for laminated composites». In: *Composites Science and Technology* 43 (1992), pp. 257–267 (cit. on p. 19).

[9] P. Linde, J. Pleitner, H.d. Boer, and C. Carmone. «Modelling and Simulation of Fibre Metal Laminates». In: *ABAQUS Users' Conference*. 2004, pp. 421–439 (cit. on p. 26).

[10] M. Bak. *Cohesive zone modeling and viscous regularization, Michael Bak Blog*. URL: `https://caeai.com/blog/cohesive-zone-modeling-and-viscous-regularization`. (accessed: 15.02.2020) (cit. on p. 29).

[11] SIMULIA. *Abaqus Analysis User's Guide*. URL: `http://dsk.ippt.pan.pl/docs/abaqus/v6.13/books/usb/default.htm?startat=pt09ch37s01alm63.html`. (accessed: 10.04.2020) (cit. on pp. 29, 67, 69).

[12] Unknown. *Lecture 6 Writing a UMAT or VUMAT*. URL: `https://imechanica.org/files/Writing%5C%20a%5C%20UMAT.pdf`. (accessed: 10.04.2020) (cit. on p. 35).

[13] C. Zweben, W. Smith, and M. Wardle. *Test Methods for Fiber Tensile Strength, Composite Flexural Modulus, and Properties of Fabric-Reinforced Laminates*. In STP674-EB Composite Materials: Testing and Design (Fifth Conference), ed. S. Tsai, (pp. 228-262). West Conshohocken, PA: ASTM International, 1979. DOI: `https://doi.org/10.1520/STP36912S` (cit. on p. 40).

[14] *ASTM C393 / C393M-16, Standard Test Method for Core Shear Properties of Sandwich Constructions by Beam Flexure*. West Conshohocken, PA: ASTM International, 1916. URL: `www.astm.org` (cit. on p. 40).

[15] Adrian P. Mouritz, ed. *Introduction to Aerospace Materials*. Woodhead, 2012. ISBN: 9781855739468 (cit. on p. 41).

[16] J.I. Cardesa Dueñas. *Notas sobre Dinámica de Fluidos computacional*. 2014 (cit. on p. 46).

[17] V. Médeau. «Rupture des composites tissés 3D : de la caractérisation expérimentale à la simulation robuste des effets d'échelle». PhD thesis. Toulouse, France: Université de Toulouse, published by ISAE, Institut Supérieur de l'Aéronautique et de l'Espace, 2019. URL: `https://depozit.isae.fr/theses/2019/2019_Medeau_Victor_D.pdf` (cit. on pp. 56–58).

[18] A.A. Griffith. *The phenomena of rupture and flow in solids*. The Royal Society Pulishing, 1921, pp. 163–198. DOI: `110.1098/rsta.1921.0006` (cit. on p. 56).

[19] J.-L. Chaboche and J. Lemaitre. *Mécanique des matériaux solides*. DUNOD, 2001. ISBN: 9782100810901 (cit. on p. 56).

[20] M.J. Laffan, S.T. Pinho, P. Robinson, and L. Iannucci. «Measurement of the in situ ply fracture toughness associated with mode I fibre tensile failure in FRP. Part I : Data reduction». In: *Composites Science and Technology* 70.4 (May 2012), pp. 606–613 (cit. on p. 58).

[21] *ASTM D5528-13, Standard Test Method for Mode I Interlaminar Fracture Toughness of Unidirectional Fiber-Reinforced Polymer Matrix Composites*. West Conshohocken, PA: ASTM International, 2013. URL: `www.astm.org` (cit. on p. 59).

[22] *Operating- Instruction Cracklength Measuring System FRACTOMAT and KRAK- GAGE*. RUMUL (cit. on p. 62).

[23] Unknown. *Fractomat measuring system.* URL: https://adhesivenetworks.com/product/tti-fractomat-1078-crack-length-measuring-and-control-system/ (cit. on p. 64).

[24] A. Turon, C.G. Dávila, P.P. Camanho, and J. Costa. «An Engineering Solution for solving Mesh Size Effects in the Simulation of Delamination with Cohesive Zone Models». In: *Retrieved from NTRS, NASA Technical Report Server* (Jan. 2007). URL: https://ntrs.nasa.gov/search.jsp?R=20070038334 (cit. on p. 68).

[25] *ASTM D7136 / D7136M-15, Standard Test Method for Measuring the Damage Resistance of a Fiber-Reinforced Polymer Matrix Composite to a Drop-Weight Impact Event.* West Conshohocken, PA: ASTM International, 2015. URL: www.astm.org (cit. on p. 80).